

1 Hydrodynamic and biochemical impacts on the development of 2 hypoxia in the Louisiana–Texas shelf Part 1: roles of nutrient 3 limitation and plankton community

4 Yanda Ou¹ and Z. George Xue^{1,2,3}

5 ¹Department of Oceanography and Coastal Sciences, Louisiana State University, Baton Rouge, LA, 70803, USA.

6 ²Center for Computation and Technology, Louisiana State University, Baton Rouge, LA, 70803, USA.

7 ³Coastal Studies Institute, Louisiana State University, Baton Rouge, LA, 70803, USA

8 *Correspondence to:* Z. George Xue (zxue@lsu.edu)

9 **Abstract.** A three-dimensional coupled hydrodynamic–biogeochemical model with multiple nutrient and plankton functional
10 groups was developed and adapted to the Gulf of Mexico to investigate the role of nutrients and the complexity of plankton
11 community in dissolved oxygen (DO) dynamics. A 15-year hindcast was achieved covering the period of 2006–2020.
12 Extensive model validation against *in situ* data demonstrates that the model was capable of reproducing vertical distributions
13 of DO, spatial distributions of bottom DO concentration, as well as their interannual variations. Model results indicated that
14 while nitrogen (N) limitation was more commonly found in the shallow (< 20 m) middle and west shelf, phosphorus (P) and
15 silicon (Si) limitations could be more spreading on the shelf than previously reported. The seasonality of primary and secondary
16 production exhibited a bi-peak (in late spring and early summer) pattern, which was contributed by both nanophytoplankton
17 and the dominated diatom groups. DO consumption at the sediment layers was mostly contributed by zooplankton mortality
18 and egestion processes. The plankton community in the water column in general, produced more DO than it consumed. In
19 waters within 2 m above the bottom, there was a higher chance that DO consumption could exceed production. Nutrient
20 limitation, interactions (competition, grazing, and predation behaviors) among plankton groups, and shifts in net DO
21 contribution from the community (i.e., (photosynthesis - total respiration)/total biomass) complicated hypoxia development
22 under different nutrient reduction strategies. Sensitivity tests indicate that a triple riverine nutrient reduction (N, P, and Si) of
23 60 % is needed to reach the goal of a 5000 km² hypoxic zone.

25 1 Introduction

26 The Louisiana–Texas (LaTex) shelf in the northern Gulf of Mexico (nGoM) has one of the most notorious recurring hypoxia
27 in the world (bottom dissolved oxygen (DO) < 2 mg L⁻¹, Rabalais et al., 2002; Rabalais et al., 2007a; Justić and Wang, 2014).
28 Regular mid-summer cruises since 1985 show that hypoxia usually first emerges in mid-May and persists through mid-
29 September. The hypoxic zone can cover as big as 23,000 km² and has a volume of up to 140 km³ (Rabalais and Turner, 2019;

Deleted: numerical modeling and hypoxia mechanisms

Deleted: nitrogen, phosphorus, silica cycles, and

Deleted: phytoplankton

Deleted: zooplankton

Deleted: applied

Deleted: study bottom

Formatted: Font: Italic

Deleted: dissolved oxygen (DO),

Deleted: its

Deleted: Horizontal advection, vertical advection, vertical diffusion, and sedimentary oxygen consumption (SOC) were

Deleted: as the major factors modulating summer bottom DO dynamics. SOC contributes 33%–51% of summer bottom DO variability over the nearshore regions. Hydrodynamic impacts on the summer bottom DO are also remarkable as the joint contribution of the advection

Deleted: vertical diffusion reaches 28%–55% and 51%–59% in nearshore and offshore regions, respectively. Sensitivity experiments were carried out to assess the changes in the size of the hypoxic zone due to riverine nutrient reductions. Results of sensitivity experiments highlighted the nonlinear relationship between the reduction of river nutrients and changes in the size of the hypoxic zone

Deleted: can be explained

Deleted: the complexity of the lower-trophic community (e.g., competition on nutrients

Deleted: Nutrient reductions would not necessarily lead to a decrease in the size of the hypoxic zone. Instead, due to the interactions

Deleted: plankton groups, the hypoxic area could even increase under some

Deleted: -

Deleted: conditions. A

Deleted: nitrogen, phosphorus

Deleted: silica

Deleted: 80

Deleted: have shown

65 Rabalais and Baustian, 2020). [Although N is the ultimate limiting nutrient, P_i load reduction would also lead to a significant](#)
66 [reduction of the hypoxia area \(Fennel and Laurent, 2018\). Transient P limitation on the shelf \(Laurent et al., 2012; Sylvan et](#)
67 [al., 2007\) was deemed to be associated with the delayed onset and reduction of the hypoxia area. Sensitivity experiments of](#)
68 [hypoxia area reduction to different nutrient reduction strategies by Fennel and Laurent \(2018\) suggested that to meet the](#)
69 [hypoxic area reduction goal \(< 5,000 km² in a 5-year running average\) set by the Hypoxia Task Force \(2008\), a dual nutrient](#)
70 [strategy with a reduction of 48 % of total nitrogen \(N\) and inorganic phosphorus \(P\) would be the most effective way.](#)

72 Coastal eutrophication in the LaTex shelf leads to a high rate of microbial respiration and depletion of DO (Rabalais et al.,
73 2007b). Incubation studies in the LaTex shelf suggested that [sediment oxygen consumption \(SOC\)](#) accounted for 20±4 %
74 (Murrell and Lehrter, 2011) [to 25±5.3 % \(McCarthy et al., 2013\) of below-pycnocline respiration, nearly 7-fold greater than](#)
75 [the corresponding percentage in waters overlying sediments \(3.7±0.8 %, about 20 cm above sediments in McCarthy et al.,](#)
76 [2013\). Incubation experiments indicated the SOC over the total respiration rate at sediments and overlying water was ~87 %](#)
77 [\(McCarthy et al., 2013\). The numerical study by Fennel et al. \(2013\) calculated the corresponding SOC fraction which reached](#)
78 [60 % when applying the water respiration rates of Murrell and Lehrter \(2011\) and sediment respiration rates of Rowe et al.](#)
79 (2002). Another numerical study (Yu et al., 2015) also pointed out that in the LaTex shelf, oxygen consumption at the bottom
80 water layer was more associated with SOC rather than water column respiration. [According to in-situ data and statistical](#)
81 [analysis, SOC could be estimated using the bottom temperature and DO concentration \(e.g., Hetland and DiMarco, 2008\).](#)
82 [Nevertheless, many numerical studies treated SOC only associated with the abundance of organic matter in the sediment \(e.g.,](#)
83 [Justić and Wang, 2014; Fennel et al., 2006; 2011\). For example, an instantaneous remineralization parameterization used by](#)
84 [Fennel et al. \(2006, 2011\) estimated SOC as a function of sediment detritus and phytoplankton. Using this scheme, Große et](#)
85 [al. \(2019\) found that the simulated SOC was supported by Mississippi N supply \(51±9 %\), Atchafalaya N supply \(33±9 %\),](#)
86 [and open-boundary N supply \(16±2 %\). However, the instantaneous parameterization tends to underestimate SOC at the peak](#)
87 [of blooms yet overestimate SOC after the blooms. In a realistic environment, there should be a lag between the blooms and](#)
88 [the peak SOC \(Fennel et al., 2013\). Recently, developments of coupled sediment–water models emphasized the importance of](#)
89 [biogeochemical processes in sediments on the SOC dynamics and evolution of bottom hypoxia in the shelf \(Moriarty et al.,](#)
90 [2018; Laurent et al., 2016\). However, coupled sediment–water models are computationally more expensive than a simplified](#)
91 [parameterization of SOC. Especially for long-term simulations and time-sensitive forecasts, it is crucial to balance the model's](#)
92 [efficiency with its complexity.](#)

94 In addition to SOC and excess nutrient supply from the rivers, water column stratification also plays an important role in
95 regulating the variability of bottom DO concentration in the LaTex shelf. Strong stratification prohibits ventilation of DO and
96 thus results in reduced DO supply to the bottom water layer (Hetland and DiMarco, 2008; Bianchi et al., 2010; Fennel et al.,
97 2011, 2013, 2016; Justić and Wang, 2014; Wang and Justić, 2009; Feng et al., 2014; Yu et al., 2015; Laurent et al., 2018). On
98 the shelf, the Mississippi and the Atchafalaya plume introduces buoyancy, leading to a stable water column and weak DO

Moved down [1]: Sensitivity experiments of hypoxia area reduction to different nutrient reduction strategies by Fennel and Laurent (2018) suggested that to meet the hypoxic area reduction goal (< 5,000 km² in a 5-year running average) set by the Hypoxia Task Force (2008), a dual nutrient strategy with a reduction of 48 % of total nitrogen

Deleted: and inorganic phosphorus would be the most effective way. Although nitrogen is the ultimate limiting nutrient, phosphorus

Deleted: phosphorus

Moved (insertion) [1]

Deleted: or

Deleted: at the water

Deleted: The fraction of

Deleted: according to the measurements by

Deleted: . (

Deleted: . As mentioned

Deleted: .

Deleted: As it was commonly accepted that SOC was driven by the abundance of organic matter in the sediment, numerical studies developed SOC schemes following this nature (e.g.,

Deleted: the

Deleted: nitrogen

Deleted: nitrogen

Deleted: nitrogen

Deleted: once

Deleted: start

Deleted: sedimentary biochemical

Deleted: simple

Deleted: Therefore

Deleted: model

Moved down [2]: from both cyanobacteria and diatoms (Wawrik and Paul, 2004; Schaeffer et al., 2012; Chakraborty et al., 2017).

Moved down [3]: Cruises data in the nGoM indicated that diatoms accounted for ~50 to ~65 % (inner-shelf) and ~33 to ~64 % (mid-shelf) of chlorophyll *a* in winter and spring, and ~30 % to ~46 % (inner-shelf) during summer and fall, respectively (Chakraborty and Lohrenz, 2015). A field survey documented that the biovolume

Moved down [4]: In the Mississippi River plume, diatoms were

Deleted: and

Deleted: , especially for long-term hindcasts. ¶ ... [1]

Deleted: The phytoplankton community was highly simplified ... [2]

Formatted: Font: Italic

Deleted: river freshwater plume supported by the

Deleted: Rivers

160 ventilation processes (Mattern et al., 2013; Fennel and Testa, 2019). Due to the different distances from major river mouths,
161 the influence of freshwater-induced buoyancy would vary along the shelf. Moreover, the transports and deposition processes
162 of organic matter are affected by the coastal along-shore current systems resulting in a SOC gradient across the shelf. For
163 instance, Hetland and DiMarco (2008) pointed out that in the west of Terrebonne Bay, where stratification is usually weak,
164 bottom hypoxia is mainly controlled by bottom respiration.

165

166 The phytoplankton blooms on the shelf result from both cyanobacteria and diatoms (Wawrik and Paul, 2004; Schaeffer et al.,
167 2012; Chakraborty et al., 2017). In the Mississippi River plume, diatoms were found as the most diverse algal class accounting
168 for over 42 % of all unique genotypes observed (Wawrik and Paul, 2004). Cruises data in the nGoM indicated that diatoms
169 accounted for ~50 to ~65 % (inner-shelf) and ~33 to ~64 % (mid-shelf) of chlorophyll *a* in winter and spring, and ~30 % to
170 ~46 % (inner-shelf) during summer and fall, respectively (Chakraborty and Lohrenz, 2015). A field survey documented that
171 the biovolume contribution of diatoms to the total phytoplankton could be as high as 80 % and 70 % during the upwelling
172 seasons in 2013 and 2014, respectively (Anglès et al., 2019). While a lot of existing studies indicated N and P were more
173 limited than Si on the shelf (e.g., for cruises in 2004 in Quigg et al., 2011; for cruises in 2012 in Zhao and Quigg, 2014; for
174 cruises in 1984, 1994, 2005, 2010, and 2011 in Turner and Rabalais, 2013), Si limitation has also been reported for both plume
175 and shelf water. Based on cruises studies in the plume of the Mississippi River in 1992 and 1993, strong Si limitation in spring
176 was found due to the increasing N:Si ratio in the Mississippi River water (Nelson and Dortch, 1996). Cruise measurements in
177 1987 and 1988 also suggested the likelihood of Si limitation, which sometimes overwhelmed the N limitation (Dortch and
178 Whitledge, 1992).

179

180 Numerical studies for hypoxia in the LaTex shelf were developed mostly based on observations that emphasized N and P as
181 limiting nutrients (e.g., Hetland and DiMarco, 2008; Fennel et al., 2006, 2011, 2013; Laurent et al., 2012; Laurent and Fennel,
182 2014; Fennel and Laurent, 2018; Justić et al., 2003; Justić et al., 2007; Justić and Wang, 2014; Große et al., 2019; Moriarty et
183 al., 2018). In addition, most existing models utilized an over-simplified lower trophic level model (one phytoplankton + one
184 zooplankton function group or only one phytoplankton group). The recycling of nutrients in water columns and the associated
185 biogeochemical processes, which may be important to hypoxia evolution (e.g., in the Chesapeake Bay by Testa and Kemp,
186 2012), could be over-simplified. In this study, we aimed to 1) investigate the cycling of silicate and its contribution to the
187 hypoxia evolution in the LaTex shelf; and 2) assess the impacts of the complexity of the plankton community on DO dynamics.
188 We adapted and modified a coupled physical-biogeochemical model covering the entire Gulf of Mexico (GoM) by introducing
189 the oxygen and P cycles to the North Pacific Ecosystem Model for Understanding Regional Oceanography (NEMURO, Kishi
190 et al. 2007). The model has two phytoplankton and three zooplankton functional groups for a more comprehensive
191 representation of the plankton community. We also modified the instantaneous remineralization parameterization by adding a
192 conceptual sedimentary organic pool (represented by a sedimentary particulate organic N pool, PON_{sed}; Fig. 1) to allow the
193 accumulation of organic matter in the sediment. The sedimentary organic matter pool in our study is supported by a complex

Deleted: different

Deleted: gradients

Moved (insertion) [2]

Moved (insertion) [4]

Moved (insertion) [3]

Formatted: Font: Italic

Deleted: Despite the above efforts, there are still knowledge gaps in our understanding of the mechanism of hypoxia development as well as a feasible way to reduce the size of the hypoxic zone. First of all, the LaTex shelf is a vast water body and the contribution of sedimentary biochemical and hydrodynamics to hypoxia development is location-dependent. Fennel et al. (2016)(Fennel et al., 2016) divided the shelf into six subregions for model validation purposes instead of for quantifying biochemical and hydrodynamic impacts on bottom DO variability in different shelf regions. A recent study by Ruiz Xonchuk et al. (2021) tried to fill such a gap by decomposing the oxygen equation and found that advection and sediment oxygen demand were the two main contributors to the oxygen budget. But they focused more on the impacts of the temporal and spatial scales of physical processes on bottom DO variability over the west shelf (between 95°W and 92.5°W). Secondly, existing biogeochemical models (e.g.,

Deleted:) utilized an over-simplified lower-trophic ecosystem (one phytoplankton + one zooplankton function groups or only one phytoplankton group) with one or two embedded nutrient flows (nitrogen or nitrogen+phosphorus). These models could not differentiate the contribution of different plankton groups or the interaction among them in hypoxia development. The nutrients reduction strategies proposed by existing models (mostly based on nitrogen loads; Scavia et al., 2013

Moved down [5]: ; Obenour et al., 2015; Turner et al., 2012;

Deleted: Laurent and Fennel (2019) may be problematic as bottom DO's responses to decreased nutrient loads may not be linear or quasilinear due to the complexity of the lower trophic community. ¶

¶ In this study, we

Deleted: phosphorus

Deleted: nitrogen pool, PON_{sed}; Fig. 1) to allow the accumulation of organic matter in the sediment. Although the SOC scheme applied is similar to that in Justić and Wang (2014), the sedimentary organic matter pool in our study is supported by a more complex plankton community, including three phytoplankton functional groups and two zooplankton functional groups. The influence of the community complexity can be reflected in the SOC and eventually in the bottom DO variability. Based on a 15-year (2006–2020) numerical hindcast, we aimed to 1) understand the contributions of different factors in hypoxia development in different parts of the LaTex shelf; and 2) assess the outcomes of different riverine nutrient reduction scenarios regarding the reduction of the hypoxic zone. In addition, the daily outputs of physical and biochemical conditions will be used to develop a hypoxia prediction model using machine learning techniques (see an accompanying paper in Part 2). In the following sections, model description and modification, model set-ups, and data availability were given in Section 2 (Methods), followed by extensive model validations (Section 3). The main findings of this study and relevant discussion are presented in Section 4.

246 [plankton community, including two phytoplankton and three zooplankton functional groups. The influence of the community](#)
247 [is represented in the biogeochemical processes in water columns and sediments and eventually be reflected in the bottom DO](#)
248 [variability.](#)

249 2 Methods

250 2.1 Coupled hydrodynamic–biogeochemical model

251 We adapted the three-dimensional, free-surface, topography-following community model, the Regional Ocean Model System
252 (ROMS, version 3.7), on the platform of Coupled Ocean–Atmosphere–Wave–Sediment Transport (COAWST) modeling
253 system (Warner et al., 2010) to the GoM (Gulf–COAWST). ROMS solves finite difference approximations of Reynolds
254 Averaged Navier–Stokes equations by applying hydrostatic and Boussinesq approximations with a split explicit time-stepping
255 algorithm (Haidvogel et al., 2000; Shepetchkin and McWilliams, 2005, 2009). The biogeochemical model applied is primarily
256 based on the NEMURO developed by Kishi et al. (2007). NEMURO is a concentration-based, lower-trophic-level ecosystem
257 model developed and parameterized for the North Pacific. The original NEMURO model has 11 concentration-based state
258 variables, including nitrate (NO_3), ammonium (NH_4), small and large phytoplankton biomass (PS and PL), small, large, and
259 predatory zooplankton biomass (ZS, ZL, and ZP), particulate and dissolved organic [N](#) (PON and DON), particulate silica
260 (Opal), and silicic acid ($\text{Si}(\text{OH})_4$). NEMURO is known for its capability to distinguish ZS, ZL, and ZP and [to provide](#) a detailed
261 analysis of the dynamics of different functional groups. It was widely used in studies of plankton biomass on regional scales
262 (Fiechter and Moore 2009; Gomez et al., 2018; Shropshire et al., 2020). The embedded [Si](#) cycle permits the inclusion of a
263 diatom group (i.e., PL), the dominant phytoplankton group in the nGoM.

264 2.2 Model modification

265 In a recent effort, Shropshire et al. (2020) adapted and modified NEMURO to the GoM with five structural changes. (1) The
266 grazing pathway of ZL on PS was removed since, in the GoM, the PS group is predominated by cyanobacteria and
267 picoeukaryotes, which are too small for direct feeding by most mesozooplankton (i.e., [ZL](#)). (2) Linear function of mortality
268 was applied for PS, PL, ZS, and ZL, while quadratic mortality was used for ZP, accounting for predation pressure of unmodeled
269 predators, like planktivorous fish. (3) The ammonium inhibition term in [the](#) nitrate limitation function was no longer considered
270 exponentially but followed the parameterization by Parker (1993). (4) Light limitation on photosynthesis was replaced with
271 Platt et al.'s (1980) functional form, which was also implemented in the newer version of NEMURO. (5) Constant C: Chl ratio
272 was replaced with a variable C: Chl model according to the formulation by Li et al. (2010).

273

274 However, neither the modified (Shropshire et al., 2020) nor the original (Kishi et al., 2007) NEMURO model considered [P](#)
275 and oxygen cycles. In this study, we introduced a [P](#) cycle into NEMURO, including three concentration-based state variables
276 as phosphate (PO_4), particulate organic [P](#) (POP), and dissolved organic [P](#) (DOP). The [P](#) limitation on phytoplankton growth

Deleted: nitrogen

Deleted: provides

Deleted: silicon

Deleted: PL

Deleted: phosphorus

Deleted: phosphorus

Deleted: phosphorus

Deleted: phosphorus

Deleted: phosphate

286 was introduced using the Michaelis–Menten formula. In the NEMURO model, N serves as the common “currency”, while P
 287 and Si are converted to N using the Redfield ratio of $P: N: Si=1: 16: 16$. In the river-dominated LaTex shelf, inorganic and
 288 organic nutrients are supplied mainly by rivers. In our model, riverine PO_4 (Fig. C1), DOP, and POP were prescribed based on
 289 water quality measurements at river gages. When no measurement was available, the PO_4 , DOP, and POP were approximated
 290 using total nitrate+nitrite (NO_3+NO_2), dissolved organic N (DON), and particulate organic N (PON) measurements,
 291 respectively, via the Redfield ratio of $P: N=1: 16$. We neglected the POP settling process but preserved these pools by
 292 introducing the stoichiometric ratio between P and N instead. In other words, the sinking process of POP was implicitly
 293 included by building linkages between PON and POP concentrations, as the sinking of PON was considered in the model.
 294 Governing equations for P state variables were given according to Eqs. 1–3. Please also refer to the appendices for more details
 295 on expressions of modified terms (Appendix A), state variables (Appendix Table B1), source and sink terms (Appendix Table
 296 B2), and values of parameters (Appendix Table B4).

$$298 \frac{d(PO_4)}{dt} = (ResPSn + ResPLn) \cdot RPO4N$$

$$299 \quad + (DecP2N + DecD2N) \cdot RPO4N$$

$$300 \quad + (ExcZSn + ExcZLn + ExcZPn) \cdot RPO4N$$

$$297 \quad - (GppPSn + GppPLn) \cdot RPO4N, \quad (1)$$

$$302 \frac{d(DOP)}{dt} = (DecP2D - DecD2N) \cdot RPO4N$$

$$301 \quad + (ExcPSn + ExcPLn) \cdot RPO4N, \quad (2)$$

$$303 \frac{d(POP)}{dt} = (MorPSn + MorPLn + MorZSn + MorZLn + MorZPn) \cdot RPO4N$$

$$304 \quad + (EgeZSn + EgeZLn + EgeZPn) \cdot RPO4N$$

$$305 \quad - (DecP2N + DecP2D) \cdot RPO4N, \quad (3)$$

307 We further adapted the oxygen cycle developed by Fennel et al. (2006, 2013) to NEMURO for hypoxia simulations. However,
 308 our model's [biogeochemical processes](#) are slightly different due to the different plankton functional groups considered. [Sources](#)
 309 for oxygen are contributed by [the](#) photosynthesis of two phytoplankton functional groups, while the sinks are attributed to
 310 respirations of two phytoplankton functional groups, metabolism of three zooplankton functional groups, light-dependent
 311 nitrification (Olson, 1981; Fennel et al., 2006), aerobic decomposition of particulate and dissolved organic matter (measured
 312 as PON, and DON, respectively), and SOC. Wanninkhof's (1992) parameterization was implemented for estimates of oxygen
 313 air–sea flux. The [biogeochemical](#) dynamics of oxygen were adopted as follows (Eq. 4; also see detailed descriptions of
 314 variables and parameters in Appendix A–B):

$$315 \frac{d(Oxyg)}{dt} = (rOxNO_3 \cdot GppNPS + rOxNH_4 \cdot GppAPS)$$

$$316 \quad + (rOxNO_3 \cdot GppNPL + rOxNH_4 \cdot GppAPL)$$

Deleted: nitrogen

Deleted: phosphorus

Deleted: silicon

Deleted: nitrogen

Deleted: nitrogen

Deleted: nitrogen

Deleted: phosphorus

Deleted: nitrogen

Deleted: phosphorus

Deleted: Equations

Deleted: biochemical dynamics of oxygen

Deleted: Biochemical sources

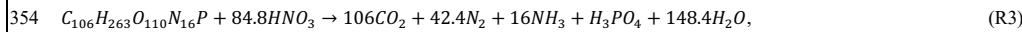
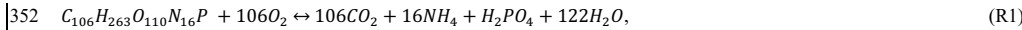
Deleted: biochemical

$$\begin{aligned}
331 & -ResPSn \cdot [Rnews \cdot rOxNO_3 + (1 - Rnews) \cdot rOxNH_4] \\
332 & -ResPLn \cdot [RnewL \cdot rOxNO_3 + (1 - RnewL) \cdot rOxNH_4] \\
333 & -rOxNH_4 \cdot (ExcZSn + ExcZLn + ExcZPn) \\
334 & -2 \cdot Nit \cdot LgtlimN \cdot r \\
335 & -rOxNH_4 \cdot (DecD2N + DecP2N) \cdot r \\
336 & -SOC \cdot THK_{bot}, \tag{4}
\end{aligned}$$

337 A PON_{sed} pool due to vertical sinking processes of PON was introduced for parameterization of SOC. The SOC scheme (Fennel
338 et al., 2006) is known as the instantaneous consumption of DO. As soon as the PON falls into the sediment bed, PON will be
339 decomposed instantaneously. This scheme tends to underestimate SOC at the peak of blooms and to overestimate SOC after
340 blooms since the lag in SOC demand is neglected (Fennel et al., 2013). We considered such temporal delays in SOC by
341 introducing a PON_{sed} pool. A portion of sinking PON ends up with PON_{sed} , while the rest is buried (PON_{burial}) and is removed
342 from the system. The parameterization is shown in the following. 1) Organic matter settling down at the conceptual sediment
343 layer is remineralized at a temperature-dependent aerobic remineralization rate, K_{P2N} . 2) Sediment oxygen is consumed only
344 in the oxidation of sedimentary organic matter (represented by PON_{sed}) and the nitrification of ammonium to nitrate (Fennel
345 et al., 2006). 3) Oxygen consumption at the conceptual sediment layer directly contributes to oxygen concentration decreases
346 only at the bottom water column. 4) Sediment denitrification is linearly related to SOC according to observational-based
347 estimates by Seitzinger and Giblin (1996), but the relationship was modified by Fennel et al. (2006) with a slightly smaller
348 slope of denitrification on SOC rate, i.e.,

$$349 \text{denitrification (mmolN m}^{-2} \text{ day}^{-1}) = 0.105 \times SOC \text{ (mmolO}_2 \text{ m}^{-2} \text{ day}^{-1}), \tag{5}$$

350 5) Aerobic decomposition of PON_{sed} , sediment nitrification, and denitrification follow chemical equations according to
351 (Fennel et al., 2006):



355
356 6) Nitrate produced in sediments (Eq. R2) is used for denitrification (Eq. R3). The linear assumption in 4) implicitly builds
357 relationships among the reactions listed in assumption 5). Let's assume that the production rate of NH_4 by aerobic
358 decomposition (Eq. R1) of organic matter is $M \text{ mmol m}^{-3} \text{ day}^{-1}$, and that the fraction of denitrification-produced CO_2 (Eq. R3)
359 to the total CO_2 production (Eqs. R1 and R3) is x . According to the linear assumption abovementioned, the consumption rate
360 of NO_3 during denitrification (Eq. R3) is proportional to the total consumption rate of O_2 in the sediment (Eqs. R1 and R2),
361 yielding $\frac{84.8Mx}{16(1-x)} = 0.105 \times \left[\frac{106M}{16} + \frac{84.8Mx}{8(1-x)} \right]$ and further $x \approx 0.1425$. The oxygen consumption rate (Eq. 6) and organic matter

Deleted: ·

Deleted: · r

Deleted: sedimentary particulate organic nitrogen (

Deleted:)

Deleted: overlying water or bottom water column. Here, we did not distinguish the overlying water and bottom water column since no dynamic sediment module was considered.

Deleted:

Deleted: Only a portion of NH_4 provided by the aerobic respiration...

Deleted: (R1)

Deleted: as the source element in the nitrification (Eq. (R2)), while all NO_3 produced by nitrification is used as the source element in

Deleted: (

Deleted:).

Deleted: (

Deleted:))

Deleted: (

Deleted:))

Deleted: Eq. (

Deleted: (

Deleted: (

Deleted:))

Deleted: (

Deleted:))

Deleted: Eq. (

Deleted:)

Deleted: (

Deleted:),

Deleted: (

Deleted:))

393 consumption rate (Eq. 7) due to the coupled aerobic decomposition, nitrification, and denitrification processes can be obtained
 394 by substituting the x value into the stoichiometric ratios according to Eqs. R1-R3.

$$395 \text{Oxygen}_{consumption} = \frac{106M}{16} + \frac{84.8Mx}{8(1-x)} = 8.3865M, \quad (6)$$

$$396 \text{OM}_{consumption} = \frac{M}{16} + \frac{Mx}{16(1-x)} = 0.0729M, \quad (7)$$

397 Accordingly, the SOC and consumption rate of PON_{sed} are given, respectively as follows:

$$398 \text{SOC} = \text{Oxygen}_{consumption} \cdot \text{THK}_{bot} = 8.3865M \cdot \text{THK}_{bot}, \quad (8)$$

$$399 \text{PON}_{sedconsumption} = 16 \cdot \text{OM}_{consumption} \cdot \text{THK}_{bot} = 1.1662M \cdot \text{THK}_{bot}, \quad (9)$$

400 where,

$$401 M = \frac{\text{PON}_{sed} \cdot \text{VP2N}_0 \cdot \exp(K_{P2N} \cdot \text{TMP})}{\text{THK}_{bot}}, \quad (10)$$

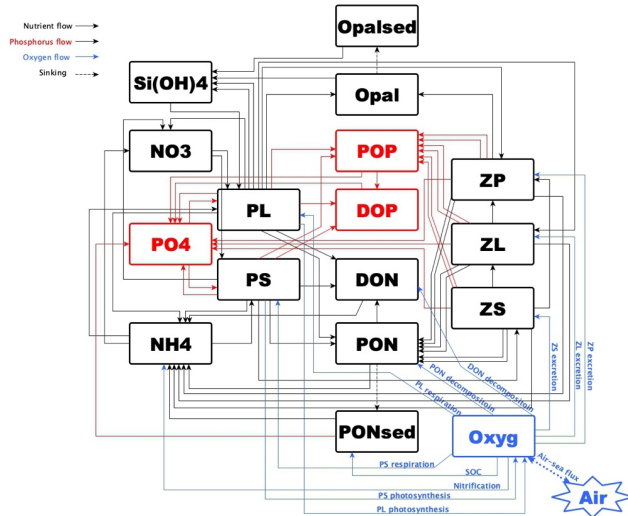
$$402 \text{THK}_{bot} = \text{thickness of bottom water column}, \quad (11)$$

403
 404 We further added light inhibition on the nitrification (Olson, 1981) and oxygen dependency on nitrification and aerobic
 405 decomposition. These parametrizations were applied following descriptions by Fennel et al. (2006, 2013). For the oxygen-
 406 dependent term, an oxygen threshold was specified below which no aerobic respiration or nitrification occurred. Detailed
 407 equations were listed in Appendix A. The structure of the newly modified NEMURO model was shown in a schematic diagram
 408 in Fig. 1.

Deleted: (
 Deleted:)
 Deleted: Eq. (
 Deleted:)-(
 Deleted:).

Deleted: For further comparison with the DO concentration, we transferred the SOC rate into a volume-based unit ($\text{mg L}^{-1} \text{day}^{-1}$) dividing the rate by THK_{bot} . For simplification, the terminology of SOC was still applied to represent the transferred SOC rate in the following discussion.

Deleted: Figure



421 **Figure 1. Schematic diagram of the modified NEMURO model. Note that the P flow and the oxygen flow are two newly added flows**
422 **to the original NEMURO model.**

Deleted: phosphorus

423 2.3 Model set-ups

424 The coupled model was applied to the GoM using Arakawa C-grid with a horizontal resolution of ~5 km (Fig. 2a). There are
425 334 and 357 interior rho points in the east-west and north-south directions, respectively. The model includes 36 sigma layers
426 vertically. The wetting and drying scheme (Warner et al., 2013) was implemented for a more accurate representation of shallow
427 water. The computational time step (i.e., baroclinic time step) was set to 240 seconds while the number of barotropic time
428 steps between each baroclinic time step was set to 30. Model hindcast was carried out from 1 August 2006 to 26 August 2020
429 with the first 5 months as a spin-up period. Model results were output on a daily interval at UTC 00: 00.

Deleted: Figure

430

431 The physical model set-ups largely followed an earlier Gulf-COAWST application (Zang et al., 2018, 2019, 2020). Open
432 boundaries were set at the south and east forced by daily water level, horizontal components of 3-D current velocity, horizontal
433 components of depth-integrated current velocity, 3-D water salinity, and 3-D water temperature derived from the Hybrid
434 Coordinate Ocean Model (HYCOM) global analysis products (Bleck and Boudra, 1981; Bleck, 2002) with data assimilated
435 via the Navy Coupled Ocean Data Assimilation system (Cummings, 2005; Cummings and Smedstad, 2013; Fox et al., 2002;
436 Helber et al., 2013). For lateral boundary conditions, we utilized Chapman implicit for free surface and water level (Chapman,
437 1985), Flather for depth-integrated momentum (Flather, 1976), gradient for mixing total kinetic energy, and mixed radiation-
438 nudging conditions for 3-D momentum, temperature, and salinity (Marchesiello et al., 2001). The nudging time steps for the
439 mixed radiation-nudging condition were set to 1 day for inflows and 30 days for outflows. The boundary nudging technique
440 was performed at the computational grids along the open boundary. The boundary condition types for passive biological and
441 chemical tracers (i.e., PS, PL, ZS, ZL, ZP, NO₃, NH₄, PON, DON, Si(OH)₄, opal, PO₄, POP, DOP, and Oxyg) were all
442 prescribed as radiation.

Deleted: (Flather, 1976)

443

444 Initial conditions for water level, horizontal components of 3-D current velocity, horizontal components of depth-integrated
445 current velocity, 3-D water salinity, and 3-D water temperature were provided by the same HYCOM products as well. Initial
446 conditions for concentrations of NO₃, PO₄, and Si(OH)₄ were interpolated from measurements provided by the World Ocean
447 Database (WOD, Boyer et al., 2018). Initial conditions for DO concentration were given by World Ocean Atlas (WOA, Garcia
448 et al., 2018). At the sediment layer, PON_{sed} , PON_{burial} , $opal_{sed}$, and $opal_{burial}$ were initialized as 0.1 mmol m^{-3} . Other biological
449 and chemical tracers were initialized as 0.1 mmol m^{-3} due to the lack of observations.

Deleted: biochemical

450

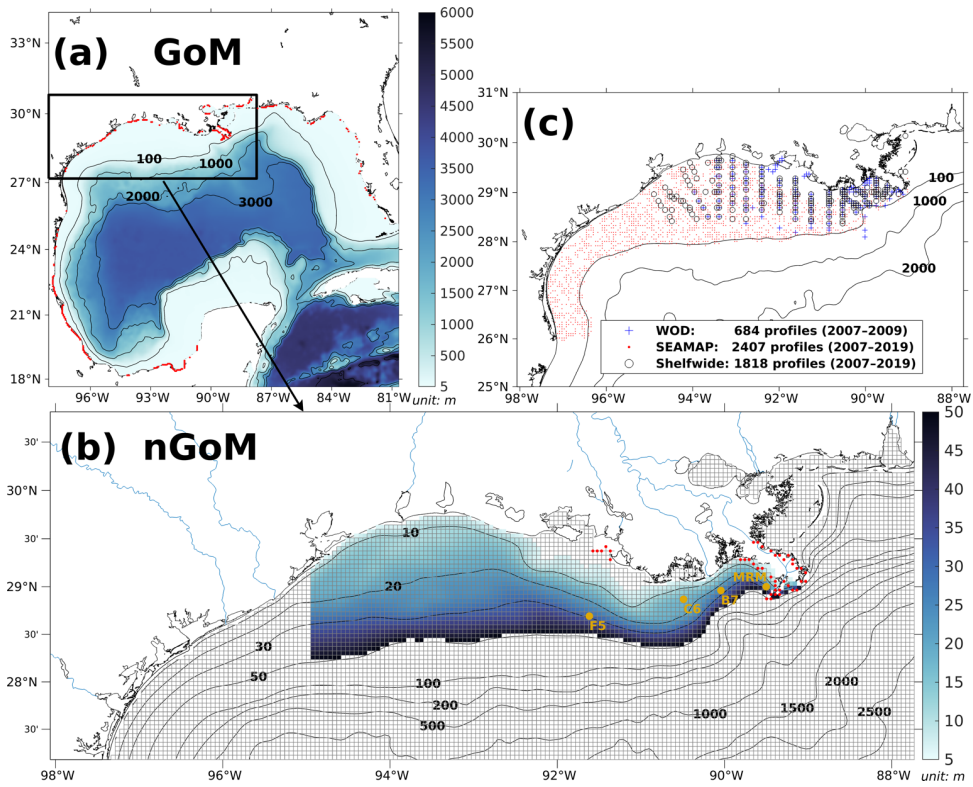
451 Atmospheric forcings, including surface wind velocity at 10 m height above sea level, net longwave radiation flux, net
452 shortwave radiation flux, precipitation rate, air temperature 2 m above sea level, sea surface air pressure, and relative humidity
453 2 m above sea level, were derived from the National Centers for Environmental Prediction (NCEP) Climate Forecast System
454 Reanalysis (CFSR) 6-hourly products (for years prior to 2011, Saha et al., 2010) and NCEP CFS Version 2 (CFSv2) 6-hourly

Deleted: Other biochemical

460 products (for years starting from 2011, Saha et al., 2011) with a horizontal resolution of ~35 km and ~22 km, respectively. In
461 our model, 63 rivers were considered as horizontal point source forcings along the coastal GoM. They were split into 280
462 points (red dots in Fig. 2a) sources transporting time-varying salinity (nearly zero), temperature, 3-D horizontal momentum
463 (based on the magnitude of river discharges), nutrients (NO_3 , NH_4 , PO_4 , $\text{Si}(\text{OH})_4$, PON, DON, POP, and DOP; Fig. C1), and
464 DO to the computational domain. Locations of river point sources of the Mississippi and the Atchafalaya Rivers were shown
465 as red dots in Fig. 2b. For reconstructions of time series of river forcing terms, we composed measurements from various
466 sources, including U.S. Geological Survey (USGS) National Water Information System (NWIS), National Oceanic and
467 Atmospheric Administration (NOAA) Tides and Currents System (TCS), NOAA National Estuarine Research Reserve System
468 (NERRS), and Mexico National Water Commission (CONAGUA, for rivers in Mexico's territory). Daily averaged river
469 discharges were given based on measurements by USGS NWIS and CONAGUA. The magnitude of river discharges was
470 multiplied by 1.4 to account for adjacent watershed areas and the lateral inflow of tributaries (Warner et al., 2005). River
471 temperature and salinity time series were reconstructed from measurements by USGS NWIS, NOAA TCS, and NOAA
472 NERRS. River nutrient concentrations were provided monthly by USGS NWIS and NOAA NERRS and were extended to
473 daily time series with values in the corresponding months. Riverine DO concentration was set to be a constant (258 mmol m^{-3})
474 assuming that riverine DO was saturated at 25°C under 1 atm. Besides, tidal forcings were introduced in the hydrodynamic
475 model taking into account of influences of tidal elevations and tidal currents. There were 13 tidal constituents considered in
476 the model including M2, S2, N2, K2, K1, O1, P1, Q1, MF, MM, M4, MS4, and MN4.

477

Deleted: Figure



479
 480 **Figure 2.** (a) Bathymetry of the entire domain of the Gulf–COAWST, (b) zoom-in bathymetry plot of the northern Gulf of Mexico
 481 (nGoM), and (c) locations of observed inorganic nutrient and DO profiles derived from WOD, SEAMAP, and NOAA’s shelf-wide
 482 cruises. In (a), locations of river point sources are denoted by red dots. In (b), only bathymetry between 6 and 50 m was mapped
 483 with colors; computational meshes were split by solid grey lines; main river channels are denoted by solid blue curves; locations of
 484 river point sources of the Mississippi and the Atchafalaya [Rivers](#) are indicated by red dots; sampling locations for SOC and
 485 overlaying water respiration measurements by McCarthy et al. (2013) are denoted by dark yellow dots.

Deleted: rivers

486 3 Biogeochemical model validations

487 3.1 Available measurements

488 In this section, biogeochemical model validations were conducted for inorganic nutrient concentration profiles (i.e., NO_3 , PO_4 ,
 489 and Si(OH)_4), ratios of diatom and total phytoplankton, SOC, DO concentration profiles, spatial distributions of bottom DO

Deleted: ratios of SOC and overlaying water respiration,

492 concentration, and temporal variability of the hypoxic area against multiple [field and lab data sets](#). Validation of the
493 hydrodynamic model can be found in Zang et al. (2019).

494

495 Inorganic nutrient concentration profiles from WOD were used for model validation. WOD measurements cover the period
496 from 11 January 2007 to 5 July 2009 including 478 NO₃ profiles, 409 PO₄ profiles, and 217 Si(OH)₄ profiles. The diatom
497 percentage of total phytoplankton was derived from measurements by Chakraborty and Lohrenz (2015) and Schaeffer et al.

498 (2012). The SOC measurements were from an incubation study (McCarthy et al., 2013). Available DO concentration profiles
499 were obtained from the NOAA-supported mid-summer shelf-wide cruises and Summer Groundfish Survey in GoM supported

500 by Southeast Area Monitoring and Assessment Program (SEAMAP) conducted annually by the Gulf States Marine Fisheries
501 Commission. The shelf-wide cruises provided 1818 measured profiles with 85140 available records from 2007 to 2019. There

502 were at least 83 DO profiles for each summer (June–August, except 2016) from the shelf-wide cruise observations. The
503 selected SEAMAP DO dataset covers a time range from 2007 to 2019 with measurements including 2407 profiles with 77415

504 sampled records. Locations of the selected profiles from different archives were shown in [Fig. 2c](#). Summer measurements by
505 the shelf-wide cruises were used [to validate](#) spatial patterns of bottom DO concentration and time series of summer hypoxic

506 areas. Estimated hypoxic areas by the cruises are available from 2007 to 2020 with a range from 5,480 km² to 22,720 km².

507 3.2 Nutrients concentration profiles

508 Modeled results showed good agreements with WOD [nutrient profiles \(Fig. 3a, 3c, and 3e, averaged every 2 m from the surface](#)
509 [to 50 m depth\) in terms of vertical distribution and magnitudes. The surface waters were rich in NO₃ \(Fig. 3a\) but oligotrophic](#)

510 [in PO₄ \(Fig. 3c\) and Si\(OH\)₄ \(Fig. 3e\), indicating possibly high diatom productivity \(Table 1\) and possible P or Si limitation](#)
511 [in the photic zone. Previous numerical studies did not provide comparisons for nutrient profiles in the shallow LaTex shelf](#)

512 [region but focused more on the validation for surface nutrient concentration. Although surface nutrients are important for](#)
513 [plankton blooms, the nutrient concentration at other water layers is also critical in affecting the shelf production dynamics.](#)

514 [The simulated profiles were linearly interpolated to the observed depth for point-to-point comparisons. Biases were](#)
515 [summarized and shown against the distance to the Mississippi River mouth \(Fig. 3b, 3d, and 3f\). An overall overestimation of](#)

516 [NO₃ was found, especially around the mouths of the Mississippi River \(distances < 70 km\), where most of the biases were](#)
517 [between ± 50 mmol m⁻³. Biases around the Atchafalaya River mouth \(distances between 250 to 260 km\) were detected](#)

518 [negatively with a wider range than that around the Mississippi River mouth. In other locations, most NO₃ biases are within ±](#)
519 [25 mmol m⁻³. There is no pronounced overestimation or underestimation detected for the PO₄ biases, which are mostly within](#)

520 [± 1 mmol m⁻³, except for waters around the Mississippi River mouth. The PO₄ biases ranged from -3 to -2 mmol m⁻³ for profiles](#)
521 [close to the mouth \(distances < 16 km\). Slight underestimation was found in the Si\(OH\)₄ concentration biases, especially for](#)

522 [profiles around the Atchafalaya River mouth \(distances = 211 km\). Most of the Si\(OH\)₄ biases ranged from -20 to 5 mmol m⁻³](#)
523 [and were smaller than the magnitude of the NO₃ biases. Mean NO₃ concentrations from the Mississippi and Atchafalaya](#)

524 [Rivers were 99 ± 34 mmol m⁻³ \(mean ± 1sd\) and 66 ± 29 mmol m⁻³, respectively. Mean riverine PO₄ concentrations were 2.7](#)

Deleted: data sets derived from cruise measurements and literature. Model simulated profiles were linearly interpolated to depths of the observed profiles for a quantitative comparison

Deleted: and overlaying water respiration

Deleted: WOD,

Deleted: ,

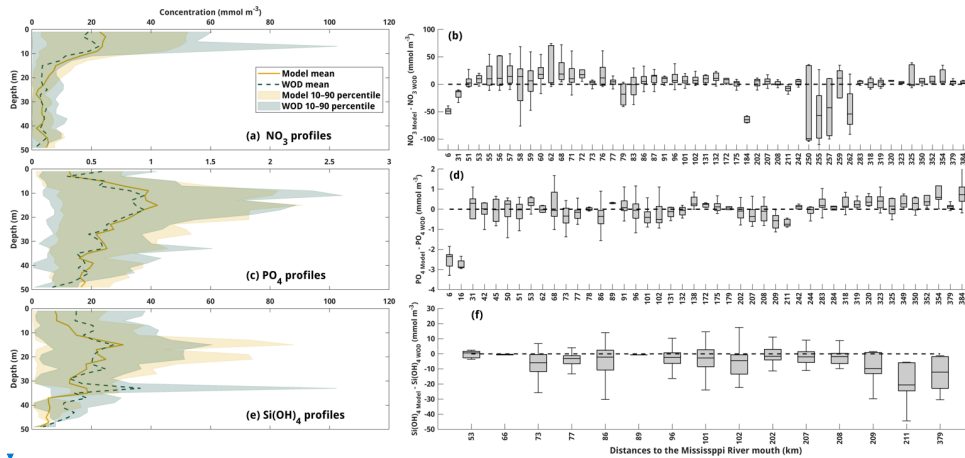
Deleted: There were 445 DO profiles (11 January 2007 to 5 July 2009) from WOD.

Deleted: Figure

Deleted: for the validation of

Deleted: nutrient profiles (Fig. 3a, 3d, and 3g, averaged every 2 m from the surface to 50 m depth) in terms of vertical patterns and magnitudes. The surface waters were rich in NO₃ (Fig. 3a) but oligotrophic in PO₄ (Fig. 3d) and Si(OH)₄ (Fig. 3g), indicating a possibly high diatom productivity (Baronas et al., 2016) and possible phosphorous or silicon limitation in the photic zone. NO₃ concentrations decreased drastically at a depth between 10 and 15 m and were maintained at a low level from 15 to 50 m. A bi-peak structure was found in both PO₄ and Si(OH)₄ concentration profiles. The first peak (also the higher ones) of PO₄ concentration occurred at around 10–20 m depth while the second peak was at around 35 m depth as illustrated by the averaged values and corresponding 10–90 percentiles. In contrast, the high peak of Si(OH)₄ concentration occurred at around 35 m depth while the low peak at the depth of around 15 m, which is consistent with biogenic silica remineralization at lower water columns (Baronas et al., 2016). The simulated profiles were linearly interpolated to the observed depth for point-to-point comparisons. The probability histograms of concentration differences illustrated that our model generally overestimated NO₃ (Fig. 3b) and PO₄ (Fig. 3e) but underestimated Si(OH)₄ (Fig. 3h). About 60% of total NO₃ differences fell within a range from -10 to 10 mmol m⁻³ with 43 % in the positive interval (i.e., from 0 to 10 mmol m⁻³). The corresponding statistics of PO₄ comparisons within a range of ±0.4 mmol m⁻³ were 53 % (-0.4–0.4 mmol m⁻³), 31 % (0–0.4 mmol m⁻³), and 22 % (-0.4–0 mmol m⁻³), respectively. Approximately 13 % of observed Si(OH)₄ were overestimated within 10 mmol m⁻³ and ~51 % were underestimated within 10 mmol m⁻³. At surface layers (0–5 m), similar probability patterns in nutrient biases were found but with slightly different statistics (Fig. 3c, 3f, and 3i). For example, about 34 % of NO₃ concentrations were overestimated within 10 mmol m⁻³ compared to 10 % of surface measurements underestimated within 10 mmol m⁻³. Mean NO₃ concentrations from the Mississippi and the Atchafalaya Rivers were 99 ± 34 mmol m⁻³ (mean ± 1sd) and 66 ± 29 mmol m⁻³, respectively. Mean riverine PO₄ concentrations were 2.7 ± 0.7 mmol m⁻³ and 2.3 ± 0.7 mmol m⁻³, respectively, and mean riverine Si(OH)₄ concentrations were 118 ± 23 mmol m⁻³ and 116 ± 21 mmol m⁻³, respectively. The nutrient concentrations bias between simulations and observations is acceptable concerning the strong influences of high riverine nutrient loads on the shelf

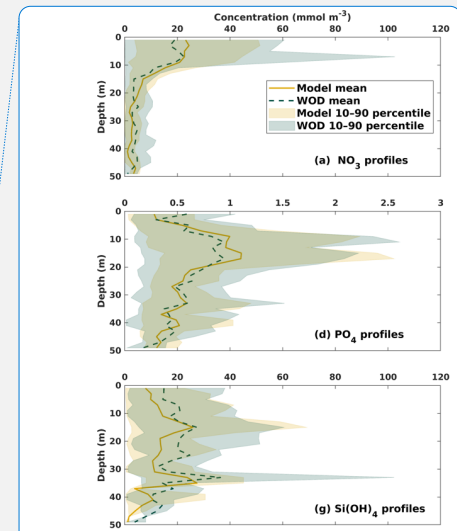
575 $\pm 0.7 \text{ mmol m}^{-3}$ and $2.3 \pm 0.7 \text{ mmol m}^{-3}$, respectively, and mean riverine Si(OH)_4 concentrations were $118 \pm 23 \text{ mmol m}^{-3}$ and
 576 $116 \pm 21 \text{ mmol m}^{-3}$, respectively. The nutrient concentrations bias between simulations and observations is acceptable,
 577 considering the possible transient influence from the riverine nutrient loads during a survey.



578
 579 **Figure 3. Profile comparisons between model hindcasts and WOD measurements for concentrations of (a)–(b) NO_3 , (c)–(d) PO_4 , and**
 580 **(e)–(f) Si(OH)_4 . Box charts on the right-hand side show the minimums, maximums, first quartiles, third quartiles, and medians of**
 581 **the concentration differences between the hindcast and measured profiles.**

582 3.3 Diatom ratios

583 Both measured and model-simulated Si(OH)_4 profiles suggested strong diatom productivity in the photic zone (Fig. 3e). Cruise
 584 observations confirmed that the LaTex phytoplankton community is dominated by the diatom group (Schaeffer et al., 2012;
 585 Chakraborty and Lohrenz, 2015). Regional averages (Fig. C2 in Appendix C), vertical averages (only the surface, middle, and
 586 bottom layers were chosen), and monthly averages were applied to the concentration ratio of diatom and total phytoplankton
 587 according to the sampled locations, sampled layers, and sampled months, respectively, of the cruise studies by Schaeffer et al.
 588 (2012) and Chakraborty and Lohrenz (2015). The modeled ratios well reproduced the measured ones in terms of magnitudes,
 589 monthly variability, and cross-shelf variability (Table 1). During the cruise periods in 2008, the range of modeled diatom
 590 percentage (79% to 99%) matched well with the measurements (79% to 88%) except for June 2008, when underestimations
 591 were found. In 2009, our model results agreed well with the measurements in inner shelf waters but overestimated the
 592 measurements in the mid-shelf regions, especially in the summer and fall of 2009. The measured percentages exhibited salient
 593 monthly variations with higher values in winter and spring and low ones in summer and fall. In the cross-shelf direction, the
 594 phytoplankton community shifted from a highly diatom-dominated one in the inner shelf waters to a less diatom-dominated
 595 one in the mid-shelf waters, especially in summer. Such patterns were well captured by our model.



- Deleted:
- Deleted: c
- Deleted:)–(f
- Deleted: g)–(i
- Deleted: Note that
- Deleted: thick vertical lines in (b), (c), (e), (f), (h),
- Deleted: (i) denote
- Deleted: difference of 0 separating
- Deleted: positive
- Deleted: negative intervals
- Deleted:
- Deleted: 3g

608

609 **Table 1. Comparison of simulated (mean \pm 1SD) and measured (mean \pm 1SD in parentheses) diatom percentage of the total**
 610 **phytoplankton. Note that the statistics for the simulated percentages were conducted based on concentration values and averaged**
 611 **over the cruise months and over given regions that cover the cruise sampling locations (Fig. C2). The measured percentages by**
 612 **Schaeffer et al. (2012) (for measurements in 2008) were calculated based on biovolume values, while those by Chakraborty and**
 613 **Lohrenz (2015) (for measurements in 2009) were given by chlorophyll *a* attributed to different phytoplankton groups.**

	Diatom/total phytoplankton \times 100%	
	Inner shelf	Midshelf
February 2008	99 \pm 4 (88 \pm 16)	
April 2008	99 \pm 2 (71 \pm 16)	
May 2008	79 \pm 39 (79 \pm 22)	
June 2008	29 \pm 42(85 \pm 10)	
January 2009	60 \pm 29 (66 \pm 21)	57 \pm 14 (47 \pm 14)
April 2009	50 \pm 33 (59 \pm 14)	51 \pm 19 (33 \pm 29)
July 2009	41 \pm 33 (40 \pm 13)	33 \pm 24 (13 \pm 16)
October–November 2009	50 \pm 33 (46 \pm 14)	38 \pm 19(19 \pm 17)
March 2010	49 \pm 35 (50 \pm 14)	52 \pm 26 (64 \pm 12)

614

615 3.4 SOC rates

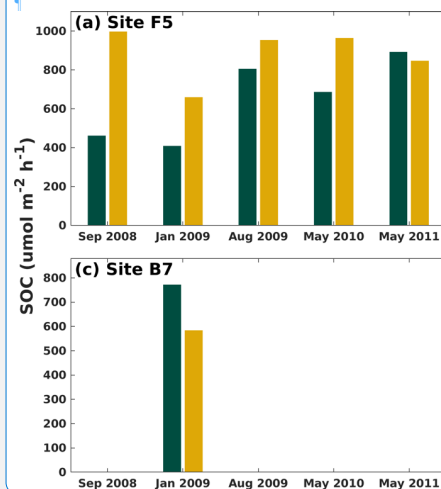
616 [Modeled SOC rates were compared against the laboratory incubation by McCarthy et al. \(2013\) at five shelf sites \(location see](#)
 617 [the Fig. 1 in that paper\) using sediment and water samples collected during six cruises \(i.e., July 2008, September 2008, January](#)
 618 [2009, August 2009, May 2010, and May 2011\). The modeled SOC was averaged over the cruise months for four shelf sites](#)
 619 [\(i.e., F5, C6, B7, and MRM; Fig. 2b\). Our model could well capture the SOC magnitude. The model generally overestimated](#)
 620 [the SOC at sites F5 and C6 except for January 2009 and May 2010 at site C6 and underestimated SOC at sites B7 and MRM](#)
 621 [\(except for August 2009\) \(Fig. 4\). The largest overestimations were found on September 2008 when measurements were](#)
 622 [carried out shortly after Hurricanes Gustav and Ike. These measurements tended to provide a low SOC but a high water column](#)
 623 [respiration, possibly induced by the mixing incurred by storms. Note that the model results shown in Fig. 4 were averaged](#)
 624 [over an entire month because no exact cruise date information was reported by McCarthy et al. \(2013\).](#)

625

626

Deleted: and overlaying water respiration

Deleted: provided incubation measurements of the SOC rates and overlaying water respiration at five shelf water sites (Fig. 1 in McCarthy et al., 2013) using sediment and water samples collected during six cruises (i.e., July 2008, September 2008, January 2009, August 2009, May 2010, and May 2011). Modeled SOC rate and SOC/overlaying water respiration ratio were then compared against the measurements. The modeled overlaying water respiration rate was approximated by the rate calculated at the bottom water column considering biochemical processes that occurred at that layer, i.e., phytoplankton respiration rates, zooplankton metabolism rates, aerobic decomposition rates of PON and DON, and nitrification rate. The modeled SOC and ratio of SOC/overlaying water respiration were averaged over the cruise months for four shelf sites (i.e., F5, C6, B7, and MRM; Fig. 2b). Our model could well capture the SOC magnitude and variability. Both measured and modeled ratios of SOC/overlaying water respiration were found greater than 1, highlighting the importance of SOC in bottom DO dynamics (Fig. 5). The model generally overestimated the SOC at sites F5 and C6 except for January 2009 and May 2010 at site C6, and underestimated SOC at sites B7 and MRM (Fig. 4). The modeled ratio agreed with the measurements except for site MRM in August 2009. Such a bias might result from the prescription of river inputs along the model boundary for diverting momentum and concentration tracers from the river point sources to the computational grid cells. The scheme could lead to an overshoot of fresh water at the near-mouth grid cells and a short residence time for organic matter in the water column and an underestimation of the overlaying water respiration rate. As the model results were averaged over an entire month but not over the exact cruise date due to the lack of cruise information in McCarthy et al. (2013), we considered model-simulated SOC and ratio of SOC/overlaying water respiration acceptable.



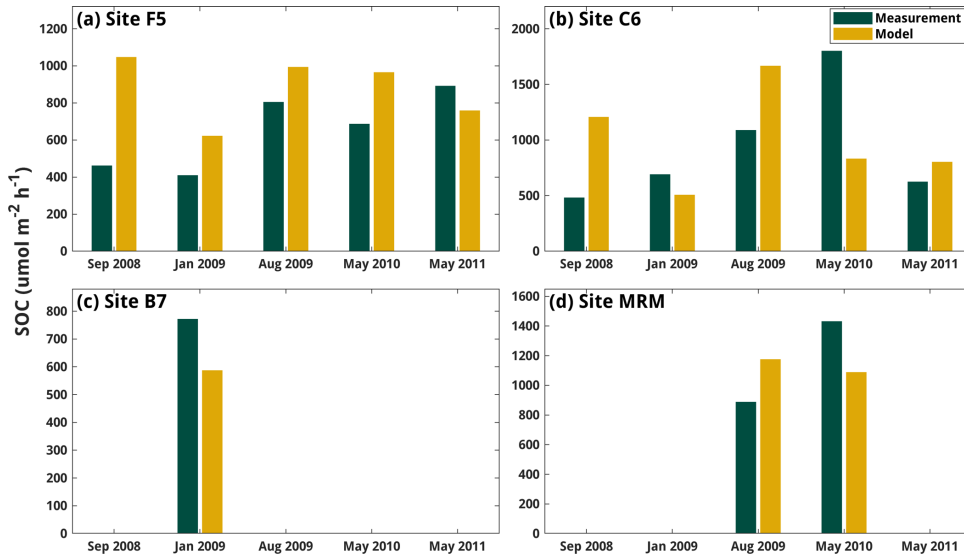
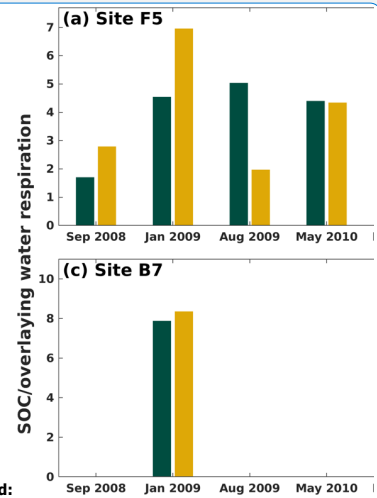


Figure 4. Comparison of modeled and measured SOC (unit: $\mu\text{mol m}^{-2} \text{h}^{-1}$) at four LaTex shelf sites (Fig. 2b). Note that the measurements are provided by McCarthy et al.'s (2013) incubation study.

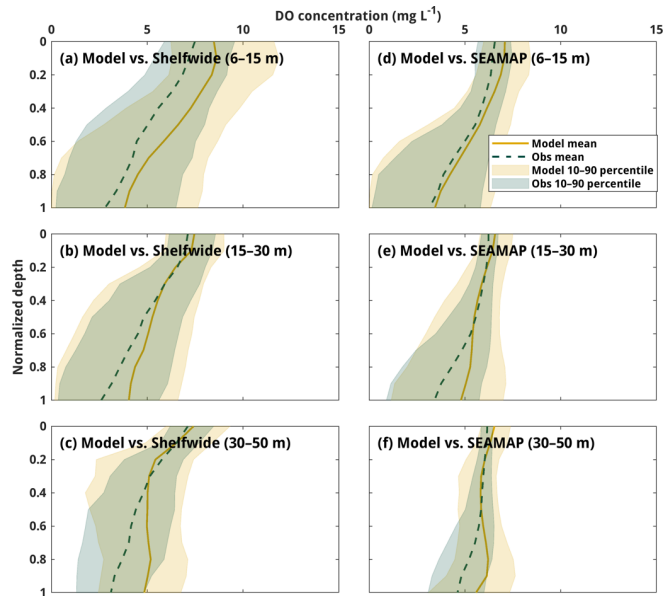
3.5 DO profiles

Both simulated and observed DO profiles were averaged for different depth ranges (Fig. 5) and compared against normalized depths ranging from 0 (surface) to 1 (bottom). The observed DO vertical structures were well captured by the model, with the 10–90 percentiles of modeled DO overlapping the measured ones well. We noticed the model tended to overestimate the observed DO by $\sim 1 \text{ mg L}^{-1}$ on average, especially in lower water columns for profiles with greater depths, which can be ascribed to the model's relatively coarse vertical resolution in deeper waters. The vertical coordinate transformations and vertical stretching functions applied to the model provided a finer resolution around the surface and relatively coarse ones around the bottom (1 to 2 m for each layer), while the shelf-wide and SEAMAP measurements were almost equally distributed along the vertical direction. We noted our model was less biased against the SEAMAP than the shelf-wide data as the latter sometimes has several measurements within one meter. In shallow waters (6–15 m), DO was somewhat more overestimated around the surface than in layers below (Fig. 5a and 5d). ROMS tends to overmix the water column in shallow water regardless of the vertical mixing parameterizations chosen (Robertson and Hartlipp, 2017). Despite the slight overestimations of DO profiles, our model results provided similar and even better performances than previous numerical studies. For example, DO concentration biases against profile measurements in Yu et al. (2015) were within 2 mg L^{-1} .



Deleted: Figure 5. Comparison of modeled and measured (McCarthy et al., 2013) ratios of SOC/overlying water respiration at four LaTex shelf sites.

Deleted: Both simulated and observed DO profiles were averaged every 2 m from the surface to 50 m depth (Fig. 6a, 6c, and 6e). The observed DO vertical structures, such as the "zigzag" shape in the WOD profiles and "C" shape in the shelf-wide and SEAMAP profiles, were well captured by the model. The 10–90 percentile of modeled DO overlap the measured ones. Probability histograms of relative bias between the model and measurements reveal that the model overestimated the measured DO (Fig. 6b, 6d, and 6f). There were 45% (27%) of the WOD DO samples were overestimated (underestimated) by 50%. When compared to the shelf-wide cruise measurements, the probability histogram of the relative bias showed a bell-shaped distribution with a peak around zero. 28%, 44%, and 66% of observations were misestimated by $\pm 10\%$, $\pm 20\%$, and $\pm 50\%$, respectively (Fig. 6d). Our model seemed to agree well with SEAMAP data. There were 36% (20%), 50% (26%), and 61% (31%) of records being overestimated (underestimated) by 10%, 20%, and 50%, respectively (Fig. 6f).



718
719 **Figure 5.** Comparisons of DO profiles between model hindcasts and measurements by (a-c) NOAA's shelf-wide cruises and (d-f)
720 SEAMAP. The normalized depths of 0 and 1 represent the surface and bottom, respectively.

722 3.6 Spatial distributions of bottom DO and temporal variability of hypoxic area

723 As the annual NOAA shelf-wide cruises were conducted from the east shelf to the west in the summer, the model simulated
724 bottom DO was resampled following the cruise periods. For example, if the westmost location of the cruise is 90°W on day 1,
725 the simulated bottom DO concentration over the east of 90°W on that day is extracted. On the following day, if the westmost
726 location of the cruise is 91°W, the simulation between 91°W and 90°W on day 2 is extracted, and so forth. All the extracted
727 frames were blended to reconstruct the spatial distribution of simulated bottom DO concentration during the summer cruise
728 period. Simulated results outside the LaTex shelf and over the deep (> 50 m) and shallow (< 6 m) water regions were excluded
729 since observations were unavailable. Model results showed a good agreement with the observations in terms of interannual
730 variability and spatial extent of bottom hypoxic waters (Fig. 6). The spatial distribution of the hypoxic regions varied over
731 different summers. For example, the hypoxic area was small and was primarily restricted to nearshore (<20 m) regions during
732 the summers of 2007, 2009, 2010, 2012, 2014, and 2018. The size of the hypoxic zone was more prominent and extended
733 offshore in 2008, 2011, 2013, and 2019. The spatial dispersion of hypoxic waters occurred mostly over the west of the LaTex

Deleted: 6

Deleted: b) WOD, (

Deleted: -d

Deleted: ,

Deleted: e

Formatted: English (UK)

Formatted: English (UK)

Formatted: English (UK)

Formatted: English (UK)

Formatted: English (UK)

Formatted: English (UK)

Deleted: Probability histograms of relative percentage differences between modeled and observed DO are in the right column. The thick vertical lines in the histograms denote the percentage difference of 0.

Formatted: Normal

Deleted: extract

Deleted: over these regions. Numerical

Deleted: 7

Deleted: in

747 shelf, where bathymetry gradients were gentle. Over the eastern shelf, the hypoxic water was mostly constrained within a
748 narrow belt. In the meantime, the western and eastern hypoxic [waters were](#) not always merged but were separated at around
749 91 °W (e.g., 2007, 2010, 2012, 2014, 2017, and 2018). These results suggested that the hypoxia development on the LaTex
750 shelf was complex and generally followed the bathymetry and distances from the major river mouths.

751

752 The daily time series of the size of the hypoxic zone was calculated over the LaTex shelf (6–50 m; Fig. [7](#)). There was a good
753 agreement between simulated hypoxia zone size and that captured by the shelf-wide cruises in terms of variability and
754 magnitude. The overall R^2 was found as 0.47 and varied yearly (Table 2). The 5-year running R^2 increased from 0.02 for the
755 first 5-year period (2007–2010) to 0.91 for the last 5-year period (2015–2020, excluding 2016). The [lower \$R^2\$](#) before 2010
756 could be attributed to the coarse resolution of the atmospheric forcings (~ 35 km, CFSR). Since 2011, CFSRv2 provided
757 forcings with a higher resolution of 22 km. [Underestimations](#) were found in 2007, 2010, 2012, and 2014 with a root-mean-
758 squared error (RMSE) of 9988 km², while minor underestimations were simulated in 2008, 2017, 2018, and 2020 (RMSE=4862
759 km²). The model tended to slightly overestimate the measurements in other summers of interest (i.e., 2009, 2011, 2013, 2015,
760 and 2019; RMSE=2132 km²). Nevertheless, those biases were acceptable considering the relative sporadic converges of cruise
761 data.

Deleted: water was

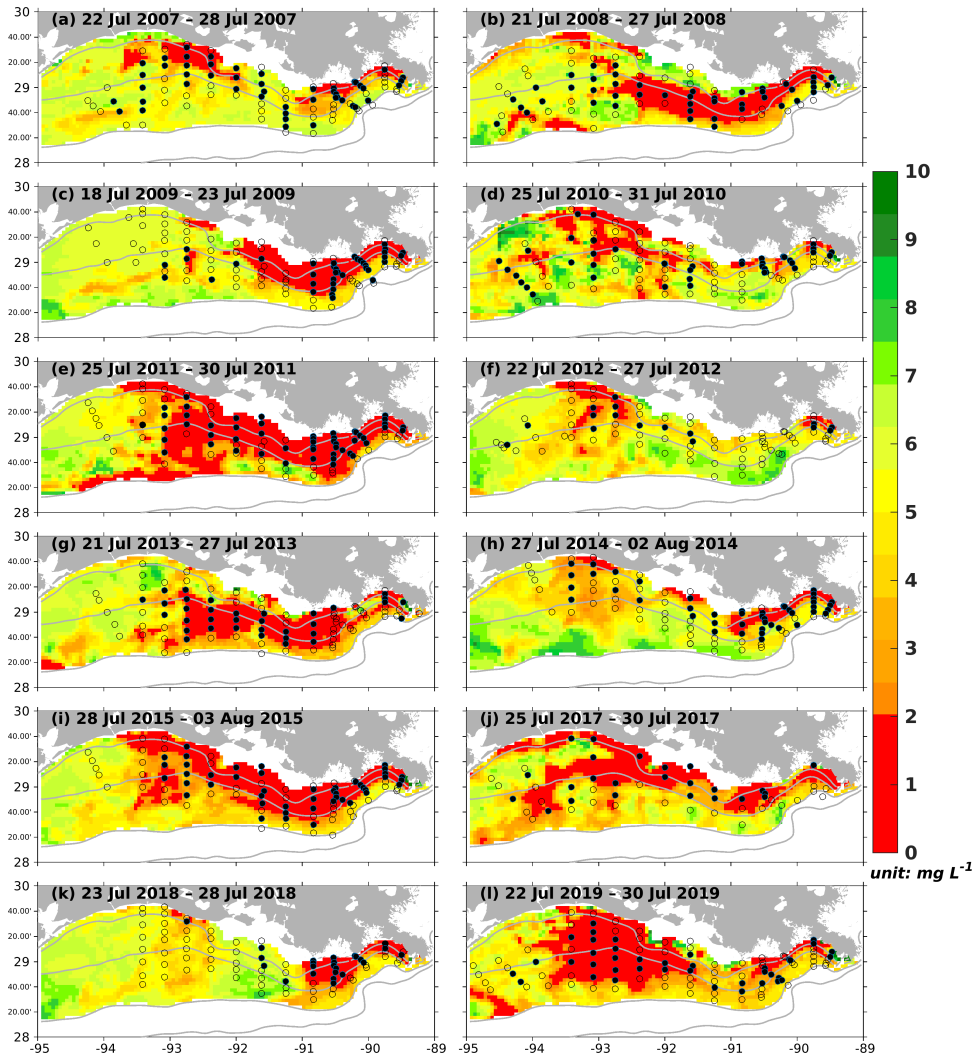
Deleted: 8

Deleted: poor performance

Deleted:) provided by

Deleted: .

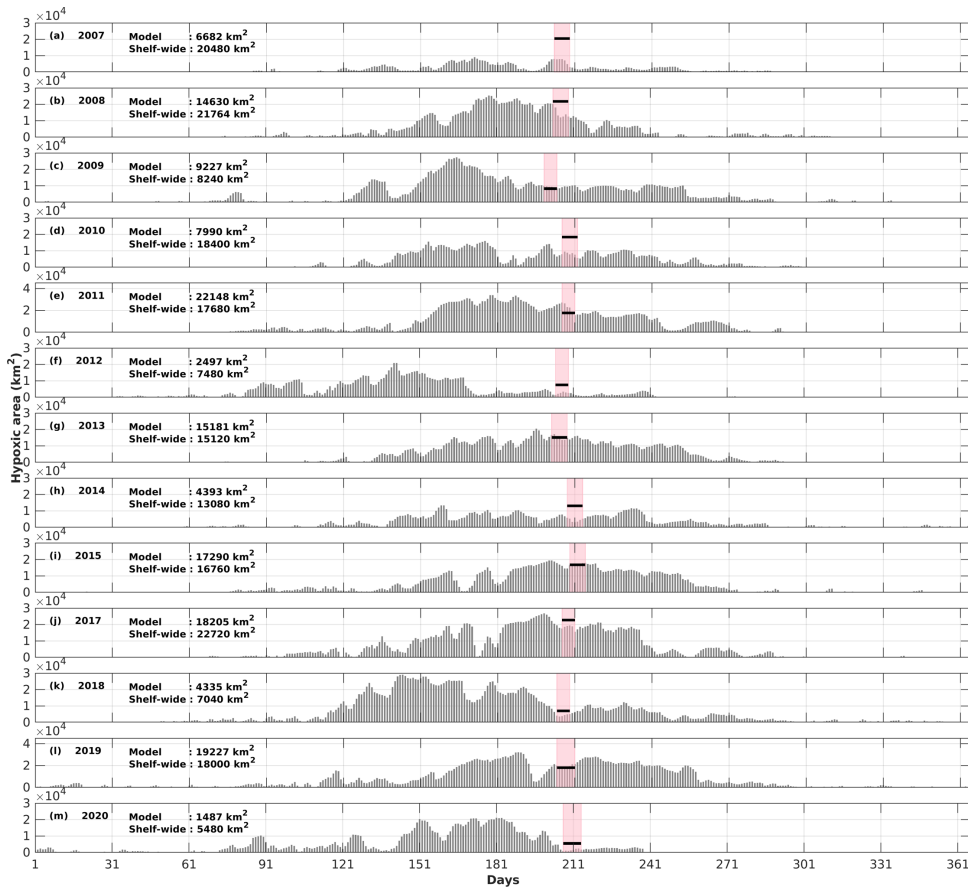
Deleted: Notable underestimations



768

769 Figure 6. Modeled summer bottom DO concentration (colored patches) and NOAA's summer shelf-wide hypoxia observations (black
 770 dots and open circles). The black dots and the open circles are indicators of observed bottom hypoxia and normoxia, respectively.
 771 The solid grey lines indicate bathymetry of 10, 20, 50, and 100 m, respectively.

Deleted: 7



773

774 **Figure 7.** Comparison of the hypoxic area (in km²) between model simulations and shelf-wide cruise observations from 2007 to 2020
 775 (except 2016). The pink patches denote the cruises periods while the solid black lines represent the measured hypoxic area.

Deleted: 8

776

777

778

779

781 **Table 2. The overall (2007–2020) and 5-year running R^2 of summer hypoxic area between model simulations and shelf-wide**
 782 **measurements. Note that the comparison in the year 2016 was excluded due to the lack of measurement.**

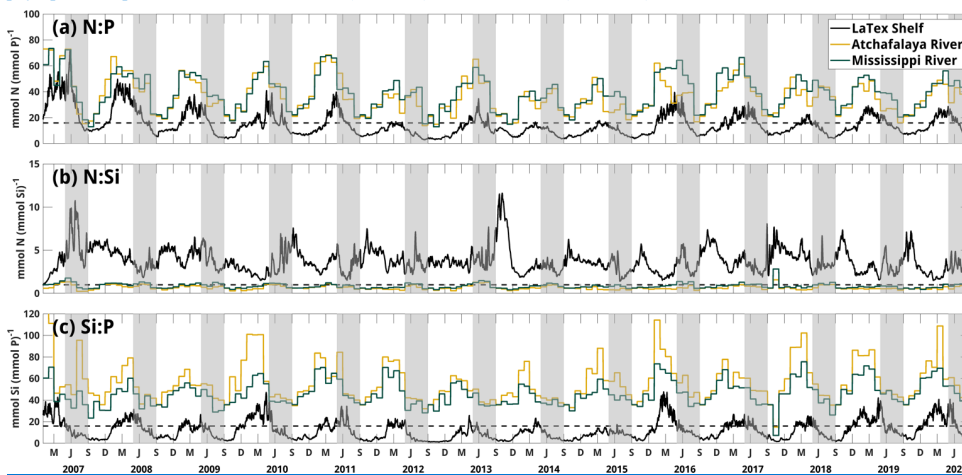
Year ranges	R^2	Year ranges	R^2
2007–2020 (overall)	0.47	2011–2015	0.82
2007–2011	0.02	2012–2017	0.75
2008–2012	0.39	2013–2018	0.71
2009–2013	0.41	2014–2019	0.73
2010–2014	0.44	2015–2020	0.91

783

784 4 Results

785 4.1 Nutrient limitation

786 [Riverine nutrient loads from the Mississippi and Atchafalaya Rivers were calculated based on measurements from the USGS](#)
 787 [NWIS. During the investigated period \(2007–2020\), the riverine N:P ratio was higher than 16:1 during spring and reached its](#)
 788 [minimum in summer. Riverine N:Si ratio fluctuated around 1:1 and was slightly higher in late spring and summer than in other](#)
 789 [seasons \(Fig. 8\). The rivers transported excessive inorganic N and Si to the shelf but much less P when compared to the](#)
 790 [Redfield ratio of N:P:Si=16:1:16. Ratios of integrated nutrient concentration in the shelf \(Fig. 8\) suggested that P was usually](#)
 791 [limited in spring when compared to N and Si. In most summers, Si limitation might be more important in regulating](#)
 792 [phytoplankton production than N limitation \(N:Si>1:1\) and P limitation \(Si:P<16:1\).](#)



793

Formatted: Superscript

Formatted: Superscript

Formatted Table

Deleted: and discussion

Deleted: 4.1 Factors controlling subregion bottom DO variability

Fennel et al. (2016)(Fennel et al., 2016) divided the inner shelf (<50 m water depth) into six subregions (Fig. 9a) largely following the bathymetry and distances from the major river mouths: from east to west, two west-Mississippi regions (6–20 m nearshore and 20–50 m offshore regions, similar hereinafter), two mid-Atchafalaya regions, and two west-Atchafalaya regions. Focusing on the bottom DO concentration balance, we calculated five hydrodynamic-related terms (i.e., the local rate of changes in bottom DO, horizontal advection of bottom DO, horizontal diffusion of bottom DO, vertical advection of bottom DO, and vertical diffusion of bottom DO) and two biochemical-related terms (i.e., biochemical-induced changes in DO at the bottom water column, and SOC). The biochemistry at the bottom water column includes processes of phytoplankton photosynthesis, phytoplankton respiration, zooplankton metabolism, aerobic decomposition of PON and DON, and nitrification. The summation of these seven terms contributes directly to the total changes in bottom DO concentration. The contribution of a given term was estimated by the percentage of the corresponding absolute value over the summation of all the absolute terms. We then averaged the absolute percentages over the entire LaTex shelf (water depth 6–50 m) and over the six subregions, respectively.

Monthly climatology illustrated that the variability of bottom DO on the LaTex shelf was mostly controlled by four processes: horizontal advection, vertical advection, vertical diffusion, and SOC (Fig. 9b). The sum of the percentages of contributions from these four terms (absolute values) was more than 80%. The contributions of the two advection terms exhibited a salient seasonal pattern with the maximum in spring and winter and the minimum in summer. The contribution of SOC showed an opposite pattern and reached its peak (34%) in summer. It was interesting to note that no salient seasonal pattern was found in the percentage of contribution from the vertical diffusion term, which maintained around 20% over a year. The vertical diffusion of DO was determined by both vertical DO gradient and vertical stratification. The robust contribution of vertical diffusion highlighted the importance of stratification on bottom DO variability throughout the year. The importance of DO advection and SOC on bottom DO balance was also documented by Ruiz Xomchuk et al. (2021), where, however, vertical diffusion was proposed as a minor contributor. Such a disagreement could result from the water layers investigated. Vertical diffusion of DO across the layer 10 m above the bottom was discussed in Ruiz Xomchuk et al. (2021), while here we estimated vertical diffusion of DO across the bottom layer.

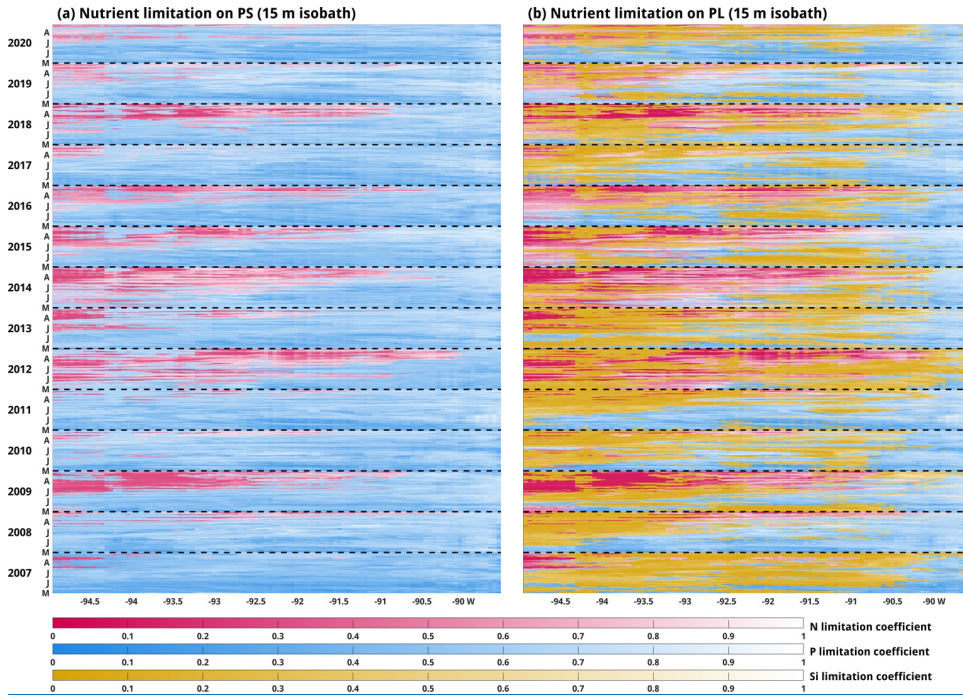
The contributions of the four terms on the bottom DO varied in different subregions. In the nearshore regions (6–20 m; Fig. 9c, 9e, and 9g), SOC played a much more important role than the other three terms in modulating the summer bottom DO concentration. The maximum contribution from SOC was 33%–51% while the contributions of two advection terms were only ~10% or even lower. In contrast, over the offshore regions (20–50 m; Fig. 9d, 9f, and 9h), the contribution of SOC decreased notably to 19%–27% in summer and was comparable to the other three hydrodynamic-related terms (18%–26% for the horizontal advection, 17%–25% for the ve... [4]

918 Figure 8. Daily time series of ratios of nutrient loads from the Mississippi and Atchafalava Rivers and nutrient ratios averaged over
919 the LaTex shelf (Fig. 2b) from the numerical results. Note that the latter ratios are derived based on the depth-integrated nutrient
920 concentrations. The black dashed lines denote the nutrient ratios of 16:1, 1:1, and 16:1 in (a), (b), and (c), respectively. The gray
921 patches indicate the late spring and summer (May–August) period of each year. The capitalized letters M, J, S, and D in the x-axis
922 denote the first day of March, June, September, and December, respectively.

923 Nutrient limitation could vary among different phytoplankton species with different efficiencies in nutrient uptakes. In our
924 model, the Si limitation was modeled only for the PL growth. Depth-averaged nutrient limitation coefficients (see Eqs. A9–
925 A10) along multiple isobaths exhibited salient spatial and temporal patterns for both PS and PL (Fig. 9 and C3–C6). For
926 example, along the 15 m isobath (Fig. 9), in the mid and west shelf, the PS growth was usually limited by N in mid- and late
927 summer but by P in other late spring and early summer. In the east shelf, P limitation on PS growth was usually dominated
928 from May to August (Fig. 9a). Types of limited nutrients for PL exhibited a distinguishable west-east pattern along the 15 m
929 isobath: the growth of PL was usually limited by P in the east and by Si in the middle. The limited nutrients shifted between
930 N and Si on the shallow mid and west shelf in different summers. In contrast, P limitation on PS growth and Si limitation on
931 PL growth was likely to be more common in the open shelf (Fig. C3–C6). N limitation was negligible along the 30 m isobath
932 and beyond, where the growth of PS was mostly limited by P and the growth of PL by Si in the west and by P in the east,
933 respectively.

934
935 N limitation was commonly simulated in the shallow (< 20 m) middle and west shelf for the two phytoplankton groups, while
936 in other parts, primary production was more likely to be limited by P or Si. Bioassays studies by Turner and Rabalais (2013)
937 suggested that phytoplankton biomass was mostly limited by N or by a co-limitation of N and P in high salinity (> 20) waters.
938 In the shallow mid and west part of the shelf, where salinity was usually greater than 20 during summer, model results
939 suggested an N-limited environment, which agreed with the bioassays studies. However, in other parts, regardless of salinity
940 ranges, the system was more limited by P and Si. Previous bioassays studies usually neglected Si effects on production (e.g.,
941 Turner and Rabalais, 2013; Zhao and Quigg, 2014). Quigg et al. (2011) pointed out that P limitation was detected particularly
942 at sites directly adjacent to the Mississippi River plume, while Si limitation was found in four out of eight bioassays where
943 production was limited by nutrients. These measurements supported our model results regarding the importance of P and Si
944 limitation on the shelf primary production.

945



946

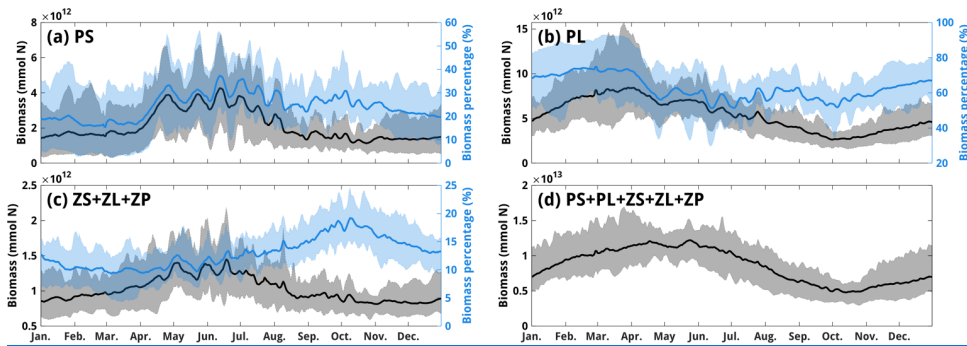
947 [Figure 9. Evolution of depth-averaged nutrient limitation coefficients for \(a\) PS and \(PL\) along the 15 m isobath during late spring](#)
 948 [and summer. The notations of M, J, J, and A in the v-axis represent the first day of May, June, July, and August, respectively. Note](#)
 949 [that a lower \(deeper colored\) coefficient represents stronger limitations on phytoplankton growth. The dashed black lines indicate](#)
 950 [the time record on May 1 of each year.](#)

951 [4.2 Plankton community dynamics](#)

952 [As suggested by previous observations \(Schaeffer et al., 2012; Chakraborty and Lohrenz; 2015\), the LaTex shelf phytoplankton](#)
 953 [community is largely supported by the diatom group, which is consistent with our model simulation. Integrated over entire](#)
 954 [water columns and the LaTex shelf, the modeled total productions \(primary + secondary productions, in mmol N\) were](#)
 955 [supported mostly by PL, which contributed ~70 % in early spring and ~50 % in summer \(Fig. 10b\). Contributions from PS](#)
 956 [biomass supported ~20 – ~35 % of total biomass from spring to summer \(Fig. 10a\) when the secondary production \(ZS+ZL+ZP\)](#)
 957 [only contributed ~10 % \(Fig. 10c\). In the meantime, the seasonality of different biomass subsets exhibited different patterns.](#)
 958 [The PS biomass reached its first peak in late April and then varied till July. The PL biomass climbed to its higher peak in early](#)
 959 [April, decreased, and rebounded slightly to its lower peak in mid-May. During summer, the PS biomass \(\$3-4 \times 10^{12}\$ mmol N\)](#)

960 was at a similar magnitude to the PL biomass ($5\text{--}6 \times 10^{12}$ mmol N). After summer, both PS and PL biomass decreased gradually
 961 to troughs in October. The seasonality of total production, therefore, exhibited a bi-peak (in late spring and early summer)
 962 pattern with the two peaks at a similar magnitude. Such a bi-peak pattern could also be found in both satellite-derived
 963 chlorophyll *a* concentration and model simulations with a similar plankton community as this study (see comparisons of
 964 modeled and satellite chlorophyll *a* concentration in Gomez et al., 2018) but was hardly captured by models using only one
 965 plankton group (e.g., Fennel et al., 2011).

966
 967 Competition of PS and PL on nutrients may provide a clue to the bi-peak production. Nutrient loads from the Mississippi and
 968 Atchafalaya Rivers usually maximize in late spring and early summer, after which the loads decrease gradually and reach the
 969 minimum in October (Fig. C1). With greater (Table B4) half-saturation coefficients on nutrients, the PL group outcompetes
 970 the PS group in a high-nutritious environment in April but would not exhibit such superiority in growth in summer when
 971 nutrient supplies decrease. Top-down effects were also detected from the time series of PS and secondary production (Fig. 10a
 972 and 10c). The PS biomass experienced a surge during April and reached its first peak around the end of April, while the
 973 secondary production did not see a salient increase until mid-April and climbed to the highest at the beginning of May. Both
 974 time series then exhibited a pronounced fluctuation after reaching their first peak and declined steadily after August. During
 975 this high-production period, the two time series were out-of-phase with the PS led by about 6 days. There was no
 976 distinguishable phase lag between the seasonality of PL and the secondary production.



978 **Figure 10.** Climatologically daily mean of (a) PS, (b) PL, (c) ZS+ZL+ZP, and (d) total production. The corresponding percentages
 979 for different biomass subsets are related to the total production and are shown as blue solid lines. The color patches indicate the
 981 range of 10–90 percentiles. Note that the biomass matrices were integrated over the entire water column and the LaTeX shelf before
 982 temporal averages.

984 We further examined the variance of the daily time series of simulated total productions (4987 records from January 2007 to
 985 August 2020). As the total production was formulated as the sum of productions by PS, PL, ZS, ZL, and ZP, the variance can
 986 be expanded mathematically, as shown in Table 3. The PL explained 63 % of the total variance, while PS explained only 20
 987 %. The daily variability of the shelf production was, therefore, mostly controlled by that of the PL. As Si and P limitations
 988 were commonly found for the growth of phytoplankton (Fig. 9 and C3–C6), more pronounced changes in total production and
 989 the resulting DO concentration would be expected when only adjusting riverine Si or P loads rather than N loads. In the
 990 meantime, the responses in different types of plankton biomass may be different to the changing nutrient loads due to the
 991 competition between PS and PL (bottom-up effects) and also grazing of zooplankton on phytoplankton (top-down effects).

992

993 **Table 3. The expansion of variance (unit: $\times 10^{22}$ mmol N²) of total production. Note that the sum of the listed variances and**
 994 **covariances is equal to the variances of the total production mathematically. Statistics are derived from the daily time series of**
 995 **plankton biomass (in mmol N) integrated over the entire water column and the LaTex shelf (color-shaded area in Fig. 2b).**
 996 **Percentages in the brackets represent variance contributions.**

<u>var(PS)</u>	<u>var(PL)</u>	<u>var(ZS)</u>	<u>var(ZL)</u>	<u>var(ZP)</u>
<u>216 (20.32 %)</u>	<u>669 (62.97 %)</u>	<u>3.14 (0.30 %)</u>	<u>4.24 (0.40 %)</u>	<u>0.21 (0.02 %)</u>
<u>2cov(PS,PL)</u>	<u>2cov(PS,ZS)</u>	<u>2cov(PS,ZL)</u>	<u>2cov(PS,ZP)</u>	<u>2cov(PL,ZS)</u>
<u>41.6 (3.92 %)</u>	<u>18.6 (1.75 %)</u>	<u>32.2 (3.03 %)</u>	<u>8.86 (0.83 %)</u>	<u>-18.2 (1.71 %)</u>
<u>2cov(PL,ZL)</u>	<u>2cov(PL,ZP)</u>	<u>2cov(ZS,ZL)</u>	<u>2cov(ZS,ZP)</u>	<u>2cov(ZL,ZP)</u>
<u>36.6 (3.45 %)</u>	<u>12.1 (1.14 %)</u>	<u>-0.03 (0.01 %)</u>	<u>0.26 (0.02 %)</u>	<u>1.35 (0.13 %)</u>
<u>sum</u>				
<u>1030</u>				

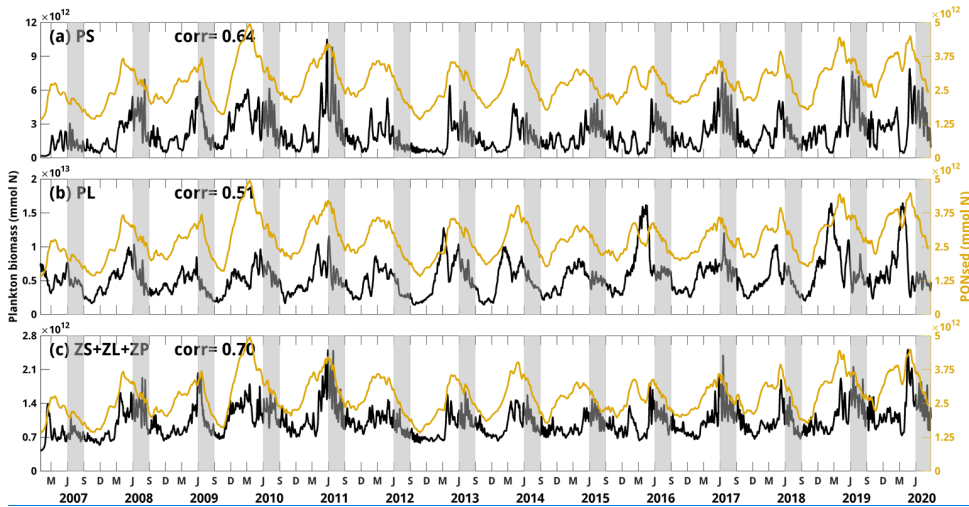
997 **4.3 Plankton contribution to PON_{sed} pool**

998 In the model, the PON_{sed} pool is supported by sinking organic matters (represented by PON), which are contributed directly
 999 from plankton detritus due to phytoplankton and zooplankton mortality and zooplankton egestion. Although PL biomass
 1000 dominated total production, the daily variability of PON_{sed} was more correlated to the PS and secondary production, with
 1001 correlation coefficients of 0.64 ($p < 0.001$) and 0.70 ($p < 0.001$), respectively, than to the PL, with a coefficient of 0.51 ($p < 0.001$)
 1002 (Fig. 11). Multiple linear regression (MLR) models were built to study the linear relationships between PON_{sed} (as the response
 1003 variable) and biomass of different types of plankton groups (i.e., PS, PL, and secondary production as explanatory variables).
 1004 All variables were normalized within a range from 0 to 1 before model construction. The highest R² was found when PON_{sed}
 1005 lagged the explanatory variables by 6 days (Table 4). Regression coefficients were found to be significantly positive between
 1006 plankton biomass and PON_{sed}. The contribution of secondary production (coefficient = 0.5388) to PON_{sed} variability was much

007 higher than the contribution from PS (0.4796) or PL (0.4758). Moreover, changes in PS and PL (both normalized) would lead
008 to similar changes in PON_{sed} even though the PL dominated the shelf total production.

009
010 The results indicate the effects of plankton community structure on PON_{sed} accumulation on the seafloor. A linear function of
011 mortality was applied to PS, PL, ZS, and ZL, while a quadratic mortality function was used for ZP. The modeled mortality
012 rates of PS, PL, ZS, and ZL are thus proportional to the corresponding plankton concentration, the mortality rate at 0 °C, and
013 a temperature-dependent term in which the temperature coefficients were parameterized as 0.0693 °C⁻¹ for all groups. The
014 mortality rate of ZP is similar to the other groups but is proportional to the square of ZP concentration. The mortality rates of
015 PS and PL at 0 °C (Mor_{PS0}=0.002 m³ mmol N⁻¹ day⁻¹ and Mor_{PL0}=0.001 m³ mmol N⁻¹ day⁻¹, respectively shown in Table B4)
016 were parameterized 11–22 times lower than those for ZS and ZL (Mor_{ZS0}=0.022 m³ mmol N⁻¹ day⁻¹ and Mor_{ZL0}=0.022 m³
017 mmol N⁻¹ day⁻¹) and 60–120 times lower than the parameter for ZP (Mor_{ZP0}=0.12 m³ mmol N⁻¹ day⁻¹). However, concentration
018 (or biomass) ratios between phytoplankton and zooplankton barely reached as high as 10 or more (Fig. 10). Therefore, mortality
019 rates of PS and PL were typically lower than the mortality rates of ZS, ZL, and ZP, given the same ambient water temperature.
020 Through mortality processes, the contribution of zooplankton biomass to water column PON and eventually PON_{sed} was
021 considered greater than that of phytoplankton biomass. In addition, a certain part of zooplankton-induced biomass contributed
022 to the water column PON via egestion processes that were not formulated for the phytoplankton groups. Therefore, the
023 contribution of the secondary production to PON_{sed} exceeded that of the primary production.

024
025 The PS mortality rate was lower than the PL mortality rate as PS concentration was usually less than (non-summer) or nearly
026 (summer) half of the PL concentration. As a result, the variability of PON_{sed} accumulation should be more sensitive to that of
027 PL biomass, which was not supported by the regression model. The top-down effects provide another angle in explaining the
028 regression coefficients. The PS supported the growth of ZS, which was at the bottom trophic level in the zooplankton
029 community. Changes in PS could be reflected in the changes in all types of zooplankton biomass through grazing and predation
030 processes in the zooplankton community (top-down effects as indicated by Fig. 10a and 10c) and further in the changes in
031 PON_{sed}. PL was grazed by ZL and ZP, which were at a higher trophic level than ZS, changes in PL could be mostly reflected
032 in biomass changes in these two groups only. Thus, despite that only half (~51 % on average; figure not shown) of the biomass
033 source in the zooplankton community was supported by PS, a considerable amount of PON_{sed} supported by zooplankton was
034 from PS. This effect offsets the high mortality rate of PL. It may explain the comparable regression coefficients for PS and PL
035 on the PON_{sed} variability.



037
038 **Figure 11. Comparisons between daily PON_{sed} and plankton biomass (i.e., (a) PS, (b) PL, and (c) secondary production). All biomass**
039 **matrices were integrated over the entire water column and the LaTex shelf.**

040
041 **Table 4. A multiple linear regression model with a response variable of PON_{sed} lagging the explanatory variables by 6 days. Note**
042 **that the model was built upon normalized daily time series.**

Linear regression model:

$$PON_{sed}(\text{lag by 6 days}) \sim I + PS + PL + \text{secondary production}$$

Estimated coefficients:

	Estimate	Std. Error	t-statistic	p-value
Intercept	0.0091	0.0036	2.5496	0.01*
PS	0.4796	0.0135	35.5370	<2E-16***
PL	0.4758	0.0084	56.5040	<2E-16***
Secondary production	0.5388	0.0134	40.0680	<2E-16***

Significance codes: 0 (***) 0.001 (**) 0.01 (*)

Number of observations: 4980, Error degrees of freedom: 4976

Root Mean Squared Error: 0.0997

R-squared: 0.74, Adjusted R-Squared: 0.74

F-statistic vs. constant model: 4.62e+03, p-value = 0

4.4 Water column DO

In this study, we focus on the responses of bottom DO to the changing nutrient, biomass, and the associated biogeochemical processes. Thus, it is necessary to compare the contribution of different plankton groups to water DO. Such contributions were quantified by ratios of total DO generated or consumed by a given plankton group over its biomass. In water above the bottom 2 m, both PS and PL tended to produce more DO than they consumed (Table 5). DO contributed by PS (per mmol N) was at least twice greater than that by PL. As PL biomass was usually greater than PS biomass (Fig. 10), such differences resulted from a higher temperature-dependent respiration rate for PL ($K_{ResPL}=0.0693\text{ }^{\circ}\text{C}^{-1}$; Table B4) than for PS ($K_{ResPS}=0.0519\text{ }^{\circ}\text{C}^{-1}$). DO consumptions by ZS and ZL metabolism were found to be three times greater than those by ZP on average. The rates of zooplankton metabolism were formulated proportionally to total biomass flows from lower trophic levels. ZS and ZL consumed more biomass through grazing than ZP, which could be reflected in the percentages of total zooplankton biomass (ZS accounted for 32 % on average, ZL for 39 %, ZP for 29 %, figure not shown). Taking all plankton functional groups as a whole, the net DO contribution by the community (per unit biomass) was found to be mostly positive (positive maximum, median, mean, first quartile, and third quartile; Table 5).

In the water within the bottom 2 m, the DO consumed by the plankton community had a higher chance to exceed the production than in the layers above (Table 5). Firstly, the DO production by the phytoplankton community within the bottom 2 m was found to be nearly half of that found in the layers above, as nutrients and light were more likely to be limited. Secondly, the first quartile of DO contribution by PL was found to be slightly negative within the bottom 2 m, while in the layers above, the corresponding statistic was positive. Finally, the net DO contribution was found to be generally positive (mean and median) but had a higher chance to be negative (minimum and first quartile) than waters above the bottom 2 m. The above statistics help us to understand how DO changes when nutrient supplies are altered. For example, if riverine nutrient supplies are reduced, photosynthesis rates will decrease. As the respiration rate of phytoplankton was formulated as a function of water temperature and phytoplankton concentration only, nutrient changes will not lead to changes in respiration rate per unit biomass. The net DO production by phytoplankton will decrease.

Table 5. Statistics of plankton contribution per unit biomass in producing or consuming DO over water layers above and within the bottom 2 m. Statistics are calculated based on depth-integrated daily matrices without spatial average or spatial integration. Note that negative signs shown denote DO consumption.

	Contributions at layers above the bottom 2 m (unit: $\times 10^{-5}\text{ mmol O}_2\text{ s}^{-1}\text{ mmol N}^{-1}$)						
	min	max	median	mean	first quartile	third quartile	Std.
PS	-1.19	27.64	7.45	7.02	3.40	10.42	4.09

PL	-2.10	58.83	2.22	3.03	1.31	3.62	3.40
ZS	0	-23.18	-6.77	-7.25	-3.76	-10.66	4.37
ZL	0	-19.78	-6.42	-6.63	-4.95	-8.10	2.72
ZP	-0.22	-9.60	-2.21	-2.60	-1.64	-3.08	1.42
Entire community	-13.76	35.40	0.99	1.25	0.24	1.94	1.84
Contributions at layers within the bottom 2 m (unit: $\times 10^{-5} \text{ mmol } O_2 \text{ s}^{-1} \text{ mmol } N^{-1}$)							
	min	max	median	mean	first quartile	third quartile	Std.
PS	-1.29	23.69	3.51	3.89	0.21	6.17	4.09
PL	-2.28	46.99	1.38	2.48	-0.40	3.74	4.29
ZS	0	-18.53	-4.17	-4.90	-1.66	-7.11	3.92
ZL	0	-19.00	-5.83	-5.72	-4.50	-7.19	2.50
ZP	0	-9.48	-1.89	-2.01	-1.45	-2.36	1.10
Entire community	-39.77	35.93	0.35	0.33	-1.74	1.75	3.71

5 Discussion

5.1 Si limitation on PL growth

Previous studies suggested that there is potential Si limitation in the LaTex shelf (Quigg et al., 2011; Nelson and Dortch, 1996; Lohrenz et al., 1999) due to the increase in riverine N:Si loads (from 1:3 to 1:1) since the 1950s (Turner et al., 1998). Over the studied period, the ratio of N:Si loads from the Mississippi and Atchafalaya Rivers was slightly greater than 1:1 during late spring and summer, while N:Si over the shelf was usually greater than 2:1 (Fig. 8b). Nelson and Dortch (1996) pointed out that within the plume, > 99 % of silicate supported by rivers was removed by biological uptake during spring and 80–95 % during summer. Cruise observations indicated strong Si limitation over the Mississippi River plume (east of 92°W) during spring and little or no Si limitation during summer (Nelson and Dortch, 1996; Lohrenz et al., 1999). Results of limitation coefficients indicated that Si was more limited than N for the growth of PL during spring and summer (Fig. 9 and C3–C6). It should be noted that the Si limitation was only related to the growth of PL in our model, while the Si limitation found in cruise studies was related to the growth of plankton assemblages. During summer, the biomass of PS and PL reached a similar magnitude showing a shift in phytoplankton composition. As the growth of PS was mostly limited by P during summer, especially over the deep or east shelf, P limitation should be considered equally important as Si limitation on the growth of total phytoplankton. Our model results also suggested that a potential co-limitation of nutrients may be more crucial to shelf productivity than the limitation of a single nutrient type. Indeed, bioassays studies illustrated that co-limitation of N+P or N+P+Si occurred and might have a greater impact on the production than single-nutrient limitation (Zhao and Quigg, 2014; Quigg et al., 2011; Turner and Rabalais, 2013).

A critical factor associated with nutrient limitation is the half-saturation coefficient of phytoplankton nutrient uptake. Uptake kinetic studies for different marine diatom species suggested a wide range of half-saturation coefficients of silicate (K_{SiOH_4} from 0.85 to 17.4 mmol Si m⁻³; Table 6). The average, median, first quartile, and third quartile of the listed measured coefficients in Table 6 were found to be 5.9, 4.5, 2.3, and 7.0 mmol Si m⁻³, respectively. In our model, the half-saturation coefficient of silicate uptake by PL was then set as 6.0 mmol Si m⁻³. We applied the average rather than the median of the published coefficients to our model since the PL group should be considered as a marine diatom assemblage. However, the K_{SiOH_4} for a diatom assemblage may shift given changing ambient silicate concentration. For example, as pointed out by Nelson and Dortch (1996), K_{SiOH_4} for the sampled phytoplankton assemblage (dominated by diatom species) remained low from 0.48 to 1.71 mmol Si m⁻³ when the ambient silicate concentration was low between 0.13 to 0.41 mmol Si m⁻³, but increased to 5.29 mmol Si m⁻³ as ambient silicate concentration was 4.72 mmol Si m⁻³. Further investigations and improvements in model parameterization for the dependency of K_{SiOH_4} on silicate concentration are therefore needed.

Table 6. Half-saturation coefficient (unit: mmol Si m⁻³) for silicate uptake by different diatom species according to multiple uptake kinetic studies.

Diatom species	K_{SiOH_4}	Reference
<i>Cylindrotheca fusiformis</i>	0.85	Del Amo and Brzezinski (1999)
<i>Nitzschia alba</i>	6.8	Azam (1974)
<i>Nitzschia alba</i>	4.5	Azam et al. (1974)
<i>Phaeodactylum tricornutum</i>	4.0, 9.2, 6.3	Del Amo and Brzezinski (1999)
<i>Thalassiosira nordenskiöldii</i>	2.8	Kristiansen and Hoell, (2002)
<i>Thalassiosira pseudonana</i>	7.04	Thamatrakoln and Hildebrand (2008)
<i>Thalassiosira pseudonana</i>	1.4	Del Amo and Brzezinski (1999)
<i>Thalassiosira pseudonana</i>	0.8, 2.3	Nelson et al. (1976)
<i>Thalassiosira weissflogii</i>	15.2, 17.4	Milligan et al. (2004)
<i>Thalassiosira weissflogii</i>	4.5	Del Amo and Brzezinski (1999)
Average	5.9	
Diatom functional group (PL)	6.0	This study

5.2 Riverine nutrient reductions

Since 2001, the Mississippi River/Gulf of Mexico Hypoxia Task Force has set up a goal of controlling the size of the mid-summer hypoxic zone below 5000 km² in a 5-year running average (Mississippi River/Gulf of Mexico Watershed Nutrient Task Force, 2001; 2008) by reducing riverine nutrient loads. Fennel and Laurent (2018) suggested that a reduction of 63 ±

1109 18% (referred to as the 2000–2016 average) in total **N** loads or a dual reduction of $48 \pm 21\%$ in total **N** and **P** loads could be
 1110 necessary to fulfill the hypoxia reduction goal. Statistic models (Scavia et al., 2013; Obenour et al., 2015; Turner et al., 2012;
 1111 Laurent and Fennel, 2019) suggested a nutrient reduction of 52%–58% related to the 1980–1996 average **should** be enough to
 1112 fulfill the goal. Nonetheless, inorganic nutrient types considered in these **statistical** models were **either N-based** (i.e., ammonia
 1113 and nitrite+nitrate) **or a combination of N** and **P-based nutrients**. The **plankton** community embedded in existing models was
 1114 simplified with one phytoplankton functional group and one zooplankton functional group (e.g., Fennel et al., 2006, 2011,
 1115 2013; Fennel and Laurent, 2018; Justić and Wang, 2014). **Here**, we aimed to explore the sensitivity of bottom DO to the riverine
 1116 nutrient discharge with different **nutrient (N, P, and Si) reduction** combinations, the corresponding changes in plankton
 1117 **community**, and **implications** for hypoxia reduction. **A total of six sensitivity experiments (Table 7) were set up with different**
 1118 **combinations of nutrient reductions**. The riverine nutrient concentration was the only variable adjusted among these sensitivity
 1119 **tests**. To remove numerical bias introduced by initial conditions, all sensitivity experiments were initialized on 1 January 2012
 1120 **based on the output of the long-term simulations and were conducted from 1 January 2012 to 26 August 2020**. Thus, any
 1121 **changes in bottom DO due to nutrient reductions should result from changes in biogeochemical processes, including changes**
 1122 **in SOC, changes in DO at the water within the bottom 2 m, and changes in DO at layers above the bottom 2 m**.

1124 **Table 7. Riverine inorganic nutrient reduction percentages for different sensitivity experiments. Note that all the runs listed were**
 1125 **initialized on 1 January 2012 and were conducted from 1 January 2012 to 26 August 2020.**

Experiment	Riverine inorganic nutrients reduction percentages (%)		
	N	P	Si
control	0	0	0
N60	60	0	0
P60	0	60	0
Si60	0	0	60
NP60	60	60	0
NSi60	60	0	60
NPSi60	60	60	60

1127 5.2.1 Responses of PON_{sed} and SOC

1128 The total biomass of PON_{sed} was likely to decrease in all nutrient reduction scenarios except for experiments Si60 and NSi60
 1129 (Fig. 12a). Responses in SOC (Fig. 12b) followed strictly with those in PON_{sed}, as SOC was formulated as a function of PON_{sed}
 1130 and water temperature and the latter remained unchanged among the six experiments. We found different responses in PON_{sed}
 1131 (or SOC) in different nutrient reduction strategies. The changes in depth-integrated plankton biomass over the entire column
 1132 can help to explain such differences (Fig. C7). As discussed above, the variability of PON_{sed} was mainly from that of secondary
 1133 production (Fig. 11 and Table 4). In most of the sensitivity tests (N60, P60, NP60, and NPSi60), the secondary production

Deleted: nitrogen... loads or a dual reduction of $48 \pm 21\%$ in total nitrogen... and phosphorus... loads could be necessary to fulfill the hypoxia reduction goal. Statistic models (Scavia et al., 2013; Obenour et al., 2015; Turner et al., 2012; Laurent and Fennel, 2019) suggested a nutrient reduction of 52%–58% related to the 1980–1996 average would...ould be enough to fulfill the goal. Nonetheless, inorganic nutrient types considered in these statistic...tatistical models were nitrogen...ither N-based (i.e., ammonia and nitrite+nitrate) or a combination of N and phosphorus...-based (i.e., phosphate) ...utrients. The lower trophic...lankton community embedded in existing models was simplified with one phytoplankton functional group and one zooplankton functional group (e.g., Fennel et al., 2006, 2011, 2013; Fennel and Laurent, 2018; Justić and Wang, 2014). When applied to the LaTeX shelf where diatom dominates the phytoplankton ... [5]

Formatted: Font color: Auto
Deleted: biomass, the complexity of the lower trophic ... [6]

Deleted: 3... Riverine inorganic nutrient reduction ... [7]

Formatted: Left

Formatted Table

Formatted: Left

Deleted: EXPcontrol

Formatted ... [8]

Formatted: Left

Deleted: EXPN20

Deleted: 20

Formatted: Left

Deleted: EXPN40

Deleted: 40

Deleted: 0

Formatted: Left

Deleted: EXPN60

Deleted: 60

Deleted: 0

Formatted: Left

Deleted: EXPN80 ... [9]

Deleted: 0

Formatted Table

Deleted: EXPP80 ... [10]

Deleted: 0

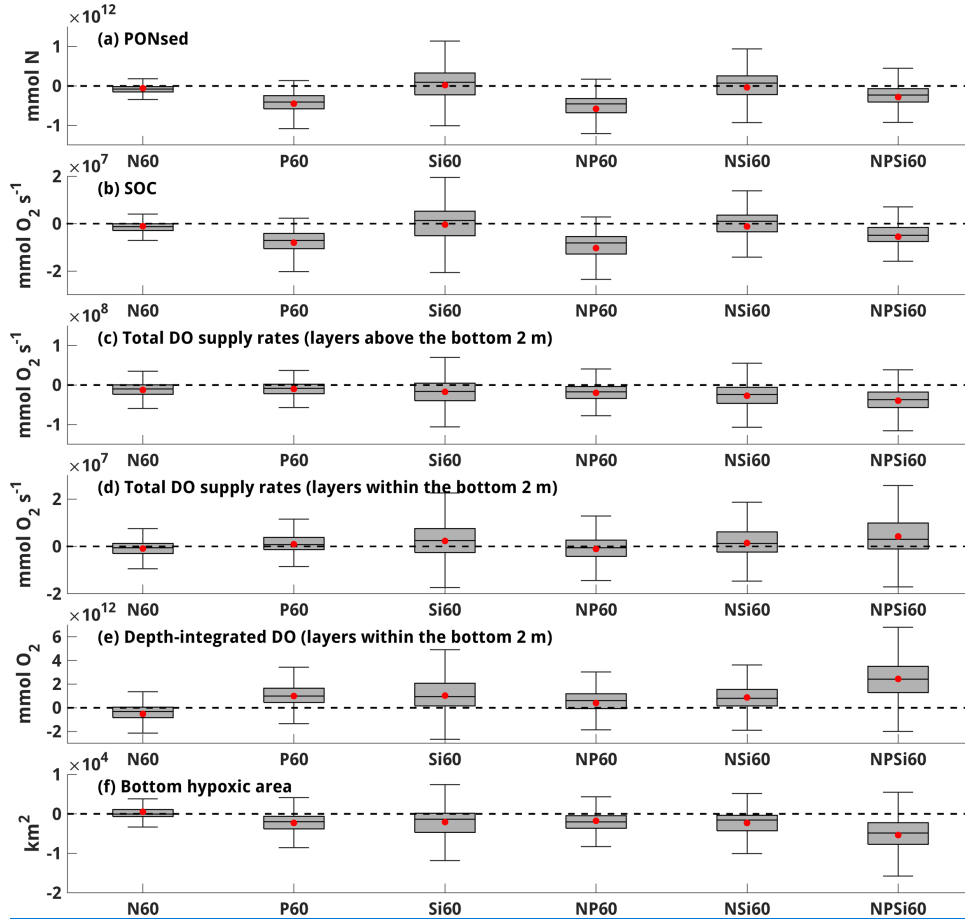
Formatted Table

Deleted: EXPSi80 ... [11]

Formatted Table

Deleted: EXPNPSi80 ... [12]

224 experienced a salient decrease (Fig. C7b) due to fewer food supply (Fig. C7c). PON_{sed} or SOC, therefore, decreased in these
225 scenarios. However, in scenarios Si60 and NSi60, secondary production did not exhibit pronounced changes (near-zero mean
226 and median; Fig C7b) but either increased or decreased in nearly half of the simulation. Such a high uncertainty could lead to
227 either an increase or a decrease in PON_{sed} biomass (Fig. 12a). On average, a slightly positive change in PON_{sed} biomass was
228 simulated, which should be a result of an enlarging ZS group (Fig. C7d) and can be explained by bottom-up and top-down
229 effects. As the growth of PL was commonly limited by Si on the shelf (Fig. 9 and C3–C6), PL biomass would generally
230 decrease (Fig. C7g) as Si loads were reduced. It would further lead to biomass decreases in ZL (Fig. C7f) and ZP (Fig. C7h),
231 both of which grazed on PL (bottom-up effects). ZS biomass would likely increase (top-down; Fig. C7d) as the predation
232 pressure from ZL and ZP was weakened. Such responses in scenarios Si60 and NSi60 can also be found for the biomass
233 integrated over the layers above the bottom 2 m (Fig. C8).



236 **Figure 12.** Responses of (a) PON_{sed} , (b) SOC, (c) total DO supply rates in layers above the bottom 2 m, (d) total DO supply rates at
 237 layers within the bottom 2 m, (e) depth-integrated DO over layers within the bottom 2 m, and (f) bottom hypoxic area. Note that
 238 total DO supply rates in (c–d) are the results of photosynthesis rates minus total water column respiration rates. Statistics shown
 239 are mean (red dots), median, first quartile, third quartile, minimum, and maximum derived from the differences between sensitivity
 240 tests and the control run during late spring and summer (May–August). A positive (negative) value indicates an increasing
 241 (decreasing) DO consumption rate by SOC in (b) but represents an increasing (decreasing) DO supply rate by water column
 242 biogeochemical processes in (c–d).

5.2.2 Responses of DO in water columns

Among the six experiments, responses in biomass regarding reduced river nutrient loads are similar at the layers above the bottom 2 m (Fig. C8) and over the entire column (Fig. C7). Changes in total DO supply rates (Fig. 12c) and total production (Fig. C8a) generally exhibited a negative pattern in all nutrient reduction scenarios. Such responses are expected in the upper water column as the plankton community produced more DO than it consumed (Table 5) even though when nutrient supplies were reduced. Decreases in total production would lead to decreases in DO supplies. The most significant decreases in total biomass and DO supplies occurred when N, P, and Si loads were all reduced by 60 % (NPSi60), while minor decreases occurred in experiment N60. Our simulations suggested that the primary production on the shelf was more limited by P and Si rather than by N only. Therefore, the changes in biomass would be less pronounced in N60 than in other scenarios.

Response in total DO supplies to nutrient reductions became more complicated when reaching down near the bottom, where net DO contribution from the community (i.e., (photosynthesis - total respiration)/total biomass) would be more likely to shift between positive and negative than in the upper water column (Table 5). But detailed responses varied from case to case. In scenario N60, most of the time, the plankton community produced more DO than it consumed in water within the bottom 2 m (same as in the control experiment), as decreases in N may not lead to a dramatic decrease in photosynthesis rate. Decreases in total production (Fig. C9a) would result in lower DO production rates (negative mean and median of changes in total DO supply rates for N60 shown in Fig. 12d). However, net DO contributions from plankton community can switch to negative when N limitation was commonly detected (e.g., 2012, 2014, and 2018, Fig. 9). The photosynthesis rates can be significantly restricted below the total respiration rates, indicating that decreases in total production would lead to less DO consumption or increase in net DO supply rates (positive interval in Fig. 12d for N60).

In scenarios P60, Si60, NSi60, and NPSi60, changes in total biomass (negative; Fig. C9a) and total DO supply rates (positive; Fig. 12d) were in opposite phases, suggesting that net DO contribution by the community was usually negative at layers within the bottom 2 m. The shifts in net DO contribution in these cases mainly result from the reductions in limited nutrients (i.e., P and Si). Photosynthesis rates decrease pronouncedly below the total respiration rates, leading to a negative net DO contribution. A great uncertainty in changes in total DO supply rates (wide range of quartiles; Fig. 12d) was found when P load reduction was not incorporated (i.e., Si60 and NSi60). It can be explained by different responses of biomass in the plankton community due to competition, bottom-up effects, and top-down effects. Reductions in Si supplies would lead to less PL (Fig. C9g) but more PS (Fig. C9e) and introduce more uncertainty in primary production (Fig., C9c). Unlike at the layers above, here, near the bottom, increases in ZS (Fig. C9d) might be more related to bottom-up effects rather than top-down effects as ZL and ZP did not exhibit pronounced changes (Fig. C9f and C9h). Such responses in ZL and ZP were a combined effect of increased food supply from PS but less from PL. Thus, high uncertainty in responses in the secondary productions was also found (Fig. C9b). In scenario NP60, within the bottom 2 m, total plankton biomass experienced a salient decrease (Fig. C9a), while changes

1276 in total DO supply rates fluctuated around zero with a slightly negative mean and median (Fig. 12d). It indicated that net DO
1277 contribution by the plankton community shifted between positive and negative in this experiment. Such complex responses in
1278 the biomass and in the plankton community's role in DO contribution highlight the need for a multi-group plankton
1279 parameterization in hypoxia simulation.

1280 5.2.3 Responses in bottom DO and hypoxic area

1281 The responses in bottom DO and hypoxic area to nutrient reductions are a combined effect of changes of DO in sediment and
1282 water column. The most significant decrease in SOC (Fig. 12b) may not necessarily lead to the most significant increase
1283 (decrease) in bottom DO (hypoxic area) (e.g., NP60; Fig. 12e–12f), while the most significant drop in DO supplies in the upper
1284 layers (Fig. 12c) may not cause a pronounced decrease in bottom DO (e.g., NPSi60; Fig. 12e–12f). The most significant
1285 increase in bottom DO was found when supplies of all three types of nutrients were reduced by 60 % (NPSi60), where the
1286 bottom hypoxic area (2012–2000) reached 5275 km². The size of the hypoxic area was also saliently reduced in P60, Si60,
1287 NP60, and NSi60. For NPSi60 and P60, SOC rates dropped saliently (Fig. 12b), corresponding with an increase in total DO
1288 supply rates by water column biogeochemical processes at layers within the bottom 2 m (Fig. 12d). Although DO supplies
1289 from the upper layers decreased in these two scenarios, bottom hypoxia would still be significantly relieved. In scenarios of
1290 Si60, NP60, and NSi60, a more significant uncertainty was found in the responses of bottom DO and hypoxic area (Fig. 12e–
1291 12f), which could be attributed to the different responses of the five plankton groups (Fig. C7 and C9).

1292
1293 Intriguingly, compared to existing models (e.g., Justić et al., 2003, 2007; Laurent and Fennel, 2014; Fennel and Laurent, 2018)
1294 or statistical studies (Scavia et al., 2013; Obenour et al., 2015; Turner et al., 2012; Laurent and Fennel, 2019), our model
1295 simulated a different response of hypoxia development when only N is reduced by 60% (N60 Fig. 12e–12f). Existing studies
1296 generally agree that a 60% reduction in N load will reduce SOC and thus relieve the hypoxic condition. In this study, For N60,
1297 as fewer productions are supported, we found the magnitude of DO reduction (less production) in the water column (both
1298 upper and bottom layers) exceeded that of SOC reduction (less consumption), resulting in a decrease in bottom DO and worsen
1299 the hypoxic condition.

1300 5 Conclusions

1301 We modified a three-dimensional coupled hydrodynamic–biogeochemical model (NEMURO) and adapted it to the Gulf of
1302 Mexico to study the bottom DO variability in the LaTex Shelf. In addition to N and Si, a P flow was embedded into the
1303 NEMURO model to account for the impacts of P limitation on hypoxia development. Built on the SOC scheme of the
1304 instantaneous remineralization developed by Fennel et al. (2006), a pool of sedimentary PON was added to account for
1305 temporal delays in SOC to the peak of plankton blooms. The model can well reproduce the vertical profiles of inorganic
1306 nutrient concentration (i.e., nitrate, phosphate, and silicate), the ratio of diatom/total phytoplankton, and the magnitude of SOC.

Moved (insertion) [5]

Deleted: A total of 16 sensitivity experiments were set up with different combinations of the riverine inorganic nutrient concentration and river freshwater discharges remained the same as in the control run. To remove numerical bias introduced by initial conditions and to reduce computational efforts, both

Deleted: control run and sensitivity experiments were initialized on 1 August 2017 and were conducted from 1 August 2017 to 26 August 2020. Initial conditions were derived from the 15-year hindcast. Analysis and comparisons were conducted based on simulations from 1 January 2018 to 26 August 2020. In summer, SOC is the prevailing factor in bottom DO changes (Fig. 9) over the shelf. When the hydrodynamics remain the same, changes in the size of hypoxia water are a result of the changes in the riverine nutrient inputs. The hypoxia averaged through the 2018–2020 summer shelf-wide cruises from the control run, and sensitivity experiments were shown in Fig. 11. To illustrate the complexity of the lower trophic community regarding decreased nutrient loads as well their contribution to the hypoxia development, simulated plankton (i.e., PS, PL, ZS, ZL, and ZP) concentration of the sensitivity experiments was also shown. ¶ (... [13])

Deleted: A

Deleted: was modified

Deleted: applied

Deleted: nitrogen

Deleted: silicon

Deleted: phosphorous

Deleted: phosphorous

Deleted: SOC,

Deleted: ratio

Deleted: /overlying water respiration

1371 The model's robustness in DO simulation was affirmed via 1) comparison of the DO profiles against cruise observations from
1372 [two](#) different databases, 2) comparison of spatial distributions of bottom DO, and 3) time series of the hypoxic area against the
1373 shelf-wide [cruise](#) observations.

Deleted: three

Deleted: cruises

1375 [Model results suggested that P and Si limitations could be more common than previously reported. N limitation was more](#)
1376 [commonly found in the shallow \(< 20 m\) middle and west shelf for both PS and PL, while in the other parts, primary production](#)
1377 [was more likely to be limited by P or Si. PL was found as a dominant plankton group accounting for about 50 – 70 % of total](#)
1378 [production during early spring and summer, explaining 63 % of the daily variability of the total production. The contribution](#)
1379 [of PS supported about 20 – 35 % of total biomass. The seasonality of total production exhibited a bi-peak \(in late spring and](#)
1380 [early summer\) pattern, which can be explained by the competition between PS and PL and was hardly captured by previous](#)
1381 [numerical models. We further explored the plankton contribution to DO budgets in water and sediment layers, respectively.](#)
1382 [We found 1\) the PON_{sed} pool was contributed mainly by zooplankton mortality and egestion, 2\) the plankton community, in](#)
1383 [general, produced more DO than it consumed in the waters above the bottom 2 m, with more uncertainty within the bottom 2](#)
1384 [m of waters.](#)

Deleted: A 15-year coupled physical-biogeochemical hindcast was achieved covering the period of 2006-2020. Three DO transport terms (i.e., horizontal advection, vertical advection, and vertical diffusion) and a biochemical term (i.e., SOC) were found as the most influential factors modulating the bottom DO dynamics in the LaTex shelf. They jointly contributed ~80% of the variability in bottom DO throughout the year. Specifically, the contribution of SOC (34%) outcompetes other factors in summer. In different subregions of the shelf, the contributions of the four terms vary with depth and distance from the Mississippi River mouth. In the nearshore regions, SOC plays a much more important role in modulating the summer bottom DO concentration with a maximum contribution of 33%–51%; while in the offshore regions, its contribution decreases notably to 19%–27% in summer, which is comparable to the contributions of the other three hydrodynamic-induced terms (18%–26% for the horizontal advection, 17%–25% for the vertical advection, and 7%–16% for the vertical diffusion). ¶

1385 [The types of limited nutrients, interactions \(competition, grazing, and predation behaviors\) among plankton groups, and the](#)
1386 [shifts in net DO contribution by the plankton community lead to complex responses in biomass, water DO, and bottom hypoxia.](#)
1387 [A 60 % reduction in all nutrient supplies would achieve the hypoxic area reduction goal set by the Task Force. The complex](#)
1388 [responses in the plankton biomass and their contribution to DO variation highlighted the importance of the complexity of the](#)
1389 [plankton community in the hypoxia evolution.](#)

¶ If the advection and vertical diffusion are considered jointly as a hydrodynamic term, the impacts of SOC (33%–51%) and hydrodynamics (28%–55%) are almost equally important in modulating the summer bottom DO in the nearshore regions, while in the offshore areas, contributions from hydrodynamics (51%–59%) outcompete the SOC impacts (19%–27%). The strong linear correlations between PEA and the advection terms suggest that increased water stability in summer leads to weaker DO exchanges from advection processes. Nevertheless, the relationship between PEA and vertical diffusion of DO across the bottom layer appears to be non-linear. As PEA starts to increase in early summer, the bottom DO starts to drop, resulting in strong vertical DO gradients at the bottom layer and enhanced vertical diffusion. As the strong water column stratification persists in mid and late summer, vertical diffusion of DO tends to be suppressed due to the weaker DO gradient resulting from the continuous DO consumption and the decreasing DO supply from the upper layers. ¶

1392 **Code/Data availability:** Model data is available at the LSU mass storage system and details are on the webpage of the Coupled
1393 Ocean Modeling Group at LSU (<https://faculty.lsu.edu/zxue/>). Data requests can be sent to the corresponding author via this
1394 webpage.

1396 **Author contribution:** Z. George Xue designed the experiments and Yanda Ou carried them out. Yanda Ou developed the
1397 model code and performed the simulations. Yanda Ou and Z. George Xue prepared the manuscript.

1399 **Competing interests:** The authors declare that they have no conflict of interest.

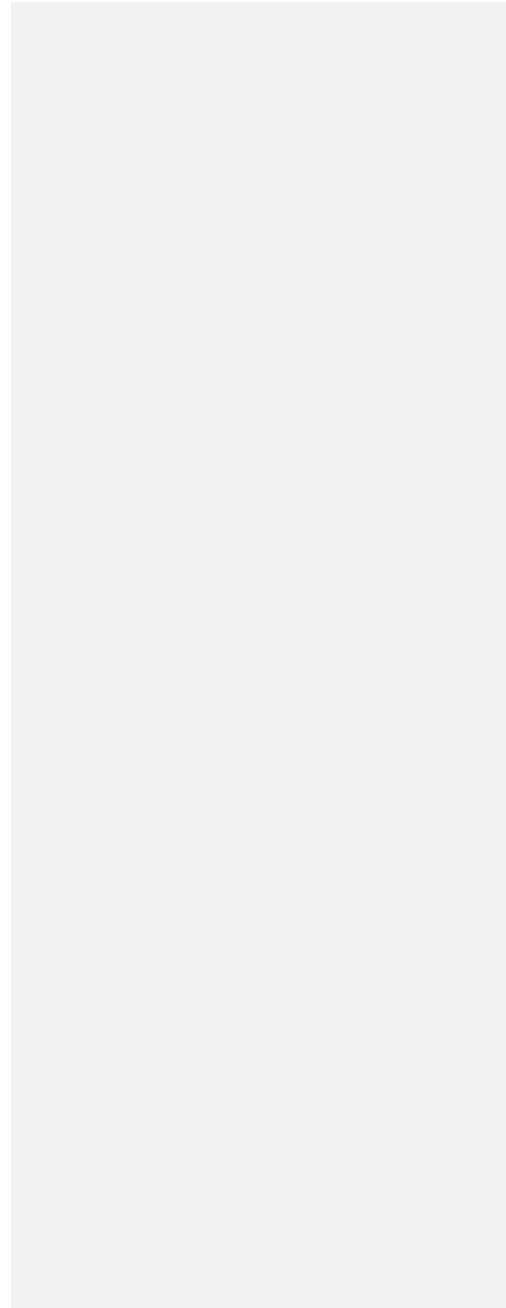
1401 **Acknowledgment:** Research support was provided through the Bureau of Ocean Energy Management (M17AC00019,
1402 M20AC10001). We thank Dr. Jerome Fiechter at UC Santa Cruz for sharing his NEMURO model codes and Dr. Katja Fennel
1403 at [Dalhousie](#) University for discussing model parameterization. The computational resource was provided by the High-
1404 Performance Computing Facility (clusters SuperMIC and QueenBee3) at Louisiana State University.

¶ We further examined the sensitivity of summer bottom DO to riverine nutrient reductions. Our sensitivity experiments highlighted the importance of the complexity of the lower-trophic community in bottom DO's response to the changing nutrient loads. Sole nutrient reductions in total nitrogen do not guarantee a hypoxic area decrease. Reduced nitrogen load can stimulate the competition between PS and PL and uncertainties to secondary productivity. Sole phosphorus reductions can, in general, reduce hypoxic area as PS and associated decreases in secondary productivity are reduced. A silicon reduction is more effective in reducing the hypoxic zone than the other two nutrients exhibited by the reductions in PL, ZS, and ZP concentration. One should also note that changes in the bottom DO are not evenly distributed over the shelf. A triple reduction strategy for all nutrients performs the best in reducing shelf hypoxic areas. When riverine nitrogen, phosphorous, and silicon loads are reduced by ~80% simultaneously, the hypoxia reduction goal of 5000 km² is likely to be achieved. ¶

Deleted:

Deleted: Dalhouse

1462
1463



1464 **Appendix A: Expressions of processes terms modified in this study**

1465 Detailed descriptions of related terms and parameters are listed in Appendix B.

1466 **A1 Update gross primary production of PS and PL due to the additional phosphate limitation**

1467 $GppPSn = GppNPS + GppAPS,$ (A1)

1468 $GppPLn = GppNPL + GppAPL,$ (A2)

1469 where,

1470 $GppNPS = PSn V_{maxS} \exp(K_{GppS} TMP) \left[1 - \exp\left(-\frac{\alpha_{PS}}{V_{maxS}} I_{PS}\right) \right] \exp\left(-\frac{\beta_{PS}}{V_{maxS}} I_{PS}\right) NutlimPS RnewS,$ (A3)

1471 $GppAPS = PSn V_{maxS} \exp(K_{GppS} TMP) \left[1 - \exp\left(-\frac{\alpha_{PS}}{V_{maxS}} I_{PS}\right) \right] \exp\left(-\frac{\beta_{PS}}{V_{maxS}} I_{PS}\right) NutlimPS (1 - RnewS),$ (A4)

1472 $GppNPL = PLn V_{maxL} \exp(K_{GppL} TMP) \left[1 - \exp\left(-\frac{\alpha_{PL}}{V_{maxL}} I_{PL}\right) \right] \exp\left(-\frac{\beta_{PL}}{V_{maxL}} I_{PL}\right) NutlimPL RnewL,$ (A5)

1473 $GppAPL = PLn V_{maxL} \exp(K_{GppL} TMP) \left[1 - \exp\left(-\frac{\alpha_{PL}}{V_{maxL}} I_{PL}\right) \right] \exp\left(-\frac{\beta_{PL}}{V_{maxL}} I_{PL}\right) NutlimPL (1 - RnewL),$ (A6)

1474

1475 $RnewS = \frac{NO_3}{(NO_3 + K_{NO_3S}) \left(1 + \frac{NH_4}{K_{NH_4S}}\right)} \frac{1}{\frac{NO_3}{(NO_3 + K_{NO_3S}) \left(1 + \frac{NH_4}{K_{NH_4S}}\right)} + \frac{NH_4}{NH_4 + K_{NH_4S}}},$ (A7)

1476 $RnewL = \frac{NO_3}{(NO_3 + K_{NO_3L}) \left(1 + \frac{NH_4}{K_{NH_4L}}\right)} \frac{1}{\frac{NO_3}{(NO_3 + K_{NO_3L}) \left(1 + \frac{NH_4}{K_{NH_4L}}\right)} + \frac{NH_4}{NH_4 + K_{NH_4L}}},$ (A8)

1477 $NutlimPS = \min\left(\frac{NO_3}{(NO_3 + K_{NO_3S}) \left(1 + \frac{NH_4}{K_{NH_4S}}\right)} + \frac{NH_4}{NH_4 + K_{NH_4S}}, \frac{PO_4}{PO_4 + K_{PO_4S}}\right),$ (A9)

1478 $NutlimPL = \min\left(\frac{NO_3}{(NO_3 + K_{NO_3L}) \left(1 + \frac{NH_4}{K_{NH_4L}}\right)} + \frac{NH_4}{NH_4 + K_{NH_4L}}, \frac{PO_4}{PO_4 + K_{PO_4L}}, \frac{SiOH_4}{SiOH_4 + K_{SiOH_4L}}\right),$ (A10)

1479 $I_{PS} = PAR \text{ frac} \exp\left\{z \text{ AttSW} + \text{AttPS} \int_z^0 [PSn(\zeta) + PLn(\zeta)] d\zeta\right\},$ (A11)

1480 $I_{PL} = PAR \text{ frac} \exp\left\{z \text{ AttSW} + \text{AttPL} \int_z^0 [PSn(\zeta) + PLn(\zeta)] d\zeta\right\},$ (A12)

1481 **A2 Update aerobic decomposition from PON to NH₄ and from DON to NH₄ due to [the](#) introduction of oxygen dependency**

1482

1483 $DecP2N = PON VP2N_0 \exp(K_{P2N} TMP) r,$ (A13)

1484 $DecD2N = PON VD2N_0 \exp(K_{D2N} TMP) r,$ (A14)

1485 where,

1486 $r = \max\left[\frac{\max(0, Oxyg - Oxyg_{th})}{K_{Oxyg} + Oxyg - Oxyg_{th}}, 0\right],$ (A15)

1487 **A3 Update water column nitrification due to [the](#) introduction of oxygen dependency and light limitation**

1488 $Nit = Nit_0 \exp(K_{Nit} TMP) LgtlimN r,$ (A16)

1489 where,

1490 $LgtlimN = 1 - \max\left(0, \frac{I_N - I_0}{I_N - I_0 + k_l}\right),$ (A17)

1491 $I_N = PAR \frac{frac}{exp} \left\{ z AttSW + \max(AttPS, AttPL) \int_z^0 [PSn(\zeta) + PLn(\zeta)] d\zeta \right\},$ (A18)

1492 **A4 Additional SOC term:**

1493 $SOC = 8.3865 PON_{sed} VP2N_0 \exp(K_{P2N} TMP),$ (A19)

1494 **Appendix B: Descriptions of terms and parameters**

1495 **Table B1. Descriptions of state variables**

Terms	Description	Unit
NH_4	Ammonium concentration	mmolN m ⁻³
NO_3	Nitrate concentration	mmolN m ⁻³
PO_4	Phosphate concentration	mmolP m ⁻³
DOP	Dissolved organic phosphorus concentration	mmolP m ⁻³
POP	Particulate organic phosphorus concentration	mmolP m ⁻³
$SiOH_4$	Silicate concentration	mmolSi m ⁻³
PSn	Small phytoplankton biomass concentration measured in nitrogen	mmolN m ⁻³
PLn	Large phytoplankton biomass concentration measured in nitrogen	mmolN m ⁻³
$Oxyg$	Dissolved oxygen concentration	mmolO ₂ m ⁻³

Deleted: phosphorous

Deleted: phosphorous

1496

1497 **Table B2 Descriptions of related terms involved in the phosphorus cycle and nutrient limitation. Superscripts “*” and “+” denote**
 1498 **that the mathematic expressions of corresponding terms are the same as those in Kishi et al. (2007) and Shropshire et al. (2020),**
 1499 **respectively. Expressions of terms with no superscript are updated and reported in Appendix A.**

Terms	Description	Unit
$DecP2N$	Decomposition rate from PON to NH ₄	mmolN m ⁻³ day ⁻¹
$DecD2N$	Decomposition rate from DON to NH ₄	mmolN m ⁻³ day ⁻¹
$DecP2D^{*+}$	Decomposition rate from PON to DON	mmolN m ⁻³ day ⁻¹
$EgeZLn^{+}$	Large zooplankton egestion rate measured in nitrogen	mmolN m ⁻³ day ⁻¹
$EgeZPn^{*+}$	Predatory zooplankton egestion rate measured in nitrogen	mmolN m ⁻³ day ⁻¹

<i>EgeZSn</i> ⁺	Small zooplankton egestion rate measured in nitrogen	mmolN m ⁻³ day ⁻¹
<i>ExcPSn</i> ⁺	Small phytoplankton extracellular excretion rate to DON and is measured in nitrogen	mmolN m ⁻³ day ⁻¹
<i>ExcPLn</i> ⁺	Large phytoplankton extracellular excretion rate to DON and is measured in nitrogen	mmolN m ⁻³ day ⁻¹
<i>ExcZSn</i> ⁺	Small zooplankton excretion rate to NH ₄ and is measured in nitrogen	mmolN m ⁻³ day ⁻¹
<i>ExcZLn</i> ⁺	Large zooplankton excretion rate to NH ₄ and is measured in nitrogen	mmolN m ⁻³ day ⁻¹
<i>ExcZPn</i> ⁺	Predatory zooplankton excretion rate to NH ₄ and is measured in nitrogen	mmolN m ⁻³ day ⁻¹
<i>GppNPS</i>	Small phytoplankton nitrate-induced gross primary production rate measured in nitrogen	mmolN m ⁻³ day ⁻¹
<i>GppAPS</i>	Small phytoplankton ammonium-induced gross primary production rate measured in nitrogen	mmolN m ⁻³ day ⁻¹
<i>GppPSn</i>	Small phytoplankton gross primary production rate measured in nitrogen	mmolN m ⁻³ day ⁻¹
<i>GppNPL</i>	Large phytoplankton nitrate-induced gross primary production rate measured in nitrogen	mmolN m ⁻³ day ⁻¹
<i>GppAPL</i>	Large phytoplankton ammonium-induced gross primary production rate measured in nitrogen	mmolN m ⁻³ day ⁻¹
<i>GppPLn</i>	Large phytoplankton gross primary production rate measured in nitrogen	mmolN m ⁻³ day ⁻¹
<i>MorPSn</i> ⁺	Small phytoplankton mortality rate measured in nitrogen	mmolN m ⁻³ day ⁻¹
<i>MorPLn</i> ⁺	Large phytoplankton mortality rate measured in nitrogen	mmolN m ⁻³ day ⁻¹
<i>MorZSn</i> ⁺	Small zooplankton mortality rate measured in nitrogen	mmolN m ⁻³ day ⁻¹
<i>MorZLn</i> ⁺	Large zooplankton mortality rate measured in nitrogen	mmolN m ⁻³ day ⁻¹
<i>MorZPn</i> ⁺	Predatory zooplankton mortality rate measured in nitrogen	mmolN m ⁻³ day ⁻¹
<i>Nit</i>	Nitrification rate	mmolN m ⁻³ day ⁻¹
<i>ResPSn</i> ⁺	Small phytoplankton respiration rate measured in nitrogen	mmolN m ⁻³ day ⁻¹
<i>ResPLn</i> ⁺	Large phytoplankton respiration rate measured in nitrogen	mmolN m ⁻³ day ⁻¹
<i>SOC</i>	Sediment oxygen consumption rate	mmolO ₂ m ⁻² day ⁻¹

1502

1503 **Table B3 Descriptions of other variables**

Terms	Description	Unit
I_{PS}	Photosynthetically available radiation for small phytoplankton	W m ⁻²
I_{PL}	Photosynthetically available radiation for large phytoplankton	W m ⁻²
I_N	Maximum photosynthetically available radiation	W m ⁻²
$LgtlimN$	Light inhibition on nitrification rate	no dimension
$NutlimPS$	Nutrient limitation term for small phytoplankton	no dimension
$NutlimPL$	Nutrient limitation term for large phytoplankton	no dimension
PAR	Net short-wave radiation on water surface	W m ⁻²
r	Oxygen inhibition on nitrification and aerobic decomposition rates	no dimension
$RnewS$	The f-ratio of small phytoplankton which is defined by the ratio of nitrate uptake to total uptake of nitrate and ammonium	no dimension
$RnewL$	The f-ratio of large phytoplankton which is defined by the ratio of nitrate uptake to total uptake of nitrate and ammonium	no dimension
$Thickness_{bot}$	Thickness of the bottom water layer	m
TMP	Water temperature	°C
z, ζ	Vertical coordinate which is negative below sea surface	m

1504

1505 **Table B4. Descriptions and values of all model parameters. Superscripts “S”, “L”, “F06”, and “F13” denote that the corresponding**
1506 **parameters follow Shropshire et al. (2020), Laurent et al. (2012), Fennel et al. (2006), and Fennel et al. (2013), respectively.**
1507 **Superscript “**” indicates the corresponding parameters are from this study.**

Parameter	Description	Units	Values
Small phytoplankton			
V_{maxS}	Small phytoplankton maximum photosynthetic rate at 0 °C	day ⁻¹	0.4 ^S
K_{NO_3S}	Small Phytoplankton half saturation constant for nitrate	mmolN m ⁻³	0.5 ^S
K_{NH_4S}	Small Phytoplankton half saturation constant for ammonium	mmolN m ⁻³	0.1 ^S
K_{PO_4S}	Small Phytoplankton half saturation constant for phosphate	mmolP m ⁻³	0.5 ^L
α_{PS}	Small phytoplankton photochemical reaction coefficient, initial slope of P-I curve	m ² W ⁻¹ day ⁻¹	0.1 ^S

β_{PS}	Small phytoplankton photoinhibition coefficient	$\text{m}^2 \text{W}^{-1} \text{day}^{-1}$	0.00045 ^S
Res_{PS0}	Small phytoplankton respiration rate at 0 °C	day^{-1}	0.03 ^S
Mor_{PS0}	Small phytoplankton mortality rate at 0 °C	$\text{m}^3 \text{mmolN}^{-1} \text{day}^{-1}$	0.002 ^S
γ_S	Ratio of extracellular excretion to photosynthesis for small phytoplankton	no dimension	0.135 ^S
K_{GPPS}	Small phytoplankton coefficient for photosynthetic rate	$^{\circ}\text{C}^{-1}$	0.0693 ^S
K_{ResPS}	Small phytoplankton coefficient for respiration	$^{\circ}\text{C}^{-1}$	0.0519 ^S
K_{MorPS}	Small phytoplankton coefficient for mortality	$^{\circ}\text{C}^{-1}$	0.0693 ^S

Large phytoplankton

V_{maxL}	Large phytoplankton maximum photosynthetic rate at 0 °C	day^{-1}	0.8 ^S
K_{NO_3L}	Large Phytoplankton constant for nitrate	mmolN m^{-3}	3.0 ^S
K_{NH_4L}	Large Phytoplankton constant for ammonium	mmolN m^{-3}	0.3 ^S
K_{PO_4L}	Large Phytoplankton constant for phosphate	mmolP m^{-3}	0.5 ^L
K_{SiOH_4L}	Large Phytoplankton constant for silicate	mmolSi m^{-3}	6.0 ^S
α_{PL}	Large phytoplankton reaction coefficient, initial slope of P-I curve	$\text{m}^2 \text{W}^{-1} \text{day}^{-1}$	0.1 ^S
β_{PL}	Large phytoplankton photoinhibition coefficient	$\text{m}^2 \text{W}^{-1} \text{day}^{-1}$	0.00045 ^S
Res_{PL0}	Large phytoplankton respiration rate at 0 °C	day^{-1}	0.03 ^S
Mor_{PL0}	Large phytoplankton mortality rate at 0 °C	$\text{m}^3 \text{mmolN}^{-1} \text{day}^{-1}$	0.001 ^S

γ_L	Ratio of extracellular excretion to photosynthesis for large phytoplankton	no dimension	0.135 ^S
K_{GppL}	Large phytoplankton coefficient for photosynthetic rate	temperature °C ⁻¹	0.0693 ^S
K_{MorPL}	Large phytoplankton coefficient for mortality	temperature °C ⁻¹	0.0693 ^S
K_{ResPL}	Large phytoplankton coefficient for respiration	temperature °C ⁻¹	0.0693 ^S

Small zooplankton

GR_{maxSps}	Small zooplankton maximum grazing rate on small phytoplankton at 0 °C	day ⁻¹	0.6 ^S
λ_S	Ivlev constant of small zooplankton	m ³ mmolN ⁻¹	1.4 ^S
$PSZS$	Small zooplankton threshold value for grazing on small phytoplankton	mmolN m ⁻³	0.043 ^S
α_{ZS}	Assimilation efficiency of small zooplankton	no dimension	0.7 ^S
β_{ZS}	Growth efficiency of small zooplankton	no dimension	0.3 ^S
$MorZS0$	Small zooplankton mortality rate at 0 °C	m ³ mmolN ⁻¹ day ⁻¹	0.022 ^S
K_{Gras}	Small zooplankton temperature coefficient for grazing	°C ⁻¹	0.0693 ^S
K_{MorZS}	Small zooplankton temperature coefficient for mortality	°C ⁻¹	0.0693 ^S

Large zooplankton

GR_{maxLps}	Large zooplankton maximum grazing rate on small phytoplankton at 0 °C	day ⁻¹	0 ^S
GR_{maxLpl}	Large zooplankton maximum grazing rate on large phytoplankton at 0 °C	day ⁻¹	0.3 ^S
GR_{maxLzs}	Large zooplankton maximum grazing rate on small zooplankton at 0 °C	day ⁻¹	0.3 ^S
λ_L	Ivlev constant of large zooplankton	m ³ mmolN ⁻¹	1.4 ^S
$PLZL$	Large zooplankton threshold value for grazing on large phytoplankton	mmolN m ⁻³	0.040 ^S

<i>ZS2ZL</i>	Large zooplankton threshold value for grazing on small zooplankton	mmolN m ⁻³	0.040 ^S
α_{ZL}	Assimilation efficiency of large zooplankton	no dimension	0.7 ^S
β_{ZL}	Growth efficiency of large zooplankton	no dimension	0.3 ^S
<i>MorZL0</i>	Large zooplankton mortality rate at 0 °C	m ³ mmolN ⁻¹ day ⁻¹	0.022 ^S
<i>KGraL</i>	Large zooplankton temperature coefficient for grazing	°C ⁻¹	0.0693 ^S
<i>KMorZL</i>	Large zooplankton temperature coefficient for mortality	°C ⁻¹	0.0693 ^S

Predatory zooplankton

<i>GRmaxPpl</i>	Predatory zooplankton maximum grazing rate on large phytoplankton at 0 °C	day ⁻¹	0.1 ^S
<i>GRmaxPzs</i>	Predatory zooplankton maximum grazing rate on small zooplankton at 0 °C	day ⁻¹	0.1 ^S
<i>GRmaxPzl</i>	Predatory zooplankton maximum grazing rate on large zooplankton at 0 °C	day ⁻¹	0.3 ^S
λ_p	Ivlev constant of predatory zooplankton	m ³ mmolN ⁻¹	1.4 ^S
<i>PL2ZP</i>	Predatory zooplankton threshold value for grazing on large phytoplankton	mmolN m ⁻³	0.040 ^S
<i>ZS2ZP</i>	Predatory zooplankton threshold value for grazing on small zooplankton	mmolN m ⁻³	0.040 ^S
<i>ZL2ZP</i>	Predatory zooplankton threshold value for grazing on large zooplankton	mmolN m ⁻³	0.040 ^S
α_{ZP}	Assimilation efficiency of predatory zooplankton	no dimension	0.7 ^S
β_{ZP}	Growth efficiency of predatory zooplankton	no dimension	0.3 ^S
<i>MorZP0</i>	Predatory zooplankton mortality rate at 0 °C	m ³ mmolN ⁻¹ day ⁻¹	0.12 ^S
<i>KGraP</i>	Predatory zooplankton temperature coefficient for grazing	°C ⁻¹	0.0693 ^S

K_{MorZP}	Predatory zooplankton temperature coefficient for mortality	$^{\circ}\text{C}^{-1}$	0.0693 ^S
ψ_{PL}	Grazing inhibition coefficient of predatory zooplankton grazing on large phytoplankton	$\text{m}^3 \text{mmolN}^{-1}$	4.605 ^S
ψ_{ZS}	Grazing inhibition coefficient of predatory zooplankton grazing on small zooplankton	$\text{m}^3 \text{mmolN}^{-1}$	3.01 ^S

Light

Att_{SW}	Light attenuation due to seawater	m^{-1}	0.03 ^S
Att_{PS}	Light attenuation due to small phytoplankton, self-shading coefficient	$\text{m}^2 \text{mmolN}^{-1}$	0.03 ^S
Att_{PL}	Light attenuation due to large phytoplankton, self-shading coefficient	$\text{m}^2 \text{mmolN}^{-1}$	0.03 ^S
$frac$	Fraction of shortwave radiation that is photosynthetically active	no dimension	0.43 ^S
I_0	Threshold of light inhibition of nitrification	W m^{-2}	0.0095 ^{F06}
k_I	Light intensity at which light inhibition of nitrification is half-saturated	W m^{-2}	0.1 ^{F06}

Water column nitrification and aerobic decomposition

Nit_0	Nitrification rate at 0 $^{\circ}\text{C}$	day^{-1}	0.003 ^S
$VP2N_0$	Decomposition rate at 0 $^{\circ}\text{C}$ (PON \rightarrow NH ₄)	day^{-1}	0.01 ^S
$VP2D_0$	Decomposition rate at 0 $^{\circ}\text{C}$ (PON \rightarrow DON)	day^{-1}	0.05 ^S
$VD2N_0$	Decomposition rate at 0 $^{\circ}\text{C}$ (DON \rightarrow NH ₄)	day^{-1}	0.02 ^S
$VO2S_0$	Decomposition rate at 0 $^{\circ}\text{C}$ (Opal \rightarrow Si(OH) ₄)	day^{-1}	0.01 ^S
K_{Nit}	Temperature coefficient for nitrification	$^{\circ}\text{C}^{-1}$	0.0693 ^S
K_{P2D}	Temperature coefficient for decomposition (PON \rightarrow DON)	$^{\circ}\text{C}^{-1}$	0.0693 ^S
K_{P2N}	Temperature coefficient for decomposition (PON \rightarrow NH ₄)	$^{\circ}\text{C}^{-1}$	0.0693 ^S
K_{D2N}	Temperature coefficient for decomposition (DON \rightarrow NH ₄)	$^{\circ}\text{C}^{-1}$	0.0693 ^S

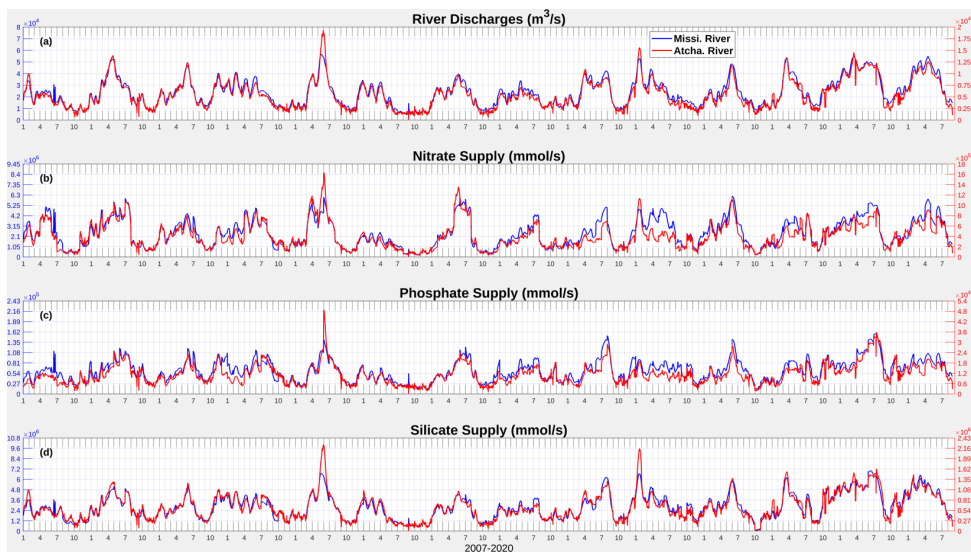
K_{O_2S}	Temperature coefficient for decomposition (Opal→Si(OH) ₄)	°C ⁻¹	0.0693 ^S
------------	---	------------------	---------------------

Other parameters

K_{Oxyg}	Oxygen concentration at which inhibition of nitrification and aerobic respiration are half-saturated	mmolO ₂ m ⁻³	3.0 ^{F13}
$Oxyg_{th}$	Oxygen concentration threshold below which no aerobic respiration or nitrification occurs	mmolO ₂ m ⁻³	6.0 ^{F13}
$RPO4N$	P: N ratio	mmolP mmolN ⁻¹	1/16 ^L
$RSiN$	Si: N ratio	mmolSi mmolN ⁻¹	1 ^S
$rOxNO_3$	Stoichiometric ratios corresponding to the oxygen produced per mol of nitrate assimilated during photosynthesis	mmolO ₂ mmolNO ₃ ⁻¹	138/16 ^{F13}
$rOxNH_4$	Stoichiometric ratios corresponding to the oxygen produced per mol of ammonium assimilated during photosynthesis	mmolO ₂ mmolNH ₄ ⁻¹	106/16 ^{F13}
$setVPON$	Sinking velocity of PON	m day ⁻¹	-5*
$setVOpal$	Sinking velocity of Opal	m day ⁻¹	-5*

1508

509 Appendix C: Supporting figures and tables



1510
1511 **Figure C1.** Daily time series (2007–2020) of river discharges of freshwater, nitrate, phosphate, and silicate from the Mississippi and
1512 Atchafalaya Rivers.

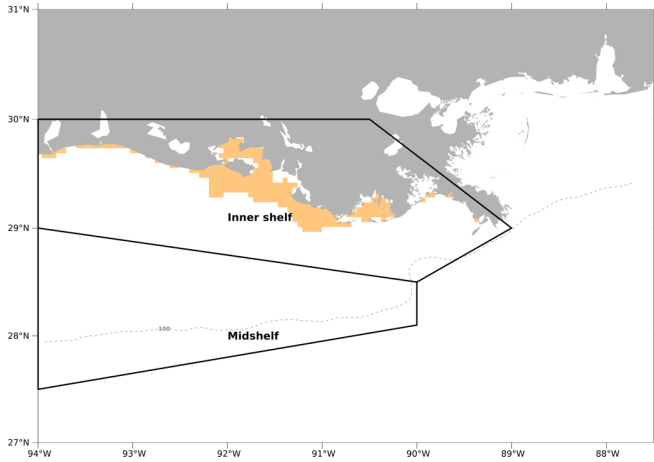
1513 **Table C1.** A correlation matrix of daily inorganic nutrient loads by the Mississippi River and the Atchafalaya River from 2007 to
1514 2020. Correlation coefficients shown are all significant ($p < 0.001$).

	Mississippi nitrate+nitrite	Atchafalaya nitrate+nitrite	Mississippi phosphate	Atchafalaya phosphate	Mississippi silicate	Atchafalaya silicate
Mississippi nitrate+nitrite	1					
Atchafalaya nitrate+nitrite	0.9123	1				
Mississippi phosphate	0.8328	0.7577	1			
Atchafalaya phosphate	0.7517	0.7913	0.9155	1		
Mississippi silicate	0.8583	0.7795	0.8759	0.7942	1	

Deleted: rivers

Atchafalaya silicate	0.7938	0.7956	0.8131	0.8148	0.9520	1
--	------------------------	------------------------	------------------------	------------------------	------------------------	-------------------

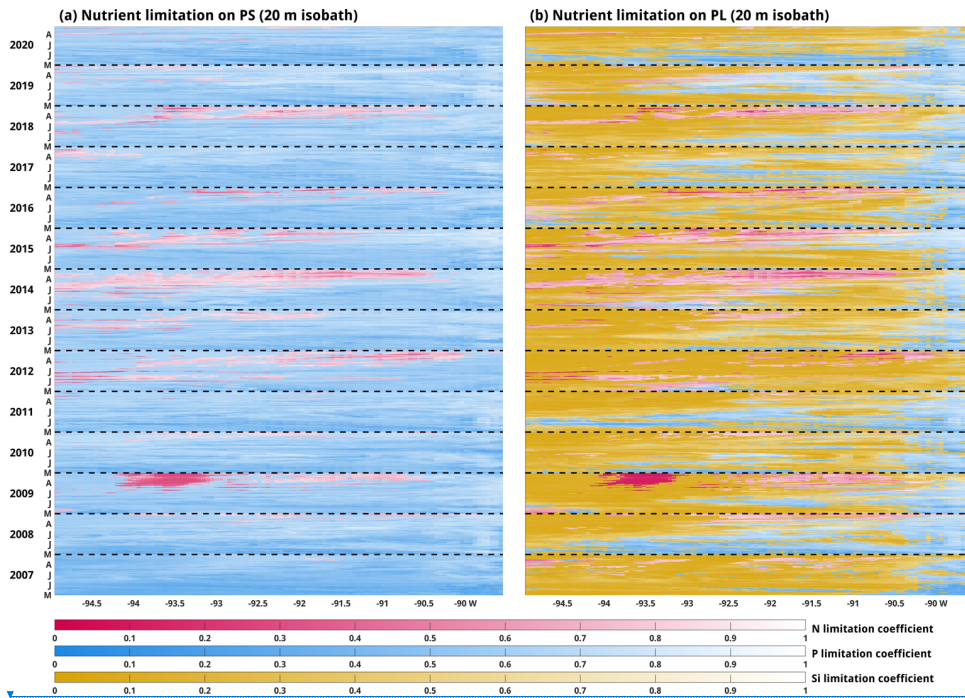
1516



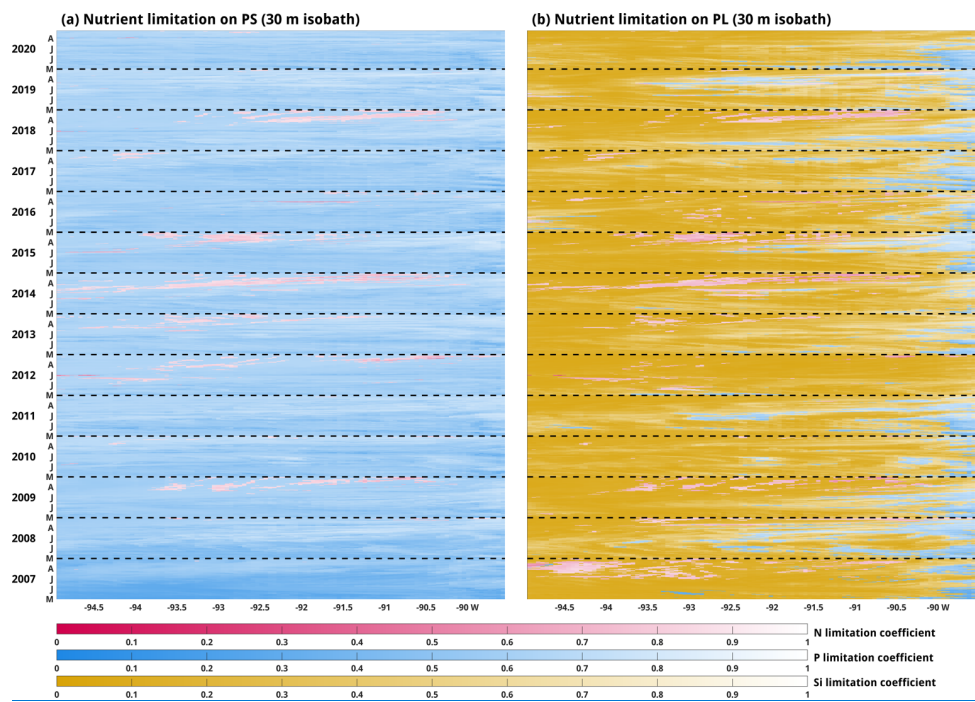
1517

1518 **Figure C2.** The model computational meshes over which the regionally averaged diatom ratios were conducted for validation
 1519 purposes. The orange-patched region covers roughly the study regions in Schaeffer et al. (2012), while the regions restricted by two
 1520 black polygons are two regions (i.e., inner shelf and midshelf) where samples were collected in Chakraborty and Lohrenz's (2015)
 1521 study.

Deleted:

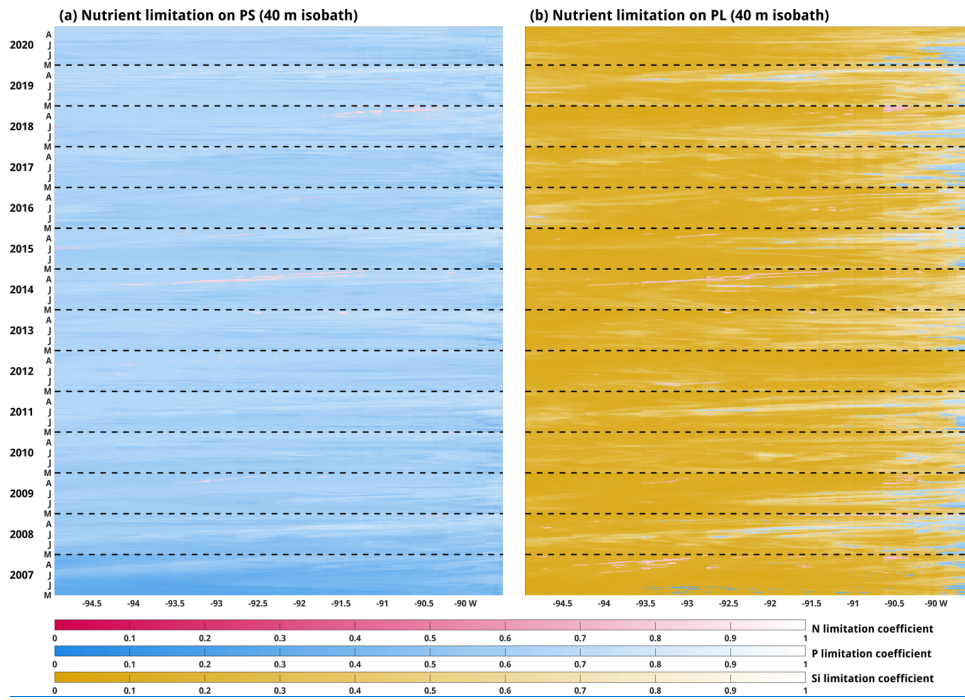


523
524 **Figure C3.** Evolution of depth-averaged nutrient limitation coefficients for (a) PS and (PL) along the 20 m isobath during late spring
525 and summer. The notations of M, J, J, and A in the y-axis represent the first day of May, June, July, and August, respectively. Note
526 that a lower (deeper colored) coefficient represents stronger limitations on phytoplankton growth. The dashed black lines indicate
527 the time record on May 1 of each year.



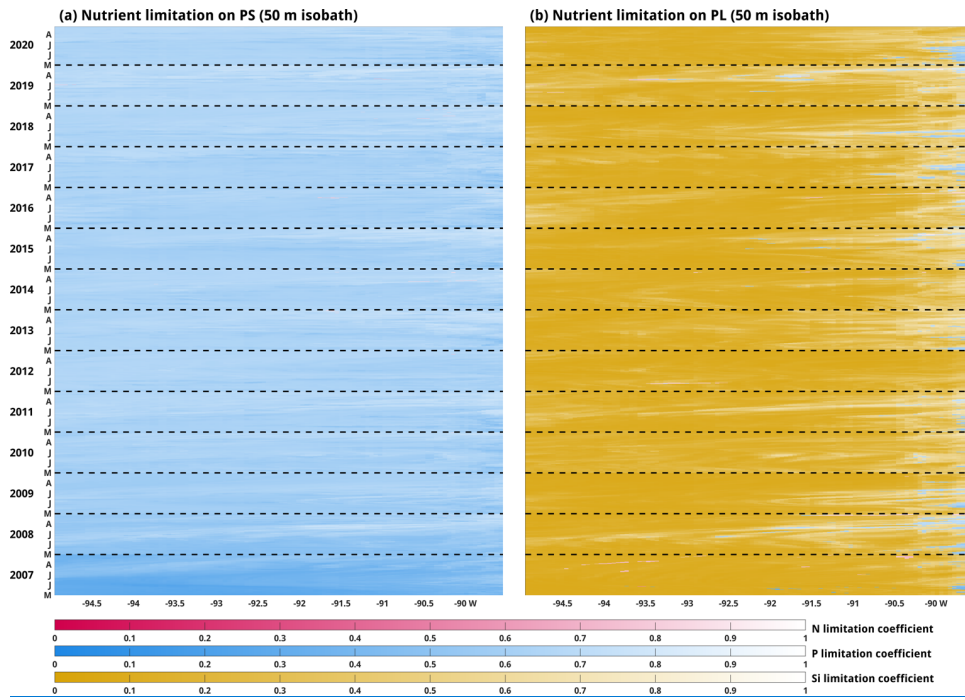
529

530 [Figure C4. Same as Figure C3, but along the 30 m isobath.](#)



531

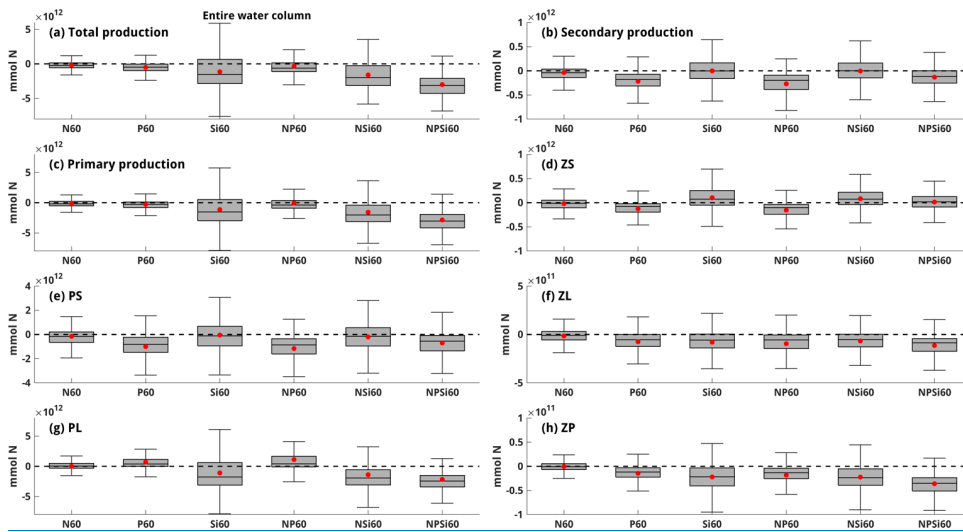
532 [Figure C5. Same as Figure C3, but along the 40 m isobath.](#)



533

534 [Figure C6. Same as Figure C3, but along the 50 m isobath.](#)

535



536

537

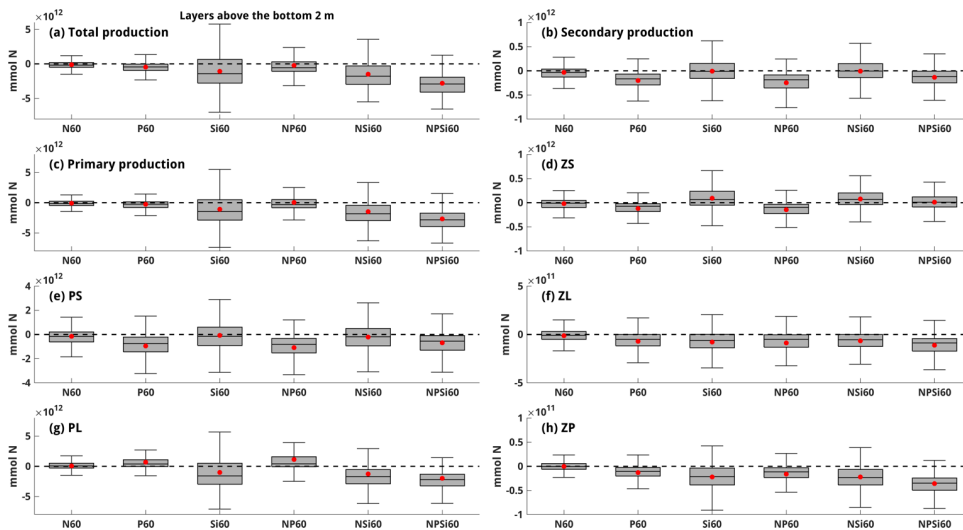
538

539

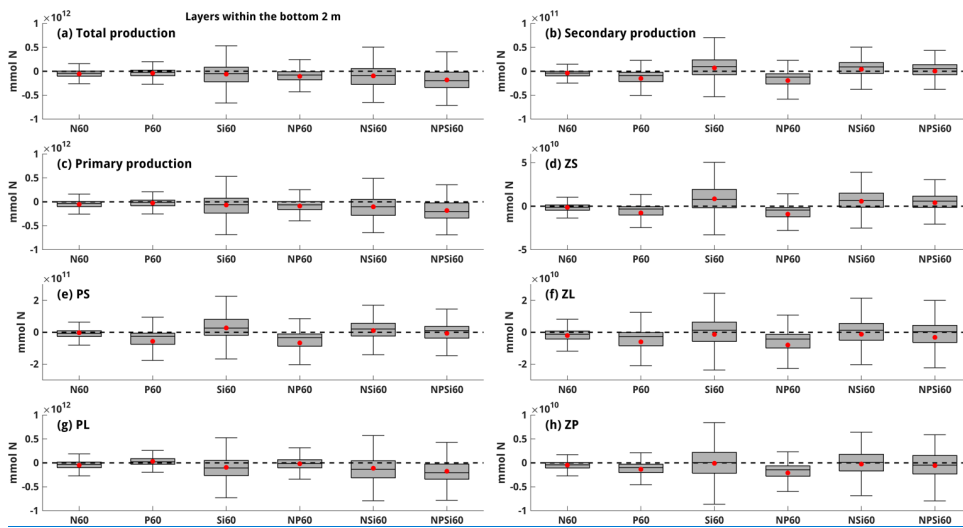
540

541

Figure C7. Responses of (a) total production, (b) secondary production, (c) primary production, (d) ZS biomass, (e) PS biomass, (f) ZL biomass, (g) PL biomass, and (h) ZP biomass to the reductions in riverine nutrient loads. All biomass matrices were integrated over the entire water column and the LaTex shelf. Statistics shown are mean (red dots), median, first quartile, third quartile, minimum, and maximum derived from the differences between sensitivity tests and the control run during late spring and summer (May–August).



542
543 [Figure C8. Same as Fig. C7, but for integrated biomass over layers above the bottom 2 m.](#)



544
545 [Figure C9. Same as Fig. C7, but for integrated biomass at layers within 2 m above the bottom.](#)

1546 **References**

- 1547 [Del Amo, Y. and Brzezinski, M. A.: The chemical form of dissolved Si taken up by marine diatoms, *J. Phycol.*, 35, 1162–1170,](https://doi.org/10.1046/j.1529-8817.1999.3561162.x)
 1548 <https://doi.org/10.1046/j.1529-8817.1999.3561162.x>, 1999.
- 1549 [Anglès, S., Jordi, A., Henrichs, D. W., and Campbell, L.: Influence of coastal upwelling and river discharge on the phytoplankton community](https://doi.org/10.1016/j.pocean.2019.02.001)
 1550 [composition in the northwestern Gulf of Mexico, *Prog. Oceanogr.*, 173, 26–36, https://doi.org/10.1016/j.pocean.2019.02.001](https://doi.org/10.1016/j.pocean.2019.02.001), 2019.
- 1551 [Azam, F.: Silicic-acid uptake in diatoms studied with \[68Ge\]germanic acid as tracer, *Planta*, 121, 205–212,](https://doi.org/10.1007/BF00389321)
 1552 <https://doi.org/10.1007/BF00389321>, 1974.
- 1553 [Azam, F., Hemmingsen, B. B., and Volcani, B. E.: Role of silicon in diatom metabolism - V. silicic acid transport and metabolism in the](https://doi.org/10.1007/BF00403050)
 1554 [heterotrophic diatom *Nitzschia alba*, *Arch. Microbiol.*, 97, 103–114, https://doi.org/10.1007/BF00403050](https://doi.org/10.1007/BF00403050), 1974.
- 1555 [Bianchi, T. S., DiMarco, S. F., Cowan, J. H., Hetland, R. D., Chapman, P., Day, J. W., and Allison, M. A.: The science of hypoxia in the](https://doi.org/10.1016/j.scitotenv.2009.11.047)
 1556 [northern Gulf of Mexico: A review, *Sci. Total Environ.*, 408, 1471–1484, https://doi.org/10.1016/j.scitotenv.2009.11.047](https://doi.org/10.1016/j.scitotenv.2009.11.047), 2010.
- 1557 [Bleck, R.: An oceanic general circulation model framed in hybrid isopycnic-Cartesian coordinates, *Ocean Model.*, 4, 55–88,](https://doi.org/10.1016/S1463-5003(01)00012-9)
 1558 [https://doi.org/10.1016/S1463-5003\(01\)00012-9](https://doi.org/10.1016/S1463-5003(01)00012-9), 2002.
- 1559 [Bleck, R. and Boudra, D. B.: Initial testing of a numerical ocean circulation model using a hybrid \(quasi-isopycnic\) vertical coordinate, *J.*
 1560 \[Phys. Oceanogr., 11, 755–770, https://doi.org/10.1175/1520-0485\\(1981\\)011<0755:TOANO>2.0.CO;2\]\(https://doi.org/10.1175/1520-0485\(1981\)011<0755:TOANO>2.0.CO;2\), 1981.](https://doi.org/10.1175/1520-0485(1981)011<0755:TOANO>2.0.CO;2)
- 1561 [Boyer, T. P., Baranova, O. K., Coleman, C., Garcia, H. E., Grodsky, A., Locarnini, R. A., Mishonov, A. V., Paver, C. R., Reagan, J. R.,](https://www.nesdis.noaa.gov/)
 1562 [Seidov, D., Smolyar, I. V., Weathers, K. W., and Zweng, M. M.: World Ocean Database 2018, Technical., edited by: Mishonov, A. V.,](https://www.nesdis.noaa.gov/)
 1563 [NOAA Atlas NESDIS 87](https://www.nesdis.noaa.gov/), 2018.
- 1564 [Chakraborty, S. and Lohrenz, S. E.: Phytoplankton community structure in the river-influenced continental margin of the northern Gulf of](https://doi.org/10.3354/meps11107)
 1565 [Mexico, *Mar. Ecol. Prog. Ser.*, 521, 31–47, https://doi.org/10.3354/meps11107](https://doi.org/10.3354/meps11107), 2015.
- 1566 [Chakraborty, S., Lohrenz, S. E., and Gundersen, K.: Photophysiological and light absorption properties of phytoplankton communities in](https://doi.org/10.1002/2016JC012092)
 1567 [the river-dominated margin of the northern Gulf of Mexico, *J. Geophys. Res. Ocean.*, 122, 4922–4938,](https://doi.org/10.1002/2016JC012092)
 1568 <https://doi.org/10.1002/2016JC012092>, 2017.
- 1569 [Chapman, D. C.: Numerical treatment of cross-shelf open boundaries in a barotropic coastal ocean model., https://doi.org/10.1175/1520-](https://doi.org/10.1175/1520-0485(1985)015<1060:ntoco>2.0.co;2)
 1570 [0485\(1985\)015<1060:ntoco>2.0.co;2](https://doi.org/10.1175/1520-0485(1985)015<1060:ntoco>2.0.co;2), 1985.
- 1571 [Cummings, J. A.: Operational multivariate ocean data assimilation, *Q. J. R. Meteorol. Soc.*, 131, 3583–3604,](https://doi.org/10.1256/qj.05.105)
 1572 <https://doi.org/10.1256/qj.05.105>, 2005.
- 1573 [Cummings, J. A. and Smedstad, O. M.: Variational Data Assimilation for the Global Ocean, in: Data Assimilation for Atmospheric, Oceanic](https://doi.org/10.1007/978-3-642-35088-7_13)
 1574 [and Hydrologic Applications, vol. II, edited by: Park, S. K. and Xu, L., Springer Berlin Heidelberg, 303–343, https://doi.org/10.1007/978-](https://doi.org/10.1007/978-3-642-35088-7_13)
 1575 [3-642-35088-7_13](https://doi.org/10.1007/978-3-642-35088-7_13), 2013.
- 1576 [Dortch, Q. and Whitledge, T. E.: Does nitrogen or silicon limit phytoplankton production in the Mississippi River plume and nearby regions?,](https://doi.org/10.1016/0278-4343(92)90065-R)
 1577 [Cont. Shelf Res., 12, 1293–1309, https://doi.org/10.1016/0278-4343\(92\)90065-R](https://doi.org/10.1016/0278-4343(92)90065-R), 1992.
- 1578 [Feng, Y., Fennel, K., Jackson, G. A., DiMarco, S. F., and Hetland, R. D.: A model study of the response of hypoxia to upwelling-favorable](https://doi.org/10.1016/j.jmarsys.2013.11.009)
 1579 [wind on the northern Gulf of Mexico shelf, *J. Mar. Syst.*, 131, 63–73, https://doi.org/10.1016/j.jmarsys.2013.11.009](https://doi.org/10.1016/j.jmarsys.2013.11.009), 2014.
- 1580 [Fennel, K. and Laurent, A.: N and P as ultimate and proximate limiting nutrients in the northern Gulf of Mexico: Implications for hypoxia](https://doi.org/10.5194/bg-15-3121-2018)
 1581 [reduction strategies, *Biogeochemistry*, 15, 3121–3131, https://doi.org/10.5194/bg-15-3121-2018](https://doi.org/10.5194/bg-15-3121-2018), 2018.
- 1582 [Fennel, K. and Testa, J. M.: Biogeochemical Controls on Coastal Hypoxia, *Ann. Rev. Mar. Sci.*, 11, 105–130,](https://doi.org/10.1146/annurev-marine-010318-095138)
 1583 <https://doi.org/10.1146/annurev-marine-010318-095138>, 2019.

Formatted: English (UK)

Deleted: Baronas, J. J., Hammond, D. E., Berelson, W. M., McManus, J., and Severmann, S.: Germanium-silicon fractionation in a river-influenced continental margin: The Northern Gulf of Mexico, *Geochim. Cosmochim. Acta*, 178, 124–142, https://doi.org/10.1016/j.gca.2016.01.028, 2016.†

Formatted: English (UK)

Formatted: English (UK)

589 Fennel, K., Wilkin, J., Levin, J., Moisan, J., O'Reilly, J., and Haidvogel, D.: Nitrogen cycling in the Middle Atlantic Bight: Results from a
590 three-dimensional model and implications for the North Atlantic nitrogen budget, *Global Biogeochem. Cycles*, 20, 1–14,
591 <https://doi.org/10.1029/2005GB002456>, 2006.

592 Fennel, K., Hetland, R., Feng, Y., and Dimarco, S.: A coupled physical-biological model of the Northern Gulf of Mexico shelf: Model
593 description, validation and analysis of phytoplankton variability, 8, 1881–1899, <https://doi.org/10.5194/bg-8-1881-2011>, 2011.

594 Fennel, K., Hu, J., Laurent, A., Marta-Almeida, M., and Hetland, R.: Sensitivity of hypoxia predictions for the northern Gulf of Mexico to
595 sediment oxygen consumption and model nesting, *J. Geophys. Res. Ocean.*, 118, 990–1002, <https://doi.org/10.1002/jgrc.20077>, 2013.

596 Fennel, K., Laurent, A., Hetland, R., Justic, D., Ko, D. S., Lehrter, J., Murrell, M., Wang, L., Yu, L., and Zhang, W.: Effects of model physics
597 on hypoxia simulations for the northern Gulf of Mexico: A model intercomparison, *J. Geophys. Res. Ocean.*, 121, 5731–5750,
598 <https://doi.org/10.1002/2015JC011516>, 2016.

599 Fiechter, J. and Moore, A. M.: Interannual spring bloom variability and Ekman pumping in the coastal Gulf of Alaska, *J. Geophys. Res.*
600 *Ocean.*, 114, 1–19, <https://doi.org/10.1029/2008JC005140>, 2009.

601 Flather, R. A.: A tidal model of the northwest European continental shelf, *Mem. la Soc. R. Sci. Liege*, **10**, 141–164, 1976.

602 Fox, D. N., Teague, W. J., Barron, C. N., Carnes, M. R., and Lee, C. M.: The Modular Ocean Data Assimilation System (MODAS), *J.*
603 *Atmos. Ocean. Technol.*, 19, 240–252, [https://doi.org/10.1175/1520-0426\(2002\)019<0240:TMODAS>2.0.CO;2](https://doi.org/10.1175/1520-0426(2002)019<0240:TMODAS>2.0.CO;2), 2002.

604 Garcia, H. E., Weathers, K., Paver, C. R., Smolyar, I., Boyer, T. P., Locarnini, R. A., Zweng, M. M., Mishonov, A. V., Baranova, O. K.,
605 Seidov, D., and Reagan, J. R.: *World Ocean Atlas 2018, Volume 3: Dissolved Oxygen, Apparent Oxygen Utilization, and Oxygen Saturation*,
606 *Technical*, edited by: Mishonov, A. V., NOAA Atlas NESDIS 83, 38 pp., 2018.

607 Gomez, F. A., Lee, S. K., Liu, Y., Hernandez, F. J., Muller-Karger, F. E., and Lamkin, J. T.: Seasonal patterns in phytoplankton biomass
608 across the northern and deep Gulf of Mexico: A numerical model study, 15, 3561–3576, <https://doi.org/10.5194/bg-15-3561-2018>, 2018.

609 Große, F., Fennel, K., and Laurent, A.: Quantifying the Relative Importance of Riverine and Open-Ocean Nitrogen Sources for Hypoxia
610 Formation in the Northern Gulf of Mexico, *J. Geophys. Res. Ocean.*, 5451–5467, <https://doi.org/10.1029/2019jc015230>, 2019.

611 Haidvogel, D. B., Arango, H. G., Hedstrom, K., Beckmann, A., Malanotte-Rizzoli, P., and Shchepetkin, A. F.: Model evaluation experiments
612 in the North Atlantic Basin: Simulations in nonlinear terrain-following coordinates, *Dyn. Atmos. Ocean.*, 32, 239–281,
613 [https://doi.org/10.1016/S0377-0265\(00\)00049-X](https://doi.org/10.1016/S0377-0265(00)00049-X), 2000.

614 Helber, R. W., Townsend, T. L., Barron, C. N., Dastugue, J. M., and Carnes, M. R.: *Validation Test Report for the Improved Synthetic*
615 *Ocean Profile (ISOP) System, Part I: Synthetic Profile Methods and Algorithm*, 2013.

616 Hetland, R. D. and DiMarco, S. F.: How does the character of oxygen demand control the structure of hypoxia on the Texas-Louisiana
617 continental shelf?, *J. Mar. Syst.*, 70, 49–62, <https://doi.org/10.1016/j.jmarsys.2007.03.002>, 2008.

618 Justic, D. and Wang, L.: Assessing temporal and spatial variability of hypoxia over the inner Louisiana-upper Texas shelf: Application of
619 an unstructured-grid three-dimensional coupled hydrodynamic-water quality model, *Cont. Shelf Res.*, 72, 163–179,
620 <https://doi.org/10.1016/j.csr.2013.08.006>, 2014.

621 Justic, D., Rabalais, N. N., and Turner, R. E.: Simulated responses of the Gulf of Mexico hypoxia to variations in climate and anthropogenic
622 nutrient loading, *J. Mar. Syst.*, 42, 115–126, [https://doi.org/10.1016/S0924-7963\(03\)00070-8](https://doi.org/10.1016/S0924-7963(03)00070-8), 2003.

623 Justic, D., Bierman, V. J. J., Scavia, D., and Hetland, R. D.: Forecasting Gulf's Hypoxia: The Next 50 Years?, 30, 791–801, 2007.

624 Kishi, M. J., Kashiwai, M., Ware, D. M., Megrey, B. A., Eslinger, D. L., Werner, F. E., Noguchi-Aita, M., Azumaya, T., Fujii, M.,
625 Hashimoto, S., Huang, D., Iizumi, H., Ishida, Y., Kang, S., Kantakov, G. A., Kim, H. cheol, Komatsu, K., Navrotsky, V. V., Smith, S. L.,
626 Tadokoro, K., Tsuda, A., Yamamura, O., Yamanaka, Y., Yokouchi, K., Yoshie, N., Zhang, J., Zuenko, Y. I., and Zvalinsky, V. I.: NEMURO-
627 a lower trophic level model for the North Pacific marine ecosystem, *Ecol. Modell.*, 202, 12–25,
628 <https://doi.org/10.1016/j.ecolmodel.2006.08.021>, 2007.

Deleted: 6

Formatted: English (UK)

- 630 [Kristiansen, S. and Hoell, E. E.: The importance of silicon for marine production, *Hydrobiologia*, 484, 21–31,](https://doi.org/10.1023/A:1021392618824.2002)
631 <https://doi.org/10.1023/A:1021392618824.2002>.
- 632 Laurent, A. and Fennel, K.: Simulated reduction of hypoxia in the northern Gulf of Mexico due to phosphorus limitation, *Elem. Sci. Anthr.*,
633 2, 1–12, <https://doi.org/10.12952/journal.elementa.000022>, 2014.
- 634 Laurent, A. and Fennel, K.: Time-Evolving, Spatially Explicit Forecasts of the Northern Gulf of Mexico Hypoxic Zone, *Environ. Sci.*
635 *Technol.*, 53, 14449–14458, <https://doi.org/10.1021/acs.est.9b05790>, 2019.
- 636 Laurent, A., Fennel, K., Hu, J., and Hetland, R.: Simulating the effects of phosphorus limitation in the Mississippi and Atchafalaya river
637 plumes, 9, 4707–4723, <https://doi.org/10.5194/bg-9-4707-2012>, 2012.
- 638 Laurent, A., Fennel, K., Wilson, R., Lehrter, J., and Devereux, R.: Parameterization of biogeochemical sediment-water fluxes using in situ
639 measurements and a diagenetic model, 13, 77–94, <https://doi.org/10.5194/bg-13-77-2016>, 2016.
- 640 Laurent, A., Fennel, K., Ko, D. S., and Lehrter, J.: Climate change projected to exacerbate impacts of coastal Eutrophication in the Northern
641 Gulf of Mexico, *J. Geophys. Res. Ocean.*, 123, 3408–3426, <https://doi.org/10.1002/2017JC013583>, 2018.
- 642 Li, Q. P., Franks, P. J. S., Landry, M. R., Goericke, R., and Taylor, A. G.: Modeling phytoplankton growth rates and chlorophyll to carbon
643 ratios in California coastal and pelagic ecosystems, *J. Geophys. Res. Biogeosciences*, 115, 1–12, <https://doi.org/10.1029/2009JG001111>,
644 2010.
- 645 [Lohrenz, S. E., Fahnenstiel, G. L., Redalje, D. G., Lang, G. A., Dagg, M. J., Whitledge, T. E., and Dortch, Q.: Nutrients, irradiance, and
646 mixing as factors regulating primary production in coastal waters impacted by the Mississippi River plume, *Cont. Shelf Res.*, 19, 1113–
647 1141, \[https://doi.org/10.1016/S0278-4343\\(99\\)00012-6\]\(https://doi.org/10.1016/S0278-4343\(99\)00012-6\), 1999.](https://doi.org/10.1016/S0278-4343(99)00012-6)
- 648 Marchesiello, P., McWilliams, J. C., and Shchepetkin, A.: Open boundary conditions for long-term integration of regional oceanic models,
649 *Ocean Model.*, 3, 1–20, [https://doi.org/10.1016/S1463-5003\(00\)00013-5](https://doi.org/10.1016/S1463-5003(00)00013-5), 2001.
- 650 Mattem, J. P., Fennel, K., and Dowd, M.: Sensitivity and uncertainty analysis of model hypoxia estimates for the Texas-Louisiana shelf, *J.*
651 *Geophys. Res. Ocean.*, 118, 1316–1332, <https://doi.org/10.1002/jgrc.20130>, 2013.
- 652 McCarthy, M. J., Carini, S. A., Liu, Z., Ostrom, N. E., and Gardner, W. S.: Oxygen consumption in the water column and sediments of the
653 northern Gulf of Mexico hypoxic zone, *Estuar. Coast. Shelf Sci.*, 123, 46–53, <https://doi.org/10.1016/j.ecss.2013.02.019>, 2013.
- 654 [Milligan, A. J., Varela, D. E., Brzezinski, M. A., and Morel, F. M. M.: Dynamics of silicon metabolism and silicon isotopic discrimination
655 in a marine diatom as a function of pCO₂, *Limnol. Oceanogr.*, 49, 322–329, <https://doi.org/10.4319/lo.2004.49.2.0322>, 2004.](https://doi.org/10.4319/lo.2004.49.2.0322)
- 656 [Mississippi River/Gulf of Mexico Watershed Nutrient Task Force: Action Plan for Reducing, Mitigating, and Controlling Hypoxia in the
657 Northern Gulf of Mexico, Washington, DC., 2001.](https://doi.org/10.1007/s12237-010-9351-9)
- 658 [Mississippi River/Gulf of Mexico Watershed Nutrient Task Force: Gulf Hypoxia Action Plan 2008 for Reducing, Mitigating, and Controlling
659 Hypoxia in the Northern Gulf of Mexico and Improving Water Quality in the Mississippi River Basin, Washington, DC., 2008.](https://doi.org/10.1007/s12237-010-9351-9)
- 660 Moriarty, J. M., Harris, C. K., Friedrichs, M. A. M., Fennel, K., and Xu, K.: Impact of Seabed Resuspension on Oxygen and Nitrogen
661 Dynamics in the Northern Gulf of Mexico: A Numerical Modeling Study, *J. Geophys. Res. Ocean.*, 123, 7237–7263,
662 <https://doi.org/10.1029/2018JC013950>, 2018.
- 663 Murrell, M. C. and Lehrter, J. C.: Sediment and Lower Water Column Oxygen Consumption in the Seasonally Hypoxic Region of the
664 Louisiana Continental Shelf, 34, 912–924, <https://doi.org/10.1007/s12237-010-9351-9>, 2011.
- 665 [Nelson, D. M. and Dortch, Q.: Silicic acid depletion and silicon limitation in the plume of the Mississippi River: Evidence from kinetic
666 studies in spring and summer, *Mar. Ecol. Prog. Ser.*, 136, 163–178, <https://doi.org/10.3354/meps136163>, 1996.](https://doi.org/10.3354/meps136163)
- 667 [Nelson, D. M., Goering, John J., Kilham, S. S., and Guillard, R. R. L.: Kinetics of silicic acid uptake and rates of silica dissolution in the
668 marine diatom *Thalassiosira pseudonana*, *J. Phycol.*, 12, 246–252, <https://doi.org/10.1111/j.1529-8817.1976.tb00510.x>, 1976.](https://doi.org/10.1111/j.1529-8817.1976.tb00510.x)

Formatted: English (UK)

Formatted: English (UK)

Formatted: English (UK)

- 1669 Obenour, D. R., Michalak, A. M., and Scavia, D.: Assessing biophysical controls on Gulf of Mexico hypoxia through probabilistic modeling,
1670 *Ecol. Appl.*, 25, 492–505, <https://doi.org/10.1890/13-2257.1>, 2015.
- 1671 Olson, R. J.: Differential photoinhibition of marine nitrifying bacteria: a possible mechanism for the formation of the primary nitrite
1672 maximum, *J. Mar. Res.*, 39, 227–238, 1981.
- 1673 Parker, R. A.: Dynamic models for ammonium inhibition of nitrate uptake by phytoplankton, *Ecol. Modell.*, 66, 113–120,
1674 [https://doi.org/10.1016/0304-3800\(93\)90042-Q](https://doi.org/10.1016/0304-3800(93)90042-Q), 1993.
- 1675 Platt, T., Gallegos, C. L., and Harrison, W. G.: Photoinhibition of photosynthesis in natural assemblages of marine phytoplankton, *J. Mar.*
1676 *Res.*, 38, 687–701, 1980.
- 1677 [Quigg, A., Sylvan, J. B., Gustafson, A. B., Fisher, T. R., Oliver, R. L., Tozzi, S., and Ammerman, J. W.: Going West: Nutrient Limitation
1678 of Primary Production in the Northern Gulf of Mexico and the Importance of the Atchafalaya River. *Aquat. Geochemistry*, 17, 519–544,
1679 <https://doi.org/10.1007/s10498-011-9134-3>, 2011.](https://doi.org/10.1007/s10498-011-9134-3)
- 1680 Rabalais, N. N. and Baustian, M. M.: Historical Shifts in Benthic Infaunal Diversity in the Northern Gulf of Mexico since the Appearance
1681 of Seasonally Severe Hypoxia, 12, <https://doi.org/10.3390/d12020049>, 2020.
- 1682 Rabalais, N. N. and Turner, R. E.: Gulf of Mexico Hypoxia: Past, Present, and Future, *Limnol. Oceanogr. Bull.*, 28, 117–124,
1683 <https://doi.org/10.1002/lob.10351>, 2019.
- 1684 Rabalais, N. N., Turner, R. E., and Wiseman, W. J.: Gulf of Mexico hypoxia, a.k.a. “The dead zone,” *Annu. Rev. Ecol. Syst.*, 33, 235–263,
1685 <https://doi.org/10.1146/annurev.ecolsys.33.010802.150513>, 2002.
- 1686 Rabalais, N. N., Turner, R. E., Sen Gupta, B. K., Boesch, D. F., Chapman, P., and Murrell, M. C.: Hypoxia in the northern Gulf of Mexico:
1687 Does the science support the plan to reduce, mitigate, and control hypoxia?, 30, 753–772, <https://doi.org/10.1007/BF02841332>, 2007a.
- 1688 Rabalais, N. N., Turner, R. E., Gupta, B. K. S., Platon, E., and Parsons, M. L.: Sediments tell the history of eutrophication and hypoxia in
1689 the northern Gulf of Mexico, *Ecol. Appl.*, 17, 129–143, <https://doi.org/10.1890/06-0644.1>, 2007b.
- 1690 [Robertson, R. and Hartlapp, P.: Surface wind mixing in the Regional Ocean Modeling System \(ROMS\). *Geosci. Lett.*, 4,
1691 <https://doi.org/10.1186/s40562-017-0090-7>, 2017.](https://doi.org/10.1186/s40562-017-0090-7)
- 1692 Rowe, G. T., Cruz Kaegi, M. E., Morse, J. W., Boland, G. S., and Escobar Briones, E. G.: Sediment community metabolism associated with
1693 continental shelf hypoxia, northern Gulf of Mexico, 25, 1097–1106, <https://doi.org/10.1007/BF02692207>, 2002.
- 1694 Saha, S., Moorthi, S., Pan, H.-L., Wu, X., Wang, J., Nadiga, S., Tripp, P., Kistler, R., Woollen, J., Behringer, D., Liu, H., Stokes, D.,
1695 Grumbine, R., Gayno, G., Wang, J., Hou, Y.-T., Chuang, H.-Y., Juang, H.-M. H., Sela, J., Iredell, M., Treadon, R., Kleist, D., Van Delst,
1696 P., Keyser, D., Derber, J., Ek, M., Meng, J., Wei, H., Yang, R., Lord, S., van den Dool, H., Kumar, A., Wang, W., Long, C., Chelliah, M.,
1697 Xue, Y., Huang, B., Schemm, J.-K., Ebisuzaki, W., Lin, R., Xie, P., Chen, M., Zhou, S., Higgins, W., Zou, C.-Z., Liu, Q., Chen, Y., Han,
1698 Y., Cucurull, L., Reynolds, R. W., Rutledge, G., and Goldberg, M.: NCEP Climate Forecast System Reanalysis (CFRS) 6-hourly Products,
1699 January 1979 to December 2010, <https://doi.org/10.5065/D69K487J>, 2010.
- 1700 Saha, S., Moorthi, S., Wu, X., Wang, J., Nadiga, S., Tripp, P., Behringer, D., Hou, Y.-T., Chuang, H., Iredell, M., Ek, M., Meng, J., Yang,
1701 R., Mendez, M. P., van den Dool, H., Zhang, Q., Wang, W., Chen, M., and Becker, E.: NCEP Climate Forecast System Version 2 (CFSv2)
1702 6-hourly Products, <https://doi.org/10.5065/D61C1TXF>, 2011.
- 1703 Scavia, D., Evans, M. A., and Obenour, D. R.: A scenario and forecast model for gulf of mexico hypoxic area and volume, *Environ. Sci.*
1704 *Technol.*, 47, 10423–10428, <https://doi.org/10.1021/es4025035>, 2013.
- 1705 Schaeffer, B. A., Kurtz, J. C., and Hein, M. K.: Phytoplankton community composition in nearshore coastal waters of Louisiana, *Mar. Pollut.*
1706 *Bull.*, 64, 1705–1712, <https://doi.org/10.1016/j.marpolbul.2012.03.017>, 2012.
- 1707 Seitzinger, S. P. and Giblin, A. E.: Estimating denitrification in North Atlantic continental shelf sediments, in: *Nitrogen Cycling in the North*
1708 *Atlantic Ocean and its Watersheds*, edited by: Howarth, R. W., Springer Dordrecht, 235–260, https://doi.org/10.1007/978-94-009-1776-7_7,
1709 1996.

Formatted: English (UK)


Formatted: English (UK)


Formatted: English (UK)

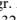
Deleted: Ruiz Xomchuk, V., Hetland, R. D., and Qu, L.: Small-Scale Variability of Bottom Oxygen in the Northern Gulf of Mexico, <https://doi.org/10.1029/2020JC016279>, 2021.


Formatted: English (UK)

- 713 Shchepetkin, A. F. and McWilliams, J. C.: The regional oceanic modeling system (ROMS): A split-explicit, free-surface, topography-
714 following-coordinate oceanic model, *Ocean Model.*, 9, 347–404, <https://doi.org/10.1016/j.ocemod.2004.08.002>, 2005.
- 715 Shchepetkin, A. F. and McWilliams, J. C.: Correction and commentary for “Ocean forecasting in terrain-following coordinates: Formulation
716 and skill assessment of the regional ocean modeling system” by Haidvogel et al., *J. Comp. Phys.* 227, pp. 3595–3624, *J. Comput. Phys.*, 228,
717 8985–9000, <https://doi.org/10.1016/j.jcp.2009.09.002>, 2009.
- 718 Shropshire, T., Morey, S., Chassignet, E., Bozec, A., Coles, V., Landry, M., Swalethorp, R., Zapfe, G., and Stukel, M.: Quantifying
719 spatiotemporal variability in zooplankton dynamics in the Gulf of Mexico with a physical-biogeochemical model, 17, 3385–3407,
720 <https://doi.org/10.5194/bg-17-3385-2020>, 2020.
- 721 Sylvan, J. B., Quigg, A., Tozzi, S., and Ammerman, J. W.: Eutrophication-induced phosphorus limitation in the Mississippi River plume:
722 Evidence from fast repetition rate fluorometry, *Limnol. Oceanogr.*, 52, 2679–2685, <https://doi.org/10.4319/lo.2007.52.6.2679>, 2007.
- 723 Testa, J. M. and Michael Kemp, W.: Hypoxia-induced shifts in nitrogen and phosphorus cycling in Chesapeake Bay, *Limnol. Oceanogr.*,
724 57, 835–850, <https://doi.org/10.4319/lo.2012.57.3.0835>, 2012.
- 725 Thamatrakoln, K. and Hildebrand, M.: Silicon uptake in diatoms revisited: A model for saturable and nonsaturable uptake kinetics and the
726 role of silicon transporters, *Plant Physiol.*, 146, 1397–1407, <https://doi.org/10.1104/pp.107.107094>, 2008.
- 727 Turner, R. and Rabalais, N.: Nitrogen and phosphorus phytoplankton growth limitation in the northern Gulf of Mexico, *Aquat. Microb.*
728 *Ecol.*, 68, 159–169, <https://doi.org/10.3354/ame01607>, 2013.
- 729 Turner, R. E., Qureshi, N., Rabalais, N. N., Dortch, Q., Justić, D., Shaw, R. F., and Cope, J.: Fluctuating silicate:nitrate ratios and coastal
730 plankton food webs, *Proc. Natl. Acad. Sci. U. S. A.*, 95, 13048–13051, <https://doi.org/10.1073/pnas.95.22.13048>, 1998.
- 731 Turner, R. E., Rabalais, N. N., and Justić, D.: Predicting summer hypoxia in the northern Gulf of Mexico: Redux, *Mar. Pollut. Bull.*, 64,
732 319–324, <https://doi.org/10.1016/j.marpolbul.2011.11.008>, 2012.
- 733 Wang, L. and Justić, D.: A modeling study of the physical processes affecting the development of seasonal hypoxia over the inner Louisiana-
734 Texas shelf: Circulation and stratification, *Cont. Shelf Res.*, 29, 1464–1476, <https://doi.org/10.1016/j.csr.2009.03.014>, 2009.
- 735 Wanninkhof, R.: Relationship Between Wind Speed and Gas Exchange Over the Ocean, *J. Geophys. Res.*, 97, 7373–7382,
736 <https://doi.org/10.1029/92JC00188>, 1992.
- 737 Warner, J. C., Geyer, W. R., and Lerczak, J. A.: Numerical modeling of an estuary: A comprehensive skill assessment, *J. Geophys. Res. C*
738 *Ocean.*, 110, 1–13, <https://doi.org/10.1029/2004JC002691>, 2005.
- 739 Warner, J. C., Armstrong, B., He, R., and Zambon, J. B.: Development of a Coupled Ocean-Atmosphere-Wave-Sediment Transport
740 (COAWST) Modeling System, *Ocean Model.*, 35, 230–244, <https://doi.org/10.1016/j.ocemod.2010.07.010>, 2010.
- 741 Warner, J. C., Defne, Z., Haas, K., and Arango, H. G.: A wetting and drying scheme for ROMS, *Comput. Geosci.*, 58, 54–61,
742 <https://doi.org/10.1016/j.cageo.2013.05.004>, 2013.
- 743 Wawrik, B. and Paul, J. H.: Phytoplankton community structure and productivity along the axis of the Mississippi River plume in
744 oligotrophic Gulf of Mexico waters, *Aquat. Microb. Ecol.*, 35, 185–196, <https://doi.org/10.3354/ame035185>, 2004.
- 745 Yu, L., Fennel, K., and Laurent, A.: A modeling study of physical controls on hypoxia generation in the northern Gulf of Mexico, *J. Geophys.*
746 *Res. Ocean.*, 120, 5019–5039, <https://doi.org/10.1002/2014JC010634>, 2015.
- 747 Zang, Z., Xue, Z. G., Bao, S., Chen, Q., Walker, N. D., Haag, A. S., Ge, Q., and Yao, Z.: Numerical study of sediment dynamics during
748 hurricane Gustav, *Ocean Model.*, 126, 29–42, <https://doi.org/10.1016/j.ocemod.2018.04.002>, 2018.
- 749 Zang, Z., Xue, Z. G., Xu, K., Bentley, S. J., Chen, Q., D’Sa, E. J., and Ge, Q.: A Two Decadal (1993–2012) Numerical Assessment of
750 Sediment Dynamics in the Northern Gulf of Mexico, 11, 938, <https://doi.org/10.3390/w11050938>, 2019.
- 751 Zang, Z., Xue, Z. G., Xu, K., Ozdemir, C. E., Chen, Q., Bentley, S. J., and Sahin, C.: A Numerical Investigation of Wave-Supported Gravity

Deleted: Simpson, J. H.: The shelf-sea fronts: implications of their existence and behaviour, *Philos. Trans. R. Soc. London. Ser. A, Math. Phys. Sci.*, 302, 531–546, <https://doi.org/10.1098/rsta.1981.0181>, 1981. 

Simpson, J. H. and Bowers, D.: Models of stratification and frontal movement in shelf seas, *Deep Sea Res. Part A, Oceanogr. Res. Pap.*, 28, 727–738, [https://doi.org/10.1016/0198-0149\(81\)90132-1](https://doi.org/10.1016/0198-0149(81)90132-1), 1981. 

Simpson, J. H. and Hunter, J. R.: Fronts in the Irish Sea, *Nature*, 250, 404–406, <https://doi.org/10.1038/250404a0>, 1974. 

Simpson, J. H., Allen, C. M., and Morris, N. C. G.: Fronts on the Continental Shelf, *J. Geophys. Res.*, 83, 4607–4614, <https://doi.org/10.1029/JC083iC09p04607>, 1978. 

Formatted: English (UK)

Formatted: English (UK)

1764 Flow During Cold Fronts Over the Atchafalaya Shelf, *J. Geophys. Res. Ocean.*, 125, 1–24, <https://doi.org/10.1029/2019JC015269>, 2020.

1765 [Zhao, Y. and Quigg, A.: Nutrient limitation in Northern Gulf of Mexico \(NGOM\): Phytoplankton communities and photosynthesis respond](#)
1766 [to nutrient pulse, *PLoS One*, 9, <https://doi.org/10.1371/journal.pone.0088732>, 2014.](#)

1767

Page 2: [1] Deleted Yanda Ou 3/14/23 4:12:00 PM

Page 2: [2] Deleted Yanda Ou 3/14/23 4:12:00 PM

Page 14: [3] Deleted Yanda Ou 3/14/23 4:12:00 PM

Page 19: [4] Deleted Yanda Ou 3/14/23 4:12:00 PM

Page 29: [5] Deleted Yanda Ou 3/14/23 4:12:00 PM

Page 29: [5] Deleted Yanda Ou 3/14/23 4:12:00 PM

Page 29: [5] Deleted Yanda Ou 3/14/23 4:12:00 PM

Page 29: [5] Deleted Yanda Ou 3/14/23 4:12:00 PM

Page 29: [5] Deleted Yanda Ou 3/14/23 4:12:00 PM

Page 29: [5] Deleted Yanda Ou 3/14/23 4:12:00 PM

Page 29: [5] Deleted Yanda Ou 3/14/23 4:12:00 PM

Page 29: [5] Deleted Yanda Ou 3/14/23 4:12:00 PM

Page 29: [5] Deleted Yanda Ou 3/14/23 4:12:00 PM

Page 29: [5] Deleted Yanda Ou 3/14/23 4:12:00 PM

Page 29: [6] Deleted Yanda Ou 3/14/23 4:12:00 PM

Page 29: [6] Deleted Yanda Ou 3/14/23 4:12:00 PM

Page 29: [7] Deleted Yanda Ou 3/14/23 4:12:00 PM

Page 29: [7] Deleted Yanda Ou 3/14/23 4:12:00 PM

Page 29: [8] Formatted Yanda Ou 3/14/23 4:12:00 PM

Font: +Body (Times New Roman), 10 pt, Not Bold, Font color: Auto

Page 29: [9] Deleted Yanda Ou 3/14/23 4:12:00 PM

NP60	60	60	0
------	----	----	---

Page 29: [10] Deleted Yanda Ou 3/14/23 4:12:00 PM

NSi60	60	0	60
-------	----	---	----

Page 29: [11] Deleted Yanda Ou 3/14/23 4:12:00 PM

NPSi60	60	60	60
--------	----	----	----

Page 29: [12] Deleted Yanda Ou 3/14/23 4:12:00 PM

Page 33: [13] Deleted Yanda Ou 3/14/23 4:12:00 PM